NORTHWESTERN UNIVERSITY

# Roles of Specialized Mucolipin-Endowed Lysosomes

A DISSERTATION

SUBMITTED TO THE GRADUATE SCHOOL

IN PARTIAL FULLFILLMENT OF THE REQUIREMENTS

For the degree

DOCTOR OF PHILOSOPHY

Field of Driskill Graduate Training Program in Life Sciences

By

Teerawat Wiwatpanit

EVANSTON, ILLINOIS

March 2018

# ABSTRACT

Mucolipins are lysosomal cation channels, with high permeability to calcium ions, that are thought to regulate endolysosomal trafficking. While mucolipin 1 is expressed in all cells, mucolipin 3 is expressed in a small subset of cells (i.e. neonatal intestinal enterocytes, cochlear hair cells and marginal cells of stria vascularis). This selective co-expression of mucolipins suggests that they may contribute to these cells' unique characteristics. For example, we found that mucolipins in fact facilitated endolysosomal trafficking in the neonatal intestinal enterocytes. In adults, protein from ingested food are digested by proteases in the acidic stomach, and the resulting free amino acids are absorbed by the enterocytes. However, during suckling period, the neonatal enterocytes are unique in that they undergo high level of endocytosis to uptake maternal nutrients. In neonates, stomach is not acidic yet and intact proteins pass into the intestine where they are endocytosed by the enterocytes for intracellular digestion through lysosomes. We found mucolipins 3 and 1 were expressed at high level in the neonatal enterocytes, and subsided by weaning. Mice lacking both mucolipins, but not either one alone, had severely vacuolated enterocytes. We demonstrated that these enlarged vacuoles resulted from the endolysosomal hybridorganelles' failure to undergo lysosomal scission after the completion of intracellular digestion of maternal milk. These enlarged vacuoles led to reduced endocytosis of nutrients which explained their growth defect, previously reported by our laboratory. We also found for the first time that human infant enterocytes also utilized this specialized mucolipin-endowed lysosomes. We reported evidence that the disruption of this specialized endolysosomal system may be the cause of necrotizing enterocolitis, a devastating pediatric intestinal disease that causes up to 80% infant mortality rate.

Unlike the enterocytes in which they exhibit high level of endocytosis and lysosomal degradation, the auditory hair cells have lower level of endocytosis compared to the neonatal intestinal enterocytes. Nevertheless, hair cells' unique feature is that they are remarkably resilient as they can survive for decades despite constant mechanical and chemical insults. The restricted co-expression in both hair cells and stria vascularis of the inner ear suggests that mucolipins may contribute to the maintenance of hearing. In fact, we found that mice lacking mucolipins 3 and 1, but not either one alone, suffered early-onset age-related hearing loss due to auditory outer hair cell death. Using mice conditionally lacking mucolipins 3 and 1 in only hair cells, but not in the stria vascularis, we found that mucolipins primarily played a role in maintaining long-term hearing in hair cells. Similar to the neonatal intestinal enterocytes lacking mucolipins, outer hair cells from these mutant mice contained vacuolated organelles. However, these enlarged organelles were lysosomes, unlike the endolysosomal hybridorganelles observed in the enterocytes of mice lacking mucolipins. Because of mucolipins co-expression in hair cells, it is reasonable to assume that the specialized mucolipin-endowed lysosomes could participate in a self-repair mechanism to recycle damaged organelles through autophagy and, therefore, promote their long-term survival. However, we found that this was not the case as shown by the normal level and distribution of autophagosomes, mitochondria and peroxisomes (organelles whose defects can lead to hair cell death and hearing loss). We found that lysosomes of outer hair cells lacking mucolipins were actually damaged themselves, becoming permeabilized, and, thus allowing toxic hydrolases, such as cathepsin D, into the cytoplasm—a known trigger of multiple cell death pathways. Here, we implicated for the first time hair cell lysosomes in age-related hearing loss, and proposed a mechanism by which toxic lysosomes could lead to outer hair cell death.

# ACKNOWLEDGEMENTS

I would like to thank my PI, Dr. Jaime García-Añoveros, for his continuing supports and advices at every step of my graduate career. With his guidance, I have gained expertise in not one but three different biological systems: intestinal, auditory and female reproductive systems. I am grateful to have worked with remarkable scientists in the Añoveros lab who have provided me valuable advices and friendship. Special thanks to former lab members, Dr. Natalie Remis and Dr. Andrew Castiglioni, who generated the transgenic mice before I joined the lab, and whose data contributed to my publications and this dissertation. I also would like to thank my thesis committee members: Dr. Mary Ann Cheatham, Dr. Catherine Hunter and Dr. Vladimir Gelfand, for continuing to challenge me intellectually and providing advices that allowed the completion of this work. In addition, I would like to thank Dr. James Bartles for all his expert advice on the auditory system.

# LIST OF ABBREVIATIONS

| | |
|---|---|
| ABR | auditory brainstem response |
| ARHL | age-related hearing loss |
| cDKO | conditional double-knockout (*Gfi1*$^{Cre/+}$;*Trpml3*$^{F/F}$;*Trpml1*$^{-/-}$) |
| DKO | double-knockout (*Trpml3*$^{-/-}$;*Trpml1*$^{-/-}$) |
| DPOAE | distortion product otoacoustic emission |
| HC | hair cell |
| IHC | inner hair cell |
| ISH | *in situ* hybridization |
| LAMP | lysosome-associated membrane protein |
| LIMP | lysosomal integral membrane protein |
| LSD | lysosomal storage disease |
| ML1 | mucolipin 1 |
| ML1KO | *Trpml1*$^{-/-}$ |
| ML3 | mucolipin 3 |
| ML3KO | *Trpml3*$^{-/-}$ |
| MLIV | mucolipidosis type IV |
| MPS | mucopolysaccharidosis |
| NEC | necrotizing enterocolitis |
| NIHL | noise-induced hearing loss |
| OHC | outer hair cell |
| SIM | structured illumination super-resolution microscope |
| TRP | transient receptor potential |
| TRPML | transient receptor potential mucolipin |
| *Va* | varitint-waddler |
| WT | wild-type |

TABLE OF CONTENTS

ABSTRACT……2

ACKNOWLEDGEMENTS……4

LIST OF ABBREVIATIONS……5

LIST OF FIGURES……9

CHAPTER 1: General Introduction……11

1.1 Transient receptor potential channel mucolipins……12

1.2 Mammalian neonatal intestine……16

1.3 Understanding pediatric gastroenterological diseases……18

1.4 A comparison between the mammalian gut epithelial cells and auditory sensory cells……20

1.5 Mammalian auditory sensory systems……21

1.6 Mouse models of age-related hearing loss……23

1.7 Overview……26

CHAPTER 2: Mucolipins and neonatal enterocytes……28

2.1 Abstract……29

2.2 Introduction……31

2.3 Results……34

2.3.1 Mucolipin 3 expression in the intestine…….…….……34

2.3.2 Pathological vacuolation in neonatal enterocytes

lacking mucolipins…….……..…….…….……44

2.3.3 Reduced endocytotic rate in neonatal enterocytes

lacking mucolipins…….……..…….…….……50

2.3.4 Pathological vacuolation in enterocytes of a rodent model

of necrotizing enterocolitis…….……...…….……55

2.3.5 Mucolipins in human infant enterocytes…….……..……59

2.4 Discussions…….…….…….……61

2.5 Materials and methods.…… …….…….……..…68

CHAPTER 3: Mucolipins and age-related hearing loss.…….……80

3.1 Abstract…….…….…….…….…….……...81

3.2 Introduction…….…….…….…….…….…82

3.3 Results…….…….…….…….…….…….....85

3.3.1 Accelerated age-related hearing loss in mice lacking mucolipins……..85

3.3.2 Cochlea degeneration in mice lacking mucolipins…….……91

3.3.3 Lysosomal pathology in hair cells lacking mucolipins…….…….96

3.4 Discussions…….…….…….…….…….…….……...109

3.5 Materials and methods…….…….…….…….117

CHAPTER 4: General discussions…….…….…….…….…….……..123

5.1 Genetic redundancy between mucolipins….…….…….…….……...124

5.2 Specialized mucolipin-endowed lysosomes….…….…….…….……...127

5.3 Future directions.. ….…….…….…….…….…….……128

5.3.1 Mucolipins and neonatal intestinal enterocytes…...…….……...128

5.3.2 Mucolipins and age-related hearing loss…….…….……129

REFERENCES …….…….……...……...…..……131

APPENDIX A..……..……..…….……...……159
***Wiwatpanit, T.**, *Lorenzen, S.M., *Cantú, J.A., Foo, C.Z., Hogan, A.K., Márquez, F., Clancy, J.C., Schipma., M.J., Cheatham, M.A., Duggan, A. and Garcia-Añoveros. J. (2018). Differentiation of nascent outer hair cells into inner hair cells in the absence of INSM1. *Nature*. Awaiting re-submission. *equal contributions

APPEXDIX B……..……..…….……...……193
García-Añoveros J, Wiwatpanit T (2014) TRPML2 and mucolipin evolution. Handb Exp Pharmacol 222:647–658.

APPENDIX C……..……..…….……...……215
Mucolipins and postpartum uterine involution

AUTHOR CONTRIBUTIONS…….……...223

LISTS OF FIGURES

**Figure 1** Mucolipin 3 is expressed in the specialized endolysosomal organelles of neonatal, but not adult, intestinal enterocytes……..37

**Figure 2** Enteroids derived from neonatal, but not adult, intestine express lysosomal mucolipin 3……...40

**Figure 3** Mucolipin 3 localizes to specialized lysosomes of neonatal enterocytes……..42

**Figure 4** Neonatal enterocytes, but not adult, lacking mucolipins 3 and 1, but not either alone, are vacuolated. ……44

**Figure 5** A single enlarged pathological vacuole fills most of the intracellular space of neonatal enterocytes lacking mucolipins 3 and 1……46

**Figure 6** The pathological vacuoles of neonatal enterocytes lacking mucolipins 3 and 1 are aberrant endolysosomal hybridorganelles……...48

**Figure 7** The pathological vacuoles in neonatal enterocytes do not alter endocytosis at P0 but eventually lead to reduced endocytosis by P7……52

**Figure 8** Human infant enterocytes contain a specialized mucolipin 3-endowed lysosomes…..……..56

**Figure 9** Human infant intestines are rich in lysosome and mucolipins……...57

**Figure 10** Human necrotizing enterocolitis (NEC) patient and rodent models of NEC suffer neonatal enterocyte vacuolation resembling that of mucolipins 3 and 1 co-deficient mice……....60

**Figure 11** Proposed model for lysosomal pathology in neonatal enterocytes lacking mucolipins 3 and 1……..……..66

**Figure 12** Co-absence of mucolipins 3 and 1 in HCs, but not either alone, causes age-related hearing loss progressing from high to low frequency…….86

**Figure 13** Mucolipin 3 is localized to HCs and the stria vascularis in both adult and neonatal cochleae……...89

**Figure 14** There is an anatomical defect in OHCs but not in the stria vascularis from cochleae lacking both mucolipins 3 and 1……..……..93

**Figure 15** Age-related hearing loss in animals lacking both mucolipins 3 and 1 is accompanied by OHC death……..95

**Figure 16** OHCs lacking mucolipins 3 and 1 possess pathologically enlarged lysosomes……...97

**Figure 17** Enlarged lysosomes in OHCs lacking mucolipins 3 and 1 do not cause defects in lysosomal degradation of damaged organelles……..101

**Figure 18** OHCs lacking mucolipins 3 and 1 exhibit lysosomal membrane permeabilization. ……..……106

**Figure 19** Upon lysosomal membrane permeabilization, enlarged lysosomes from OHCs lacking mucolipins 3 and 1 contain almost undetectable level of lysosomal cathepsin D……108

**Figure 20** Proposed model for lysosomal pathology in hair cells lacking mucolipins 3 and 1……...115

# CHAPTER 1:

# General Introduction

### 1.1 Transient receptor potential channel mucolipins

The transient receptor potential (TRP) channel constitutes a family of cation channels that are distantly related to voltage-gated $K^+$, $Na^+$ and $Ca^{2+}$ superfamilies. The mucolipin TRP (TRPML) subfamily consists of 3 vertebrate isoforms (mucolipin 1-3), coded from *Mcoln1-3* genes (also known as *Trpml1-3*) (García-Añoveros and Wiwatpanit, 2014). Their names derive from their paralog mucolipin 1, of which mutations cause the lysosomal storage disease (LSD) mucolipidosis type IV (MLIV) in humans (Bargal et al., 2000; Bach, 2001). In invertebrates, e.g. *Drosophila melanogaster, Caenorhabditis elegans* and *Dictyostelium discoideum,* there is only one mucolipin homolog: *trpml*, *cup-5* and *mcln*, respectively (Fares and Greenwald, 2001; Lima et al., 2012; Wong et al., 2012). Mucolipins are localized to the membrane of intracellular vesicles, specifically late endosomes and lysosomes, and thought to act as nonselective cation channels, although they are preferential to $Ca^{2+}$ (LaPlante et al., 2004; Zhang et al., 2009; Cheng et al., 2010; Castiglioni et al., 2011; García-Añoveros and Wiwatpanit, 2014; Remis et al., 2014; Cao et al., 2017). In heterologous expression systems, mucolipin 1, 2 and 3 elicit inwardly rectifying currents, i.e. inward currents at negative potentials and no outward currents at positive one (Grimm et al., 2007; Xu et al., 2007; Nagata et al., 2008; Samie et al., 2009; Lev et al., 2010; Zeevi et al., 2010). Studies have also demonstrated that heterologously co-expressed mammalian mucolipins can form dimers and multimers in all combinations *in vitro* (Venkatachalam et al., 2006; Grimm et al., 2010; Zeevi et al., 2010). These interactions appear to be exclusive between mucolipins as they do not co-immunoprecipitated with a distantly related channel TRP melastatin 8 (Zeevi et al., 2010).

Mucolipin 1 is the most characterized channel of this subfamily. Mucolipin 1 is ubiquitously expressed in all cells (Bach, 2001; Cheng et al., 2010; Castiglioni et al., 2011) and

mutations on *Trpml1* gene cause MLIV in humans (Bach et al., 1975, 2005; Bargal et al., 2000, 2001). MLIV is an autosomal recessive early-onset (~1 year of age) neurodegenerative disease, characterized by ophthalmological abnormalities, psychomotor retardation, iron deficiency and impaired production of gastric acids that lead to constantly elevated blood gastrin hormone level (Schiffmann et al., 1998; Bach, 2001; LaPlante et al., 2002, 2004; Geer et al., 2010; Chandra et al., 2011; Wakabayashi et al., 2011). Cells from MLIV patients exhibit an accumulation of undigested macromolecules inside enlarged vacuoles, forming toxic aggregates that result in cellular degeneration (Zeigler et al., 1992; Winchester et al., 2000; Slaugenhaupt, 2002; Vergarajauregui et al., 2008; Wakabayashi et al., 2011). *Trpml1*$^{-/-}$ (ML1KO) mice begin to exhibit mild gait deficits at 3 months progressing slowly until 6 months, at which they develop MLIV-like symptoms (ataxia, retinal degeneration and loss of body fat) and die within 8 months of age (Venugopal et al., 2007; Micsenyi et al., 2009). Studies have demonstrated that mucolipin 1 plays a prominent role in vesicle trafficking, but its specific roles appear to depend on cell types: vesicle scission in neonatal intestinal enterocytes (Remis et al., 2014), vesicle fusion in macrophages (Thompson et al., 2007) and lysosomal exocytosis in muscle fiber (Samie et al., 2013; Cheng et al., 2014).

Mucolipin 2 is the least studied channel of the TRPML subfamily because there is no known pathology associated with human diseases, and a knockout animal model is not available. The expression domains of mucolipin 2 have only been described using RT-PCR. *Trpml2* mRNA is present in human lung, trachea, stomach, colon, mammary glands, peripheral blood lymphocytes, kidney, thymus, testis, uterus, spleen, adipose tissue, and thyroid; and in mouse kidney, thymus, trachea, colon, adipose tissue, lung, liver, pancreas, and testis (Samie et al., 2009; Grimm et al., 2010; García-Añoveros and Wiwatpanit, 2014). Genetically, mucolipin 2 is

more closely related to mucolipin 3 than mucolipin 1 (García-Añoveros and Wiwatpanit, 2014). Furthermore, synthetic compounds known to activate mucolipin 3 also activate mucolipin 2 in heterologous expression systems, suggesting similar gating mechanisms for both channels (Grimm et al., 2010, 2012). A few studies have suggested subcellular functions of mucolipin 2 in heterologous expression systems. For example, the consecutively active human-mucolipin 2 expressed in *Drosophila* S2 cell leads to cell death by $Ca^{2+}$ overload (Lev et al., 2010); exogenous murine mucolipin 2 is localized to the lysosomes of chicken DT40 B-lymphocytes (Song et al., 2006). However, it remains unclear what subcellular and physiological functions of mucolipin 2 are in native cells and organs.

Previous studies described expression of *Trpml3* in melanocytes, chemosensory neurons of vomeronasal organ, olfactory epithelium, thymus, scattered cells in the lung (presumed to be alveolar macrophages) and cells of the kidney (presumed to be principal cells of the collecting duct) (Xu et al., 2007; Nagata et al., 2008; Castiglioni et al., 2011; Remis et al., 2014). Similar to mucolipin 2, there is no known pathology associated with mucolipin 3 in humans. However, its gain-of-function mutations have been extensively explored in the *varitint waddler* (*Va*) mouse models (Cable and Steel, 1998; Di Palma et al., 2002; Steel, 2002; Atiba-Davies and Noben-Trauth, 2007; Grimm et al., 2007; Xu et al., 2007; Nagata et al., 2008). *Va* mutation is a spontaneous dominant mutation on *Trpml3* gene that causes male sterility, coat color hypopigmentation, deafness and a circling behavior (Di Palma et al., 2002; Atiba-Davies and Noben-Trauth, 2007). This mutation results in an alanine-to-proline (A419P) substitution near the pore region domain of the channel (Di Palma et al., 2002). A second mutation (isoleucine-to-Threonine, I362T) occurred on *Trpml*3 of the original *Va* stock results in a less severe phenotype; this mouse line is termed $Va^J$ (Lane, 1972; Cable and Steel, 1998). The hearing and

vestibular impairments in *Va* and *Va$^J$* mice prompted the lab to first examine the expression of mucolipin in the inner ear (Nagata et al., 2008; Castiglioni et al., 2011). Previous lab members found that mucolipin 3 was expressed in inner-ear cochlear and vestibular hair cells (HCs), and marginal cells of stria vascularis, and that mucolipin 3 was also localized to lysosomes (Nagata et al., 2008; Castiglioni et al., 2011). In addition, mucolipin 3 is also expressed in vemeronasal organ (Castiglioni et al., 2011), melanocytes (Xu et al., 2007) and neonatal intestinal enterocytes (Remis et al., 2014). Several studies demonstrated that the *Va* and *Va$^J$* mutations on *Trpml3* resulted in increased open probability of the channel at negative membrane potential, causing constitutive cationic calcium currents that led to HC death that causes hearing and vestibular defects, and melanocyte death that cases pigmentation defects (Kim et al., 2007; Xu et al., 2007; Nagata et al., 2008). Nevertheless, because the *Va* and *Va$^J$* are gain-of-function mutations, they do not reveal the contribution mucolipin 3 may make in native cells and organs, which requires a null mutation lacking functional mucolipin 3 channel.

However, mice lacking functional mucolipin 3 (*Trpml3$^{-/-}$*, ML3KO)exhibit no obvious phenotype, including hearing, growth and coat color (Jörs et al., 2010; Remis et al., 2014). We therefore hypothesized that perhaps the remaining mucolipins, mucolipin 1 and 2, could act redundantly with mucolipin 3. It is worth to note that mucolipin 2 is not expressed in any mucolipin 3-expressing cell, including HCs and neonatal intestinal enterocytes (Montell, 2005; Zeevi et al., 2007; García-Añoveros and Wiwatpanit, 2014; Remis et al., 2014). However, mucolipin 1 is expressed in all cells (Bach, 2001; LaPlante et al., 2002; Bach et al., 2005) and, thus, is more likely to act redundantly with mucolipin 3. In fact, mice lack both mucolipins 3 and 1 (*Trpml3$^{-/-}$;Trpml1$^{-/-}$*, DKO) suffer growth defects during suckling period and recovered after weaning, consistent with mucolipin 3's restricted expression in neonatal, but not adult, intestinal

enterocytes (Remis et al., 2014). This discovery has led us to hypothesize that mucolipins 3 and 1 could contribute to unique functions of cells co-expressing both channels.

Because mucolipins are localized mainly to lysosomes (Puertollano and Kiselyov, 2009; Cheng et al., 2010; Castiglioni et al., 2011; Remis et al., 2014), we hypothesize that these cells and organs utilize specialized mucolipin-endowed lysosomes for their unique physiological functions. In addition, based on the growth defects observed in mice lacking both mucolipins 3 and 1, but not either one alone, we also hypothesize that mucolipins 3 and 1 act redundantly to maintain the specialized functions of cells and organs expressing both channels. In the study presented here, we will investigate the subcellular basis of specialized lysosomes in cells and organs expressing both mucolipins 3 and 1, specifically the neonatal enterocytes and auditory HCs.

**1.2 Mammalian neonatal intestine**

Digestion and absorption of nutrients from maternal milk during postnatal period of young mammals is fundamentally different from those of ingested food post-weaning (Grand et al., 1976; Henning, 1981; Alberts and Pickler, 2012). In mature digestive tract, consumed proteins start to break down in the stomach which is considered a strongly acidic environment (pH ~2), caused by secretion of gastric hydrochloric acid by parietal cells (Helander and Keeling, 1993; Goodman, 2010; Boland, 2016). This acidic environment activated an array of proteases, secreted by the stomach epithelial cells, which begin to break down the consumed proteins. Partially digested gastric content is further broken down extracellularly into amino acids in the intestine by excreted pancreatic proteases. The resulting free amino acids, di- and tri-peptides are taken up by the intestinal enterocytes through amino acid transporters located across the

brushboarder membrane of the intestinal enterocytes (Goodman, 2010; Boland, 2016).

However, this mode of digestion and absorption do not occur during suckling. Right after birth, the stomach of human newborns is less acidic (pH ~5.1 - 6.4) and proteins pass through to the intestine intact (Mason, 1962). This is likely because, in newborns, maternal antibodies and growth factors enter the intestine intact to be transferred *via* transcytosis across the enterocytes into the circulation (Kraehenbuhl et al., 1979; Ladinsky et al., 2012). In rodents, neonatal enterocytes endocytose milk proteins and deliver them to specialized lysosomes (termed giant lysosomes) for intracellular digestions (Henning, 1985; Wilson et al., 1991). After weaning, this specialized endolysosomal system disappears, as the adult-like lysosome-poor enterocytes replace the neonatal ones (Hirano and Kataoka, 1986; Wilson et al., 1991).

Other differences between adult vs neonatal digestion are the use of different digestive enzymes to accommodate the change in diet. The rodent intestinal epithelial cells undergo several changes during the suckling-to-weaning transition to accommodate solid food diet mainly containing carbohydrate, as opposed to maternal milk which is high in lipids (Henning, 1981). One important difference is the switch of brushboarder di-saccharidases from neonatal lactase (for digestions of milk carbohydrates) to adult sucrase isomaltase (for digestions of complex carbohydrate) (Henning, 1981, 1985; Manson and Weaver, 1997; Lindquist and Hernell, 2010).

Additionally, a recent study discovered that neonatal enterocytes had high expressions of mucolipins 3 and 1 (Remis et al., 2014). While mucolipin 1 expression subsides to a baseline level in adult enterocytes, mucolipin 3 is absent after weaning. Both mucolipins also exhibit spatial expression within the intestine, that is, the expression levels of mucolipins gradually increase from proximal, duodenum where digestions are prominent, to distal, ilium where

nutrient absorptions are prominent (Goodman, 2010; Remis et al., 2014). Interestingly, the differential expression of mucolipins in neonatal intestine is also consistent with the spatiotemporal replacement of suckling enterocytes with adult enterocytes (Henning, 1985; Hirano and Kataoka, 1986; Pácha, 2000; Muncan et al., 2011; Mould et al., 2015). Given the unique functions and the expression on mucolipin 3 in neonatal intestinal enterocytes, we hypothesize that they utilize specialized mucolipin-endowed lysosomes for intracellular digestions of maternal nutrients.

### 1.3 Understanding pediatric gastroenterological diseases

Neonatal intestinal dysfunction is a major cause of infant mortality worldwide and intestinal pathologies such as necrotizing enterocolitis (NEC), pediatric malabsorption syndromes and failure-to-thrive are common causes of severe illness in both premature and full-termed babies. Specifically, NEC affects pre-termed newborns at a rate of 3% per year in the United States (National Institute of Child Health and Human Development, NICHD), and leads to an average mortality of 10-80% (Hunter et al., 2008b; Lin et al., 2008). Interestingly, NEC do not occur in adults, and the reason why adults do not experience NEC is unknown. Pediatric malabsorption syndromes describe an array of conditions by which the intestine fails to absorb nutrients (Hosoyamada, 2006; Siddiqui and Osayande, 2011; Guandalini, 2017). These conditions, such as lactose intolerance, cystic fibrosis, celiac disease and Wolman disease, result in chronic diarrhea, abdominal distention and failure-to-thrive (Boldrini et al., 2004; Hosoyamada, 2006; Siddiqui and Osayande, 2011). In some cases, infants with pediatric malabsorption syndromes exhibited intestinal malformation and enterocolitis (Hosoyamada, 2006). Pediatric failure-to-thrive is a condition describing the infants' lack of growth or lack of

weight-gain affecting about 5 - 10% of children across the United States (Hirschberger and Kleinberg, 1976; Shields et al., 2012; Goh et al., 2016). This condition often accompanies the pediatric malabsorption syndromes. Despite their prevalence, most cases of these intestinal pathologies have unknown etiologies. Studies on the unique physiology of neonatal intestinal functions would shed light on the prevention and treatment of these diseases.

We recently found that murine neonatal enterocytes were rich in specialized lysosomes, harboring mucolipins 3 and 1 channels, and in their co-absences, the animals exhibited a failure-to-thrive phenotype, but the condition was recovered after weaning when the animals switched their diet from maternal milk to solid chow (Remis et al., 2014). These animals also exhibited diarrhea symptom during suckling period (Remis et al., 2014) suggesting that there might be defects on nutrient absorptions (Hosoyamada, 2006). These animals lacking mucolipins 3 and 1 could serve as a model for human pediatric conditions involving pediatric malabsorption syndromes and failure-to-thrive. However, it is unknown whether human neonatal intestinal enterocytes utilize the specialized endolysosomal system to digest maternal milk, or express mucolipin 3. Because the length of suckling period in human is arbitrary—the switch from milk to solid food is objective among parents—as opposed to 21 days in mice, human neonatal enterocytes might not contain the specialized lysosome-rich system for nutrient digested observed in rodents. The discovery of whether human have specialized “suckling-type” enterocytes would greatly benefit the diagnosis and treatments of neonatal intestinal dysfunctions. The presence of neonatal-specific enterocytes would implicate that the treatments of these diseases would have to be specific to the unique physiology of these neonatal cells, not present in adults, as conventional treatments for adult intestinal diseases might not be effective to resolve such diseases.

In addition, subcellular functions of lysosomes in human neonatal enterocytes are often ignored (Grand et al., 1976; Henning, 1981; Wilson et al., 1991; Veereman-Wauters, 1996). The only known disease associated with neonatal lysosomal pathologies is Wolman disease (Boldrini et al., 2004). Wolman disease is a LSD caused by a deficiency in lysosomal acid lipase (Hoffman et al., 1993; Boldrini et al., 2004). Hallmarks of Wolman disease are severe diarrhea and pediatric malabsorption that result in malnutrition, liver disease, adrenal gland calcification and aggregation of cholesterol esters and triglycerides in the intestines, liver, adrenal glands, neurons and brain macrophages (Hoffman et al., 1993; Krivit et al., 2000; Boldrini et al., 2004). However, this lysosomal disease in neonatal intestine is very rare—there has been only ~50 reported cases world-wide thus far. It is important to determine whether infants' intestine process the elaborated mucolipin-endowed endolysosomal system. If so, using a mouse model with dysfunctional endolysosomal system in the intestine could help elucidate pathologies in pediatric intestinal diseases as it is possible that they are results of the disruption of the specialized neonatal intestinal endolysosomal system.

### 1.4 A comparison between the mammalian gut epithelial cells and auditory sensory cells

While functionally different, the intestinal epithelial cells are morphologically similar to the inner ear sensory epithelial cells. The intestinal enterocytes have actin filament-based, bundle-like protrusions at their apical surface (microvilli) (Moxey and Trier, 1979; Fath and Burgess, 1995) similar to the stereocilia located at apical surface of the inner ear auditory HCs (Mburu et al., 2010). Stereocilia are organs responsible for hearing and balance, and studies have extensively identified molecules involved in stereocilia development, functions and maintenance (Rzadzinska et al., 2004, 2009; Mburu et al., 2010; McGrath et al., 2017). Interestingly, recent

studies have identified functional molecules present in intestinal microvilli that are required in stereocilia development and functions such as harmonin, taperin and clarin (McConnell et al., 2011; Crawley et al., 2016; Li et al., 2016a). Notably, the organization of microvilli and stereocilia tips are similar in that they require a scaffold protein harmonin to interacts with cadherin and protocadherin for their structure (Kraemer and Yap, 2003; Crawley et al., 2016; Li et al., 2016a). The overlapping structural molecules between intestinal microvilli and inner ear stereocilia suggest that they could be evolutionarily related. Because the digestive system evolutionarily emerged well before the auditory organ (Manley and Köppl, 1998; Steinmetz et al., 2017), it is possible that auditory HCs diverged from gut epithelial cells and later acquired their unique ability to transduce sound information into electrical signals to the brain. Whether the intestinal enterocytes and HCs share any subcellular and molecular machinery for their unique physiology remains unknown. Given that the lysosomal mucolipin 3 is expressed in both neonatal enterocytes and inner ear HCs, it is curious to examine whether these very functionally distinct cells employ specialized mucolipin-endowed lysosomes for their maintenance and functions.

### 1.5 Mammalian auditory system

The mammalian auditory system includes three distinct parts: the outer, the middle and the inner ears. Hearing starts at the outer ear that funnels sound vibrations to the eardrum. These sound vibrations are then amplified by the middle-ear ossicles. It is in the inner-ear cochlea, specifically the organ of Corti, where sound is transduced into electrical signals to the brain. The mammalian cochlea contains two types of sensory receptor cells, outer (OHCs) and inner hair cells (IHCs), that play distinct roles in hearing. Sound-induced vibration in the organ of Corti

mechanically stimulate OHCs. OHCs in turn mechanically amplify these vibrations, enhancing sensitivity to sounds and sharpening tuning (Cheatham et al., 2004; Dallos et al., 2006; Ashmore, 2008). This mechanical tuning of sounds, unique to OHCs, is achieved through the motor protein prestin along their basolateral membrane (Zheng et al., 2000; Cheatham et al., 2004; Dallos et al., 2008). The resulting amplified vibrations from OHCs then stimulate IHCs which release glutamate to activate afferent neurons, thus relaying sound information to the brain in the form of electrical signals (Seal et al., 2008; Flores et al., 2015).

In the cochlea, HCs are equipped with stereocilia, hair-like, actin-based protrusions at the apical surface of the cells, hence the term "hair cells" (McGrath et al., 2017). Sound-induced vibrations it the cochlea deflect stereocilia, affecting the tensions at the tip-link complex and subsequently opening and closing the non-specific mechanoelectrical transduction channels (Hudspeth, 1982; Fettiplace, 2017). For HCs to transduce sounds properly, the stria vascularis secretes $K^+$-rich fluid, termed endolymph, prompting $K^+$ as the main ions for sound transduction (Fettiplace, 2017). The stria vascularis is an epithelial segment of the spiral ligament with two main cellular layers: 1) marginal-cell layer facing the endolymph and 2) intermediate/basal-cells layer (Wangemann, 2006). The marginal cells express a high level of a voltage-gated potassium channel KCNQ1, which, coupled with another voltage-gated potassium channel KCNE1, maintains $K^+$ homeostasis in the endolymph (Yang et al., 1997; Wangemann, 2006; Fettiplace, 2017). In the absence of KCNQ1, mice have reduced volume of endolymph, and experience complete deafness (Lee et al., 2000; Casimiro et al., 2001). Interestingly, mis-localization of KCNQ1 by the absence of a lysosomal integral membrane protein-2 (LIMP2) can cause strial degeneration and HC death, resulting in progressive hearing loss (Gamp et al., 2003; Knipper et al., 2006). Although the stria vascularis does not compose of sensory cells, it is essential for HCs

to transduce sound information to the brain.

Another important component of the mammalian auditory system is the complex network of cochlear neurons. The cochlea contains 2 types of primary neurons, type I and II afferent neurons, connecting the cochlea to the brain (Flores et al., 2015; Fettiplace, 2017). IHCs, the true sensory cells, transform sound vibrations into electrical signals though the release of glutamate that activates type-I afferents (Seal et al., 2008). The remaining type II afferents innervate OHCs; however their function remains poorly understood (Dannhof and Bruns, 1993). Disruptions of synapses especially between type-I afferents and IHCs, for example: by loud noises, can disable the neurons and result in the degeneration of the neurons themselves (Kujawa and Liberman, 2009; Shi et al., 2016; Liberman, 2017). Taken together, sensory HCs, the stria vascularis and neurons are key components to relay sound information to the brain and defects in any one these components can lead to hearing impairment.

**1.6 Mouse models of age-related hearing loss**

Hearing loss is the most common sensory deficit. World health Organization estimates that 5% of global population have disabling hearing loss—328 million adults and 32 million children worldwide (WHO). The most common form of hearing loss is age-related hearing loss (ARHL) as it is one of the hallmarks of aging (Ohlemiller, 2006). Approximately, 18% of American adults aged 45-64 years old, 30% of adults aged 65-74 years old, and 50% of adults 75 years or older suffer hearing loss (NIDCD). ARHL is defined as a progressive loss of hearing from high to low frequencies that advances with age (Ohlemiller, 2006). Although contributions to ARHL can be accumulated, i.e. increasing vulnerability to damages from continuing exposure to noise, chemical and other insults (Gates and Mills, 2005; Delmaghani et al., 2015; Wong and

Ryan, 2015), in the absence of external stimuli and insults (as when animals are raised in complete silence), ARHL is still present (Sergeyenko et al., 2013; Yan et al., 2013). There is no known single cause of ARHL in human, but it is likely due to the changes in the inner ear as we grow older.

Causes of hearing loss can be: 1) sensory, at the HCs, 2) strial at, the stria vascularis and 3) neuronal, at the innervations. However, the most common cause of hearing loss, and ARHL, is the degeneration of HCs. Even though HCs have a remarkable feature that they are very resilient; they can withstand constant high-energy demands and mechanical stimulations; they survive for decades or a century in humans (Ohlemiller, 2006; Wong and Ryan, 2015; Liberman, 2017), they do degenerate leading hearing loss. In mammals, hearing loss due to HC loss is permanent because HCs do not regenerate after an early developmental period. While HC degeneration is the most common cause of ARHL, the molecular mechanism of ARHL is unclear. The inbred mouse strain C57BL/6 exhibited ARHL accompanied by HC loss (Spongr et al., 1997; Zheng et al., 1999; Ison et al., 2007). C57BL/6 animals carry the ARHL susceptibility allele *Ahl*, which encodes cadherin 23, expressed at the tiplink complex of stereocilia (Zheng et al., 1999; Noben-Trauth et al., 2003; Ison et al., 2007). Studies have suggested that mutations on cadherin 23 lead to endoplasmic reticulum stress, resulting in an accumulation of unfolded and misfolded proteins that trigger apoptosis of OHCs (Han et al., 2012; Hu et al., 2016). Defects in tight junctions between HCs and supporting cells, due to mutations in the *Usp53* gene of *mambo* mice, can also lead to OHCs loss, causing hearing defects at as early as 18 days of age (Kazmierczak et al., 2015). In addition, studies have suggested that calcium ion imbalance (Fridberger et al., 1998; Tong et al., 2016; Yu et al., 2016) or increase in radical-oxygen species (Menardo et al., 2012; Delmaghani et al., 2015) in OHCs can lead to OHCs death and ARHL.

Although not as prevalent as hearing loss due to HC degeneration, stria vascularis' dysfunction can also lead to ARHL. A recent large-scale ENU-mutagenesis genetic screening reported several alleles associated with ARHL phenotype, including a gene coding for a sodium bicarbonate transporter member 10, *Slc4a10* (Potter et al., 2016). *Slc4a10* is expressed in the spiral ligament fibrocytes, cochlear cells that, along with the strial intermediate cells, generate the highly positive potential in the endolymph (Wangemann, 2006; Marcus and Wangemann, 2010). Specifically, T-to-C mutation at nucleotide 1940 of *Slc4a10*, causes strial degeneration starting as early as at 2 months of age, accompanied by the reduction in endocohlear potentials and increased hearing thresholds (Potter et al., 2016). Although the mechanism is unknown, strial degeneration in *Slc4a10* mutant mice eventually leads to OHC degeneration at around 9 months of age at which their hearing becomes severely impaired (Potter et al., 2016). In addition, the loss of lysosomal protein LIMP2 causes strial degeneration that precedes HC loss (Gamp et al., 2003). LIMP2-deficient mice exhibit a progressive hearing loss from high to low frequencies that worsens with age, characteristics of ARHLs (Knipper et al., 2006).

Finally, the common form of neural ARHL is perhaps the loss of spiral ganglion neurons, and, hence, the synaptic loss between HCs and cochlear nerves (Schuknecht and Gacek, 1993; Kujawa and Liberman, 2006; Melgar-Rojas et al., 2015). While most studies examine this condition in the context of noise-induced hearing loss (Ohlemiller, 2006; Kujawa and Liberman, 2009; Hill et al., 2016; Kurabi et al., 2016; Shi et al., 2016), in a control condition (without noise-induced damage), cochlear synaptic loss occurs in young CBA/CaJ mice (~4 weeks of age) before the onset of age-related HC loss (~80 weeks of age) (Sergeyenko et al., 2013). Whether this neural hearing loss is specific to the CBA strain, or to mice, remains to be determined.

In conclusions, under strict experimental and cellular criteria, progressive ARHL in mice

mirrors the patterns observed in human. Most observations of aged human and animal cochlea reveal similar pathologies of the organ of Corti, stria vascularis and spiral ganglion neurons (Covell, 1953; Willott and Erway, 1998; Makary et al., 2011; Sergeyenko et al., 2013). While we cannot argue which component of the inner ear is the most important in ARHL, we can agree that sensory, strial and neural hearing loss are closely related. Given that the mouse strains and mutant models for AHRL have accelerated degeneration the organ of Corti, stria vascularis and auditory nerves, they serve powerful tools to identify the underlying genetic contributions to hearing loss in human.

**1.7 Overview**

The work presented in this dissertation elucidates the subcellular basis of lysosomal channel mucolipins 3 and 1 in two structurally similar but functionally distinct cells—i.e. neonatal intestinal enterocytes and auditory HCs—and how these channels contribute to functions and maintenance of these cells. In Chapter 2, we will discuss the role of mucolipins in the specialized endolysosomal system in neonatal intestinal enterocytes. We found that in the absences of mucolipins 3 and 1, the enterocytes became severely vacuolated. These pathological vacuoles eventually led to reduction in endocytosis of maternal milk, resulting in a failure-to-thrive condition as the animals could no longer absorb nutrients from the milk. Because these enlarged pathological vacuoles were endolysosomal in nature, we deduced that mucolipins facilitated the scission of the endolysosomal hybrid-organelles to replenish endosomes and lysosomes to the cells. In Chapter 3, we will discuss the role of mucolipins in protecting against early-onset ARHL. Using different mouse models lacking mucolipins, we found that these

channels acted mainly in HCs to maintain hearing. In the absence of both mucolipins 3 and 1, animals displayed early-onset AHRL due to OHC death. While we did not find that HCs required specialized lysosomal functions for their survival and functions, we found that mucolipins contributed to lysosomal membrane integrity. Mucolipin co-deficiency resulted in enlarged lysosomes with permeabilized membrane, leading to the release of toxic hydrolase cathepsin D into the cytoplasm that triggers OHC death. This finding represents a novel mechanism for OHC death that leads early-onset ARHL.

# CHAPTER 2:

# Mucolipins and Neonatal Enterocytes

## 2.1 Abstract

During the suckling period, neonatal intestinal enterocytes are richly equipped with endosomes and lysosomes, presumably for the uptake and intracellular digestion of maternal milk proteins. By weaning, mature intestinal enterocytes replace those rich in lysosomes. Here, we found that mouse enterocytes before weaning express high levels of two endolysosomal cation channels, mucolipins 3 and 1—products of *Trpml3* and *Trpml1* genes. Neonatal enterocytes of mice lacking both mucolipins were severely vacuolated within hours after birth. Ultrastructurally and chemically, these fast-forming vacuoles resembled those that systemically appear in epithelial cells of mucolipidosis type IV (MLIV) patients, which bear mutations in *Trpml1*. Hence, lack of both mucolipins 3 and 1 causes an accelerated MLIV-type of vacuolation in enterocytes. The vacuoles were aberrant endolysosomal hybrid-organelles, and were not generated by alterations in endocytosis or exocytosis, but likely by an imbalance between fusion of lysosomes and endosomes and their subsequent scission. These vacuolated enterocytes displayed reduced endocytosis from the intestinal lumen, a defect expected to compromise nutrient uptake. The reduction of nutrient uptake is consistent with the previously reported findings that mice lacking both mucolipins suffered a growth delay that began after birth and continued through the suckling period but recovered after weaning (Remis et al., 2014). Our results revealed genetic redundancy between lysosomal mucolipins 3 and 1 in neonatal enterocytes. Furthermore, we for the first time demonstrated the presence of specialized mucolipins-rich endolysosomal system in human neonatal enterocytes. More importantly, we found evidence that the pathological vacuolation in our *Trpml3*$^{-/-}$;*Trpml1*$^{-/-}$ (DKO) mice may represent a polygenic animal model of the poorly-understood pediatric intestinal diseases, of

unknown etiologies, such as necrotizing enterocolitis (NEC), which is often studied using pathogen-induced rodent models. Here, our results implicate lysosomes in neonatal intestinal pathologies, a major cause of infant mortality worldwide, and suggest that transient intestinal dysfunction might affect newborns with lysosomal storage disorders.

## 2.2 Introduction

In mammals, including humans, Intestinal digestion is very different before and after weaning periods (Grand et al., 1976; Henning, 1981; Alberts and Pickler, 2012). In adults, extracellular enzymes in the lumen of digestive tract digest proteins and the enterocytes lining the intestine absorb the resulting amino acids. During suckling, maternal nutrients, especially milk proteins, pass though the stomach intact as the neonatal stomach is not yet acidic, and lacks pepsin. Proteins are taken (endocytosed) whole by enterocytes for intracellular digestions through a lysosomal pathway (Gonnella and Neutra, 1984; Henning, 1985; Hamosh, 1996; Baqui et al., 1998c). For this unique form of feeding, perinatal enterocytes generate *de novo* a specialized system of endosomes and lysosomes, containing "giant lysosomes", designated for milk digestion, that lasts until weaning, when they are replaced by adult enterocytes (Henning, 1985; Wilson et al., 1991).

Mucolipins are cation channels present in the membranes of lysosomes and late endosomes, and are preferential to calcium ions (LaPlante et al., 2004; Zhang et al., 2009; Cheng et al., 2010; Castiglioni et al., 2011; García-Añoveros and Wiwatpanit, 2014; Remis et al., 2014; Cao et al., 2017). Mammals have three mucolipin paralogs, encoded by the genes *Trpml1*, *2* and *3* (García-Añoveros and Wiwatpanit, 2014). Mutations in human *Trpml1* cause mucolipidosis type IV (MLIV), a lysosomal storage disorder (LSD) characterized by severe psychomotor retardation and ophthalmological abnormalities that typically appear months after birth but within the first year of life (Bargal et al., 2000; Bach, 2001). Mice lacking mucolipin 1 (*Trpml1*$^{-/-}$, ML1KO) develop similar symptoms also about six months after birth (that is, with a similar onset in absolute time but at a much later developmental stage with respect to humans) and die within 8-10 months (Venugopal et al., 2007; Micsenyi et al., 2009). Cells of MLIV patients and

ML1KO mice display enlarged lysosomal vacuoles that are largely empty or accumulate various undigested substances, depending on cell type, but that typically contain membranous bodies with concentric lipid membranes (Zeigler et al., 1992; Winchester et al., 2000; Slaugenhaupt, 2002; Vergarajauregui et al., 2008; Wakabayashi et al., 2011). The slow onset of these subcellular abnormalities pose an obstacle to elucidating how the pathological vacuolation occurs in the absence of mucolipin 1, and have also led to the suspicion that other channels, perhaps mucolipins 2 or 3, may partially compensate for the loss of mucolipin 1.

Unlike the ubiquitously expressed mucolipin 1, mucolipin 3 is expressed in a small subset of cell types which include auditory hair cells and melanocytes of the skin (Xu et al., 2007; Nagata et al., 2008; Castiglioni et al., 2011). Gain-of-function dominant mutations on *Trpml3* (*Va* and $Va^J$) result in hyperactive ion channels that are lethal due to calcium overload in cells heterologously expressing them, causing deafness due to loss of hair cells and hypopigmentation presumably due to loss of melanocytes (Cable and Steel, 1998; Di Palma et al., 2002; Steel, 2002; Atiba-Davies and Noben-Trauth, 2007; Grimm et al., 2007; Xu et al., 2007; Nagata et al., 2008). However, these gain-of-function mutations do not clarify the role mucolipin 3 may play in the small subset of cells expressing it.

The relevance of mucolipins extends beyond the *Va* or $Va^J$ mice and MLIV to many other diseases caused by mutations in other genes (such as sphingomyelinases for Nieman-Pick); the pathologically-accumulated lipids inhibit mucolipin 1 channels, which disrupts lysosomal trafficking and thus aggravates the cellular pathology of these diseases (Shen et al., 2012; Weiss, 2012). In addition, and more importantly, many pediatric intestinal dysfunctions, such as necrotizing enterocolitis (NEC), failure-to-thrive or pediatric malabsorption syndromes, only occur in infants and have unknown etiologies (Hosoyamada, 2006; Hunter et al., 2008a; Siddiqui

and Osayande, 2011; Guandalini, 2017). The fact that only neonatal enterocytes have an elaborated specialized endolysosomal system, distinct from adults, prompts us to explore whether defects in this specialized system in neonatal enterocytes could be the underlying cause of many pediatric intestinal diseases. Hence, it is pressing to elucidate the role of mucolipins in lysosomes and the nature of the lysosomal abnormalities caused by their dysfunction in neonatal intestinal enterocytes.

Here, we found that the lysosome-containing enterocytes of the suckling mice expressed mucolipin 3 and upregulated mucolipin 1, and that mice lacking both mucolipins (but not only one of the two) suffered delayed growth together with pathological vacuolation of enterocytes throughout the period of suckling, until weaning. The vacuolated enterocytes assembled within hours of birth, and contained a pathological organelle of with both endosomal and lysosomal components that was similar to the pathological vacuoles formed in epithelial cells of MLIV patients. Following enterocyte vacuolation was a reduction of endocytosis from the intestinal lumen, a presumed cause for a deficiency in nutrient uptake that would account for the delayed growth. In addition, we found for the first time that human infant enterocytes contained the specialized mucolipin-endowed endolysosomal system. We also found that intestinal samples from rodent models for NEC and NEC patients revealed a strikingly similar pathology of vacuolated enterocytes as observed in our mouse model lacking mucolipins 3 and 1.

## 2.3 Results

### 2.3.1 Mucolipin 3 expression in the intestine

#### Enterocytes of neonatal but not adult small intestines express *Trpml3*

While all major organs express *Trpml1* (Bach, 2001; Cheng et al., 2010), only a few cell types express the paralog *Trpml3*, including inner ear hair and marginal strial cells, olfactory and vomeronasal sensory neurons, melanocytes, presumed alveolar macrophage and presumed principal cells of collecting ducts of the kidneys (Xu et al., 2007; Nagata et al., 2008; Castiglioni et al., 2011; Remis et al., 2014). In order to determine the expression profile of *Trpml3* in the intestine, we performed RNA in situ hybridization (ISH) on sagittal sections of newborn pups (P1 and P2) and on sections of adult mouse organs. While expression of *Trpml3* did not differ between neonates and adults for the cell types and organs previously reported (Remis et al., 2014), a notable exception was the epithelia of the intestinal villi, which expressed the highest levels of *Trpml3* mRNA in neonates but no detectable levels in adults (Figure 1A-D). We confirmed that the neonatal ISH signal was specifically detecting *Trpml3* mRNA because it was obtained with two non-overlapping antisense probes (one complimentary to exons 1 to 5 and the other to exons 8 to 12; Figure 1A, B) but not with control sense probes or with antisense probes in *Trpml3*$^{-/-}$ (ML3KO) tissue (Remis et al., 2014) (Figure 1C). However, the same antisense probes could not detect *Trpml3* mRNA in sections of adult intestine (Figure 1D). We also performed immunohistochemistry on intestines using antibodies raised against the N-terminus of mouse mucolipin 3 (TRPML3-NT) (Nagata et al., 2008). We noticed that neonatal intestinal samples contained high level of autofluorescence spanning most of detectable optical spectrums; we therefore performed a non-fluorescence immunohistochemistry using DAB amplification to detect mucolipin 3. We found that TRPML3-NT antibody labeled the apical region of villus

epithelial cells from neonatal (P8 and P7) *Trpml3*$^{+/+}$ (wild-type), but not ML3KO, mice (Figure 1E, F, K, M). Within intestinal villi of neonates, the cells expressing mucolipin 3 were the enterocytes, and not the secretory goblet cells or any cell within the lacteals (the internal portion of the villi, which is part of the lymphatic circulation; Figure 1E, F, K, M). However, we could not detect TRPML3-NT immunoreactivity in sections of adult (P48) *Trpml3*$^{+/+}$ (wild-type) small intestine above the weak non-specific immunoreactivity levels of ML3KO littermates (Figure 1G, H). We therefore concluded that neonatal, but not adult, enterocytes expressed *Trpml3* mRNA and mucolipin 3 protein.

Enterocytes live only for a few days, and those produced in neonates differ in many respects from those produced in adults (Grand et al., 1976; Henning, 1981; Alberts and Pickler, 2012). Neonatal enterocytes are specialized in the digestion of nutrients from suckled milk, and, as weaning approaches (~P21 in the mouse), are replaced by "mature-feeding" enterocytes equipped for the digestion and absorption of nutrients from ingested chow weaning (Grand et al., 1976; Henning, 1981; Alberts and Pickler, 2012). Quantitative RT-PCR analysis of *Trpml3* mRNA levels in small intestine from prenatal (E18.5) to adult indicates that *Trpml3* mRNA levels peak during the first postnatal week (P7), subside as weaning approaches and reach undetectable levels in adults (Figure 1I). By P14, *Trpml3* mRNA is more abundant in the distal (ileum) than proximal (duodenum) intestine (Figure 1J), consistent with the spatiotemporal replacement of suckling enterocytes with mature enterocytes weaning (Grand et al., 1976; Henning, 1981; Alberts and Pickler, 2012). Hence, intestinal enterocytes express *Trpml3* during the postnatal period of suckling, but not afterwards.

Neither ISH nor immunohistochemistry detected expression of *Trpml3* in the space between the villi, also called intervillus pockets and crypts, where the intestinal stem cells that

produce the enterocytes reside (de Santa Barbara et al., 2003) (Figure 1A, B, E). Hence, it appears that mucolipin 3 acts in the postmitotic, differentiated enterocytes of suckling mice.

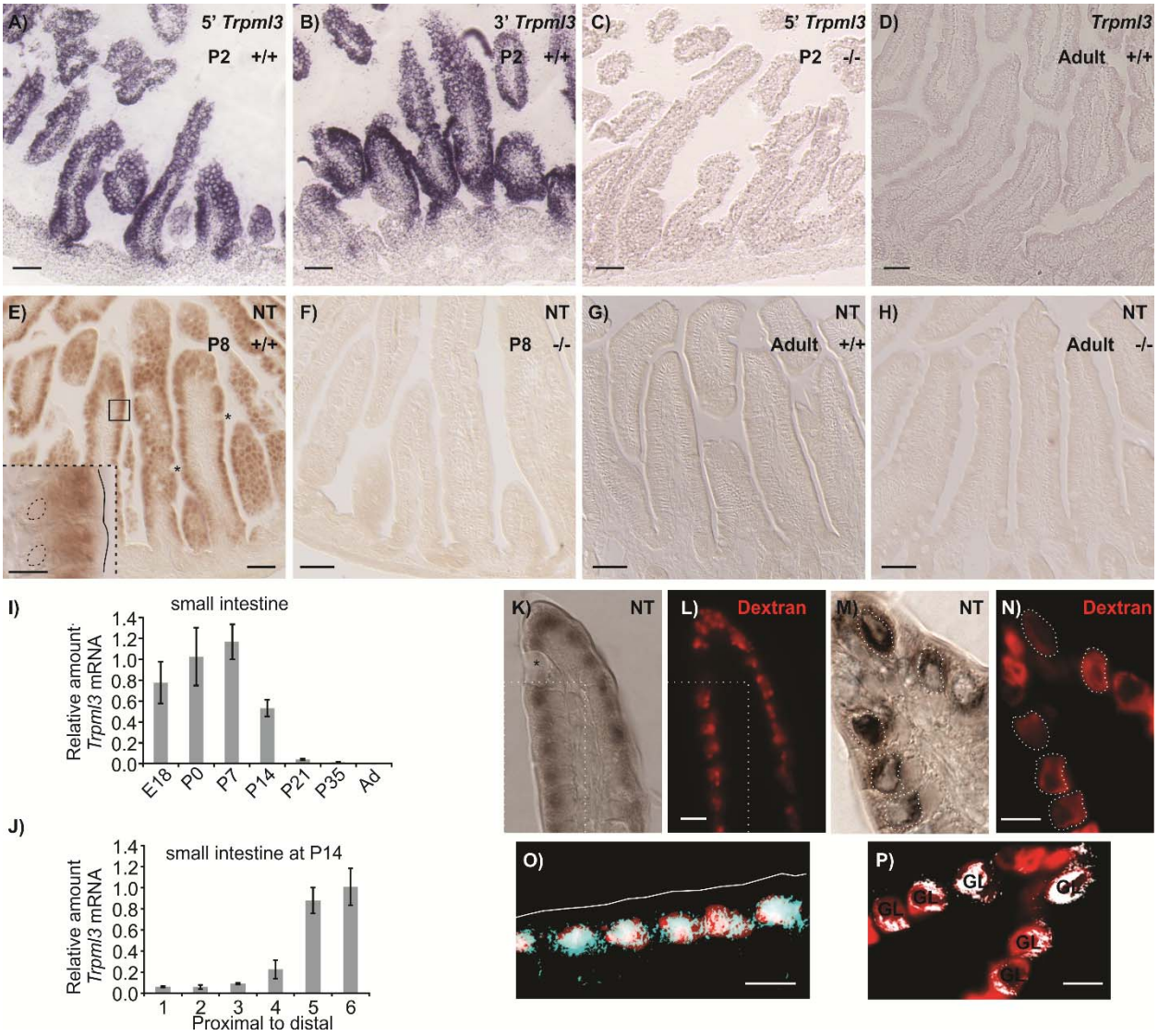


**Figure 1. Mucolipin 3 is expressed in the specialized endolysosomal organelles of neonatal, but not adult, intestinal enterocytes.** (**A-D**) *In situ* hybridization with two non-overlapping probes to *Trpml3* (complementary to 5' and 3' portions of its mRNA) reveals strong mRNA levels in (**A,B**) neonatal, but not (**D**) adult intestines. (**C**) Lack of hybridization on neonatal intestines of *Trpml3*$^{-/-}$ mice shows that the probe used specifically detects *Trpml3* mRNA. (**E-H**). Immunohistochemistry with an antibody to the N-terminus of TRPML3 (NT) on (**E,F**) neonatal and (**G,H**) adult intestines reveals that (**E**) neonatal but not (**G**) adult enterocytes express

TRPML3 protein. Goblet cells (marked with asterisks) do not express TRPML3. (**F,H**) Lack of immunoreactivity in intestines from *Trpml3*$^{-/-}$ mice confirms that the immunoreactivity in wild type intestines specifically represents TRPML3 proteins. (**I-J**) RT-qPCR reveals that (**I**) the high levels of *Trpml3* mRNA in neonatal intestines subside by weaning, and that (**J**) by P14 distal intestine (i.e., ileum) of the suckling mouse, characterized by giant lysosomes, expresses higher levels of *Trpml3*. Each bar is the average of n=3 experiments. Error bars represent SD's. (**K,M**) Immunohistochemistry on P7 intestines in which prior exposure to Texas Red-dextran has labeled lysosomes (**L,N**). Enterocytes, but not goblet cells (labeled with an asterisk on **K**), are lysosome-rich and express TRPML3 protein. (**O, P**) Merging of both images (in **O**, only the region delimited with dotted lines in **K** and **L**). (**K, L, O**) In duodenal enterocytes, which contain multiple closely spaced lysosomes, the resolution of the anti-TRPML3 immunoreactivity does not discern individual lysosomes. However, the TRPML3-immunorreactivity occupies the same area of cytoplasm than the dextran-filled lysosomes, and not the portion of cytoplasm rich in endosomes closed to the apical membrane (outlined in white on **O**). (**M, N, P**) Illeal enterocytes contain a single giant lysosome (labeled GL on **P**), which is filled with dextran and immunoreacts with antibodies to TRPML3. Dotted lines in (**M**) outline the giant lysosome boundaries as defined by Texas Red-dextran in (**N**). Hence, lysosomes of enterocytes seem to contain TRPML3 protein. Scale bars are 50 μm except in the inset in E and in K-O, where they are 10 μm. Overall these data supports that TRPML3 protein localizes to lysosomes, although localization at nearby late endosomes is also possible. (**A-J**) were performed by Remis et al., 2014.

**Mucolipin 3 localizes to the specialized endolysosomal organelles of suckling enterocytes**

A defining characteristic of suckling enterocytes is that they do not uptake free amino acids from the intestinal lumen but instead endocytose intact proteins (and perhaps some fats) from the milk and deliver them to lysosomes for digestion (Henning, 1981; Hamosh, 1996; Oshikawa et al., 1996; Manson and Weaver, 1997). The endocytosed proteins are delivered to specialized lysosomes which, in the more distal parts of the small intestine (ileum), form one giant lysosomal vacuole per enterocyte. We labeled lysosomes of neonatal mice by feeding them formula with Texas Red-conjugated dextran at P6 and examining its intracellular accumulation one day later (at P7; Figure 1L, N). Texas Red-conjugated dextran not only indicated the presence of lysosomes (as it is delivered, and retains in lysosomes) but also non-receptor mediated endocytosis in the enterocytes. Immunohistochemistry with TRPML3-NT antibody in sections of duodenum revealed immunoreactivity to the region of cytoplasm rich in lysosomes, and not in the more apical portion of cytoplasm that is richer in early endosomes (Figure 1K, L, O). In sections of ileum, where enterocytes display not a multitude of lysosomes but a single giant one, mucolipin 3 immunoreactivity also overlaps with the Dextran-filled giant lysosomal vacuoles indicating a high level of endocytosis among these cells (Figure 1M, N, P).

In an attempt to better visualize the subcellular localization of mucolipin 3 in neonatal enterocytes and bypass autofluorescence issues from intestinal crysections, we resorted to examining *in vitro* cultured enterocytes. These cultures are typically established from adult intestines (Sato et al., 2009; Koo et al., 2011; Stelzner et al., 2012). However, in collaboration with Dr. Jerrold Turner, Harvard Medical School (formerly at University of Chicago), we were able to establish enterospheres and enteroids from suckling (P3 to 4) intestines for the first time (Figure 2). We also found that enteroids were significantly less autofluorescence, thus allowing

us to use immunofluorescence to detect the presence of mucolipin 3, using TRPML3-NT antibody, in enterocytes. Here, we found that, while enterocytes from adult-derived enteroids lacked mucolipin 3, those from suckling-derived enteroids expressed it at high levels (Figure 2A, B).

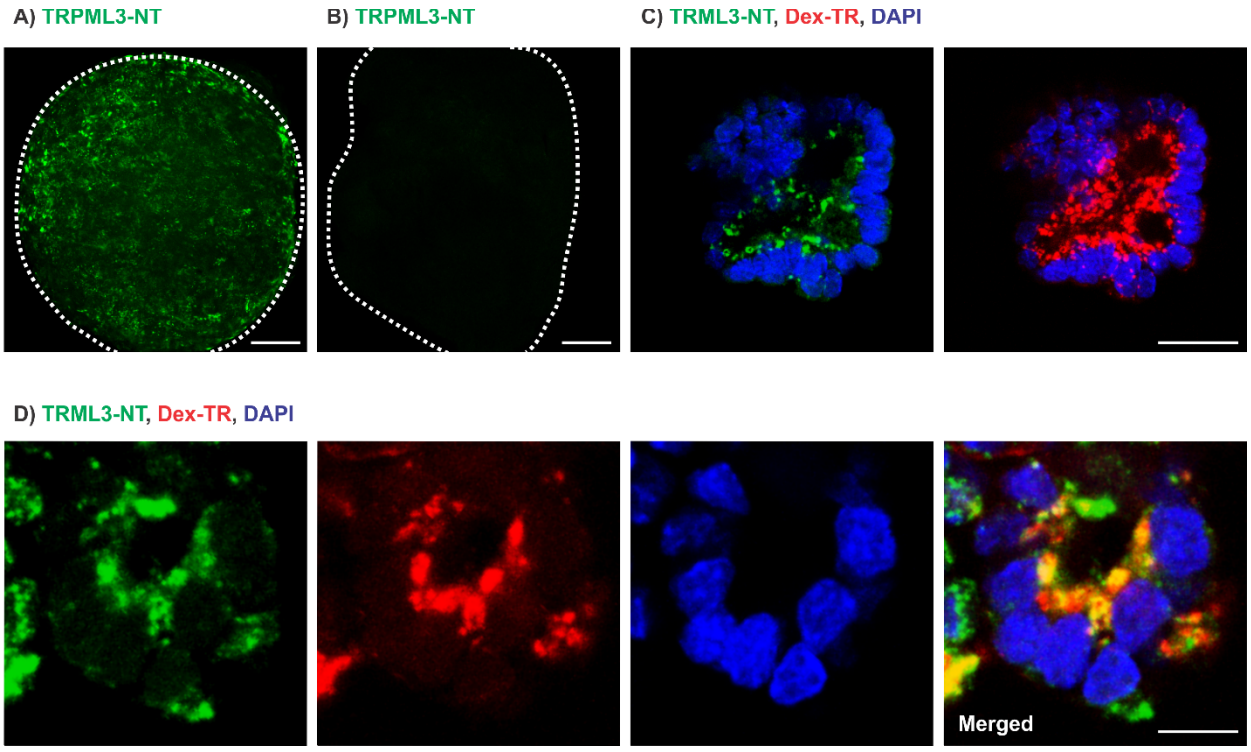


**Figure 2. Enteroids derived from neonatal, but not adult, intestine express lysosomal mucolipin 3**. (**A, B**) Immunohistochemistry on whole-mount enterospheres reveal that enterocytes derived from P3 (**A**) but not adult (**B**) intestine express mucolipin 3 (as indicated by TRPML3-NT immunoreactivity). (**C, D**) Frozen sections from enteroids derived from P3 intestine treated with Dextran-Texas Red (Dex-TR) reveal that cultured enterocytes exhibit high level of apical endocytosis and contain mucolipin 3-endowed lysosomes. Scale bars are 50 µm in (**A, B**) and 10 µm in (**C, D**).

Similar to the *in vivo* experiment (Figure 1K-P), we labelled lysosomes in the enterocytes by exposing enteroids to Texas Red-conjugated dextran before fixation and immunohistochemistry (Figure 2C, D). Interestingly, these suckling-derived enteroids displayed prominent apical endocytosis and lysosomes (Figure 2C, D). These dextran-filled lysosomes also contained high level of mucolipin 3, a similar pattern observed in non-fluorescence staining of mucolipin 3 on cryosections (Figure 1K-P). However, the high density of lysosomes in these enterocytes and the poor subcellular localization afforded by non-fluorescent immunohistochemical amplification (DAB, Figure 1K-P) or fluorescent tyramide amplification (Figure 2) prevented us from unambiguously localizing mucolipin 3 to lysosomes as the signals could be localize to much smaller endocytic complexes surrounding and/or fusing to the giant lysosome.

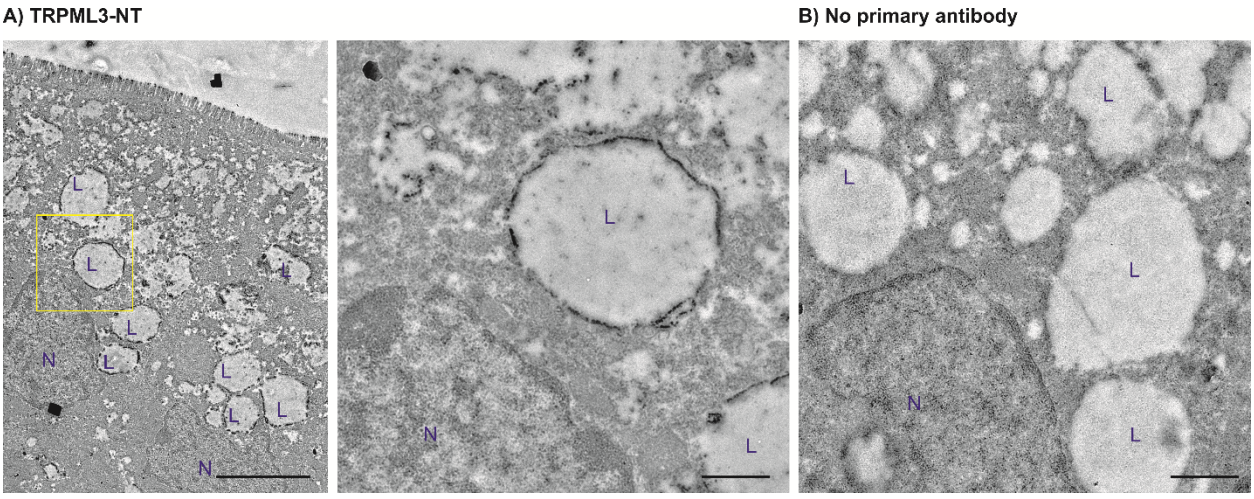


**Figure 3. Mucolipin 3 localizes to specialized lysosomes of neonatal enterocytes.** Tissues were collected from wild-type P2 pups, and mucolipin 3 was labelled with TRPML3-NT antibody with Ultra Small (0.8nm) gold particle-conjugated secondary antibody. (**A**) Ultrastructural examination iliem revealed TRPML3 immunoreactivity on the membrane of large vesicles, presumably lysosomes (L). A representative lysosome (yellow inset), with mucolipin 3 labeleld with gold particles, is shown at a high magnification (right panel). (**B**) An ultra-thin section of the same sample as in (**A**) was used without primary antibody as a negative control. Nucleus (N). Scale bars are 5 µm (**A**, left panel) and 1 µm (**A**, right panel; **B**).

In order to determine the subcellular localization of mucolipin 3 in neonatal enterocytes, we performed ultrastructural examination of the enterocytes labelled with TRPML3-NT and gold-conjugated secondary antibody (Figure 3). Because the much smaller endocytic vesicles may localize in close proximity to the giant lysosome or lysosomes, it cannot be ruled out that mucolipin 3 is present in small early- or late endosomes fusing to the lysosomes. Nevertheless, we found that TRPML3-NT antibody labelled membranes of the larger vesicles, presumably

lysosomes, of neonatal (P2) enterocytes (Figure 3A). In fact, we did not observe small endocytic vesicles clustering around the lysosomes at this neonatal stage (Figure 3). We stained an ultra-thin section of the same intestinal sampler without the primary antibody TRPML3-NT as a negative control, and found no TRPML3-NT immunoreactivity, confirming that our antibody was specific to TRPML3 protein (Figure 3B). Together with other detection methods (Figure 1-2), we concluded that mucolipin 3 channels localized to the specialized lysosomes of suckling enterocytes. This subcellular localization resembles that of other epithelial cells (LLC-PK1-CL4 and hair cells of the inner ear) in which mucolipin 3 localizes to intracellular vesicles, most of which co-express lysosomal markers (Nagata et al., 2008; Castiglioni et al., 2011).

### 2.3.2 Pathological vacuolation in neonatal enterocytes

**Pathological vacuolation of neonatal, but not adult, enterocytes of mice lacking both mucolipins 3 and 1, but not of mice lacking a single mucolipin**

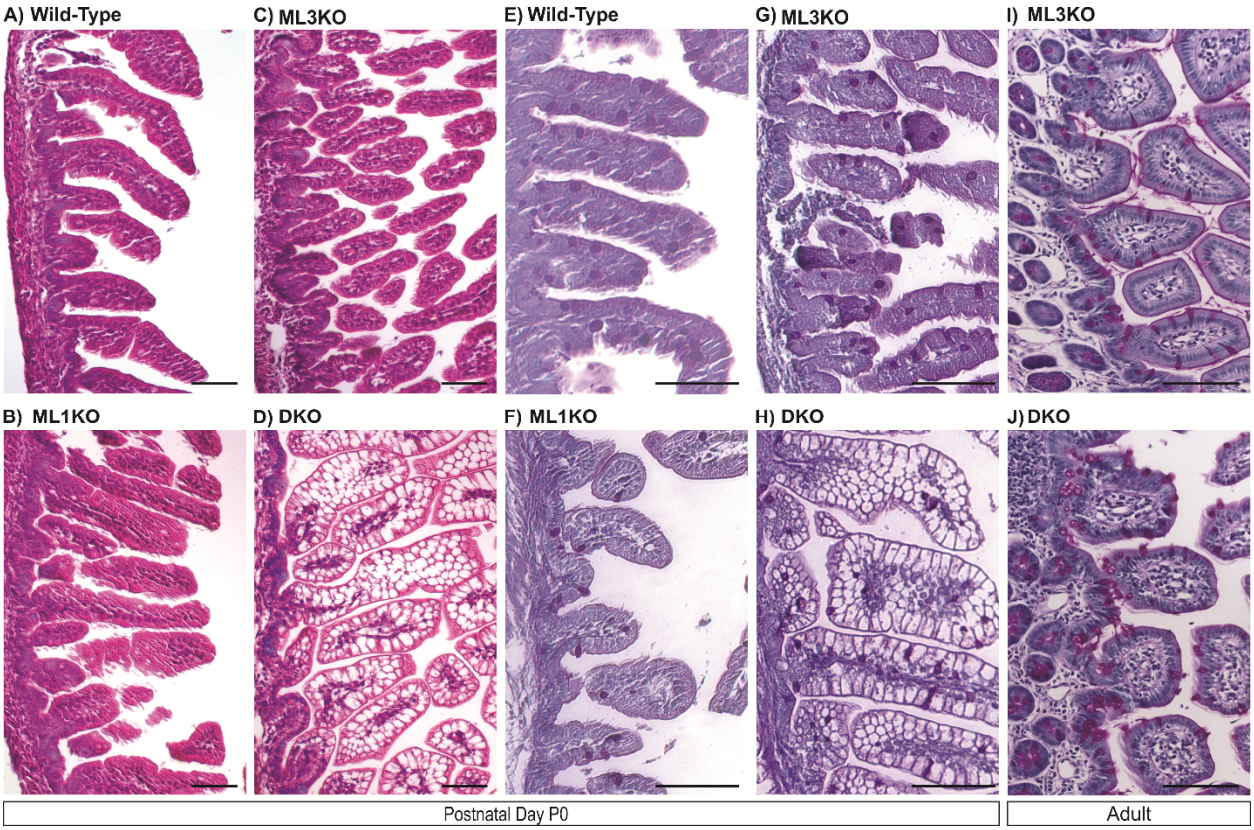


**Figure 4. Neonatal enterocytes, but not adult, lacking mucolipins 3 and 1, but not either alone, are vacuolated**. (**A-D**) Hematoxylin and eosin (H&E) staining of paraffin-embedded sections of P0 intestine reveals abnormal vacuolation in (**D**) DKO pups, but not in (**A**) wild-type, (**B**) ML1KO or (**C**) ML3KO pups. (**E, H**) Periodic acid-Schiff (PAS) staining of paraffin-embedded sections of neonatal intestines reveals that (**H**) the vacuolated intestinal cells of DKO mice are not mucin-filled, goblet cells (labeled red), which show a distribution undistinguishable from (**E**) wild-type, (**F**) ML1KO or (**G**) ML3KO pups. (**I, J**) ML3KO and (**J**) DKO mice. Scale bars are 100 μm.

Remis et al. (2014) found that mice lacking both mucolipins 3 and 1 (DKO), but not either one alone (ML1KO or ML3KO) suffered the growth defect failure-to-thrive during suckling period. This prompted us to examine the molecular basis of this pathology among neonatal mice lacking mucolipins. First, we histologically examined hematoxylin and eosin (H&E) stained paraffin sections of neonatal (P0) and adult intestines from wild-type, ML1KO, ML3KO and DKO mice. While the intestines from ML1KO or ML3KO mice were undistinguishable from those of wild-type littermates, the neonatal intestines of DKO mice were severely dysmorphic, comprised of cells with a vacuolated appearance (Figure 4A-H). In wild-type intestines, an empty, vacuolated H&E appearance is characteristic of the mucus-secreting goblet cells which contribute to only a small subset of the intestinal epithelium. However, Periodic Acid-Schiff-staining, which labels the mucin-filled goblet cells, does not label the pathologically-vacuolated cells of neonatal DKO intestines and instead reveals a normal distribution of scattered goblet cells amidst the pathologically vacuolated enterocytes (Figure 4E-H). Interestingly, in adult, there was no vacuolation of DKO enterocytes, and the intestines appeared indistinguishable between DKO and their control littermates (Figure 4I, J). The normal appearance of neonatal enterocytes from ML1KO and ML3KO mice demonstrates that these two genes may substitute or compensate for one another and that, at least in the neonatal intestine, they can act redundantly (either by performing the exact same molecular function or by performing distinct roles that lead to the same or an equivalent outcome).

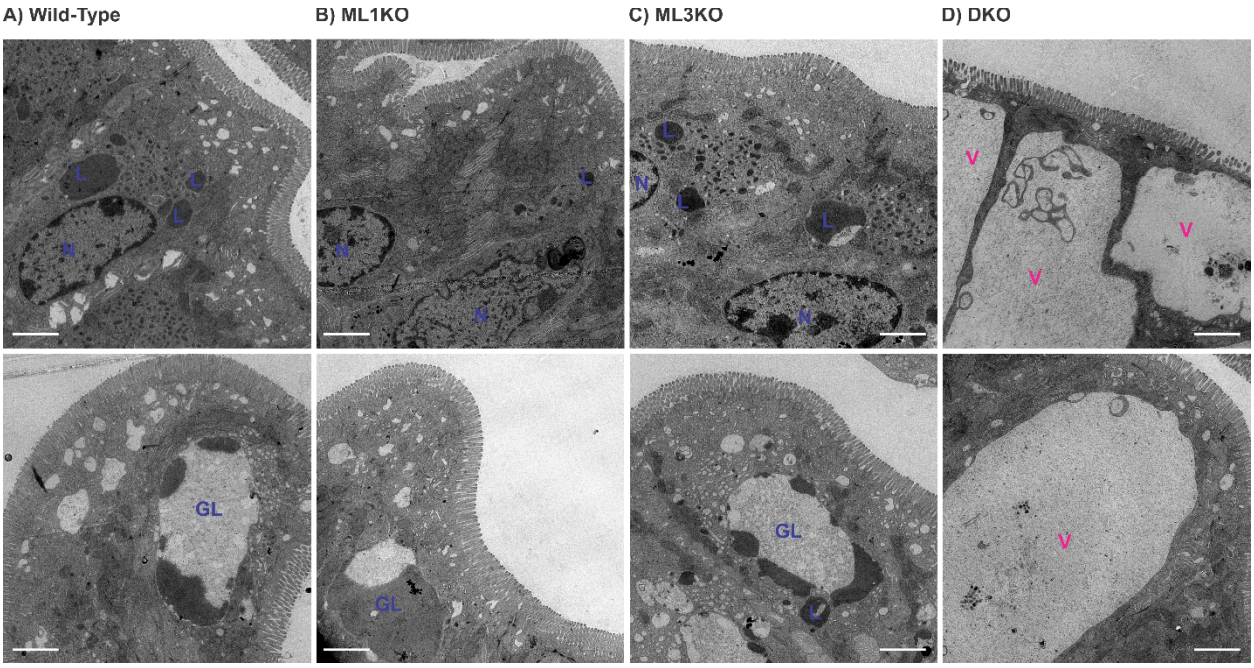


**Figure 5. A single enlarged pathological vacuole fills most of the intracellular space of neonatal enterocytes lacking mucolipins 3 and 1.** Tissues were collected from P7 pups fed with Texas Red-dextran. Ultrastructural examination of ileum from (**A**) Wild-type, (B) ML1KO, (C) ML3KO and (**D**) DKO mice at P7. These micrographs indicate that there are both lysosomes (L, upper panels) and giant lysosomes (GL, lower panels) with similar distribution and morphology between (**A**) wild-type, (**B**) ML1KO and (**C**) ML3KO. The lysosomes and giant lysosomes contain large amount of electron-dense materials, presumably dextran ready for intracellular degradation. The large pathological vacuoles (V) are only present in (**D**) DKO and, unlike the giant lysosomes in the controls, appear mostly electronluscent and take up most of the cytosolic space. Scale bars are 2 μm. Organelles present in control enterocytes are labeled in blue, whereas pathological structures are in pink. (N, nucleus).

In order to elucidate the subcellular basis of neonatal enterocyte vacuolation, we performed ultrastructural examination on neonatal intestines from DKO and their control littermates which did not contain vacuolated enterocytes (Figure 5). Electronmicrographs of P7 pups revealed that the enterocytes of wild-type, ML1KO and ML3KO ileal enterocytes had both lysosomes and the characteristic giant lysosome filled with electron dense material, presumably milk proteins accumulated for digestion (Figure 5A-C). In contrast, P7 ileal enterocytes of DKO animals lack this giant lysosome and instead have a greatly enlarged pathological vacuole that appeared mostly empty but still had some membranous whorls (Figure 5D). Despite their pathology, brush border microvilli, apical plasma membrane invaginations (endocytic figures) and endosomes of DKO enterocytes appeared normal (Figure 5). Hence, ultrastructural examination of suckling-type enterocytes from DKO mice reveals that their vacuolated appearance apparent with H&E histology results from the formation of large, vacuolar organelles of an abnormal nature that form instead of (and in the same subcellular location as) the giant lysosomes characteristic of wild-type ileal enterocytes.

**The pathological vacuoles of suckling enterocytes lacking mucolipins 1 and 3 are aberrant hybrid endolysosomal hybrid organelles**

An enlarged cytoplasmic vacuole accumulating endocytosed materials could result from an overall increase in endocytosis and/or a decrease in exocytosis, as both would increase the amount of intracellular organelle membrane. In order to elucidate how this pathological vacuole forms, we fed formula with Texas Red-conjugated dextran to pups immediately after birth and examined their intestines three hours later. At this point, enterocytes had endocytosed the dextran

which, in ML3KO control littermates, accumulated in the lysosomes (Figure 6A, A'; upper panels). On the other hand, in enterocytes from DKO mice, the dextran accumulated in the pathological vacuole, demonstrating that it accumulated endocytosed cargo normally destined to lysosomes (Figure 6A, A'; lower panels).

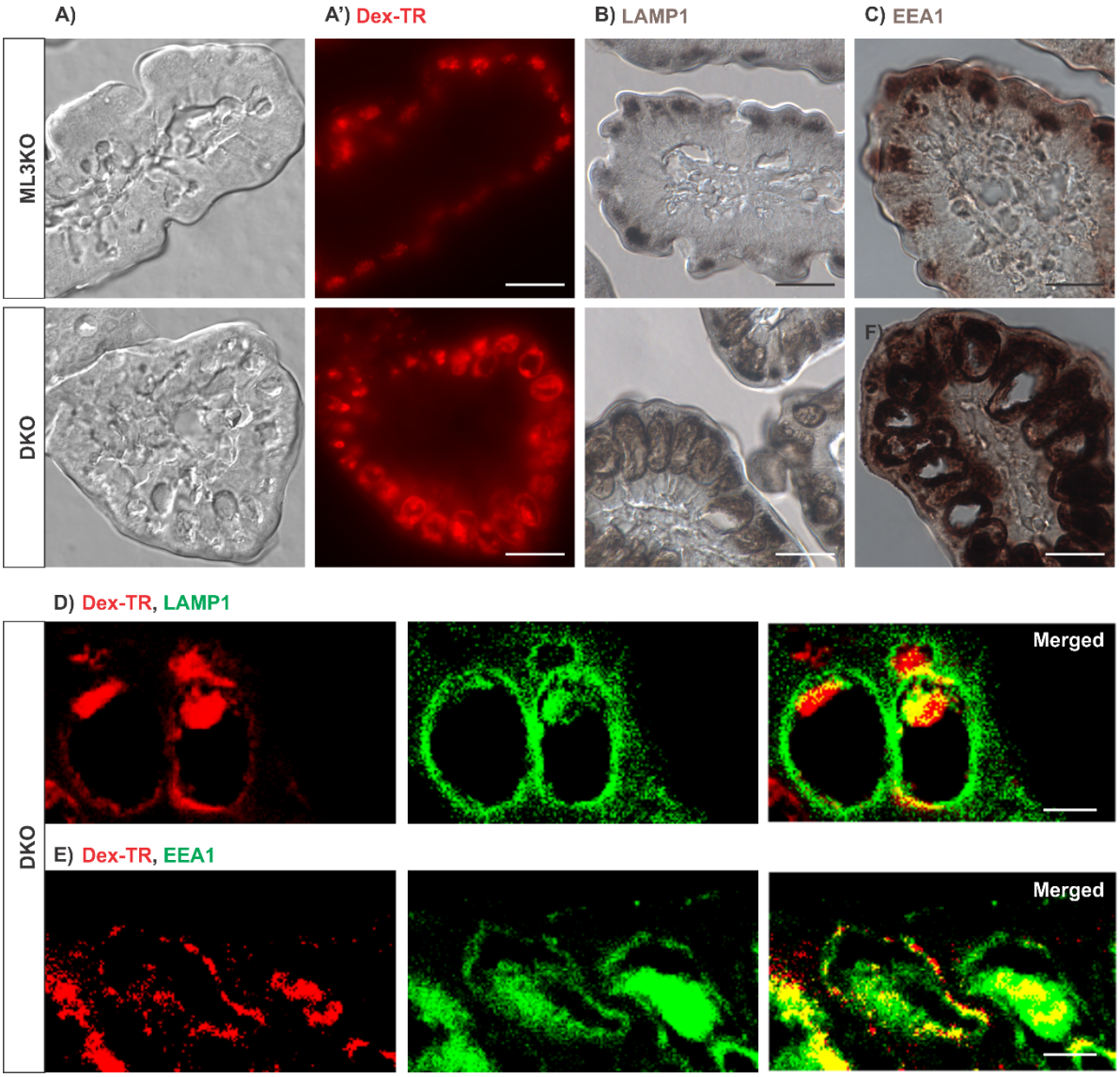


**Figure 6. The pathological vacuoles of neonatal enterocytes lacking mucolipins 3 and 1 are aberrant endolysosomal hybridorganelles.** Cryosections of intestines from 3 hour old control ML3KO and DKO littermates that had been fed formula with Dextran-Texas Red (Dex-TR)

immediately after birth. (**A**) Nomarski and fluorescent (**A'**) images of the same sections reveal that neonatal enterocytes endocytose the ingested Dextran-Texas Red, which accumulates in the apical lysosomes of ML3KO control enterocytes (upper panel) and in the pathological vacuoles of DKO enterocytes (lower panel). Immunoreactivities of the lysosomal marker LAMP1 (**B**) and to the early endosomal marker EEA1 (**C**) reveal that the pathological vacuoles of DKO enterocytes contain endosomal and lysosomal components and thus may result from the fusion of both types of organelles. (**G-E**) Confocal optical sections of immunofluorescent staining for LAMP1 (**D**) or EEA1 (**E**) on DKO intestines from the same P0 animal used in (**B, C**) reveal that endocytosed dextran accumulates in the pathological vacuoles, which contain both LAMP1 and EEA1. Due to the high level of neonatal enterocytes autofluorescence, which spans most of the detectable optical

Three proposed roles for mucolipin channels are to: 1) release calcium from lysosomes to trigger their fusion with endosomes or vice versa; 2) once fused into a transient hybrid organelle, release calcium from it to trigger scission and thus reformation of lysosomes and endosomes; and 3) release calcium for focal lysosomal exocytosis (Reddy et al., 2001; LaPlante et al., 2004; Piper and Luzio, 2004; Treusch et al., 2004; Grati et al., 2006; Puertollano and Kiselyov, 2009; Dong et al., 2010; Shen et al., 2012). In the first case, we would expect that the enlarged pathological vacuole of DKO enterocytes, filled with endocytosed materials, would be an enlarged endosome or lysosome resulting from a block in fusion between these organelles. In the second case, we would expect that the enlarged pathological vacuole would be a hybrid organelle resulting from the continuous fusion of endosomes with lysosomes without the subsequent

scission. By labeling with antibodies to a lysosomal marker (lysosome-associated membrane protein 1, LAMP1) and an early endosome marker (early endosomes antigen 1, EEA1), we found that the pathological vacuole of DKO enterocytes were both lysosomal and endosomal in nature (Figure 6B-E). Such a pathologically enlarged endolysosomal hybrid organelle would not result from the proposed block in fusion between endosomes of lysosomes, but instead from an increase in the rate of fusion or a subsequent decrease in the rate of scission.(Piper and Luzio, 2004; Treusch et al., 2004; Thompson et al., 2007; Puertollano and Kiselyov, 2009; Dong et al., 2010).

Given that mucolipins' roles in lysosomal exocytosis has been described in cell membrane repair mechanism of damaged muscle fiber (Reddy et al., 2001), it is unlikely that neonatal enterocytes would require such elaborated self-repair mechanism because the enterocytes' turnover rate, and the generation of new enterocytes from the intestinal stem cells are very rapid (every 2-6 days) (Mayhew et al., 1999; Williams et al., 2015). While we cannot rule out the possibility that mucolipin 3 and 1 codeficiency may cause defects in lysosomal exocytosis, our evidence suggested that mucolipins in fact facilitated lysosomal scission of the endolysosomal hybrid-organelles in the neonatal enterocytes.

### 2.3.3 Reduced endocytotic rate in neonatal enterocytes lacking mucolipins

In order to elucidate the mechanism leading to growth defect among suckling DKO mice, we assessed non-receptor mediated endocytosis by quantifying the amount of Texas Red-conjugated dextran that entered duodenal enterocytes of neonatal pups upon feeding. The reduction of endocytosis of maternal nutrients could lead to failure-to-thrive in

DKO pups. However, at birth, we found that despite the different subcellular distribution of endocytosed dextran (in a pathologically large vacuole in DKO enterocytes versus multiple lysosomes in enterocytes of ML3KO control littermates), the average net amount per enterocyte did not differ with genotype and subcellular pathology (Figure 7A, B). We also quantified the number of plasma membrane invaginations (termed endocytic figures) which represent endocytotic or exocytotic events (Figure 7C, D) from suckling enterocytes at P0. We found that, despite the intracellular vacuolation of DKO enterocytes, the number of invaginations at their plasma membrane did not differ from that of control littermates. Altogether, at birth, we found no evidence for an increased rate of endocytosis, or a decreased rate of exocytosis, that might account for the endolysosomal vacuolar enlargement of DKO enterocytes.

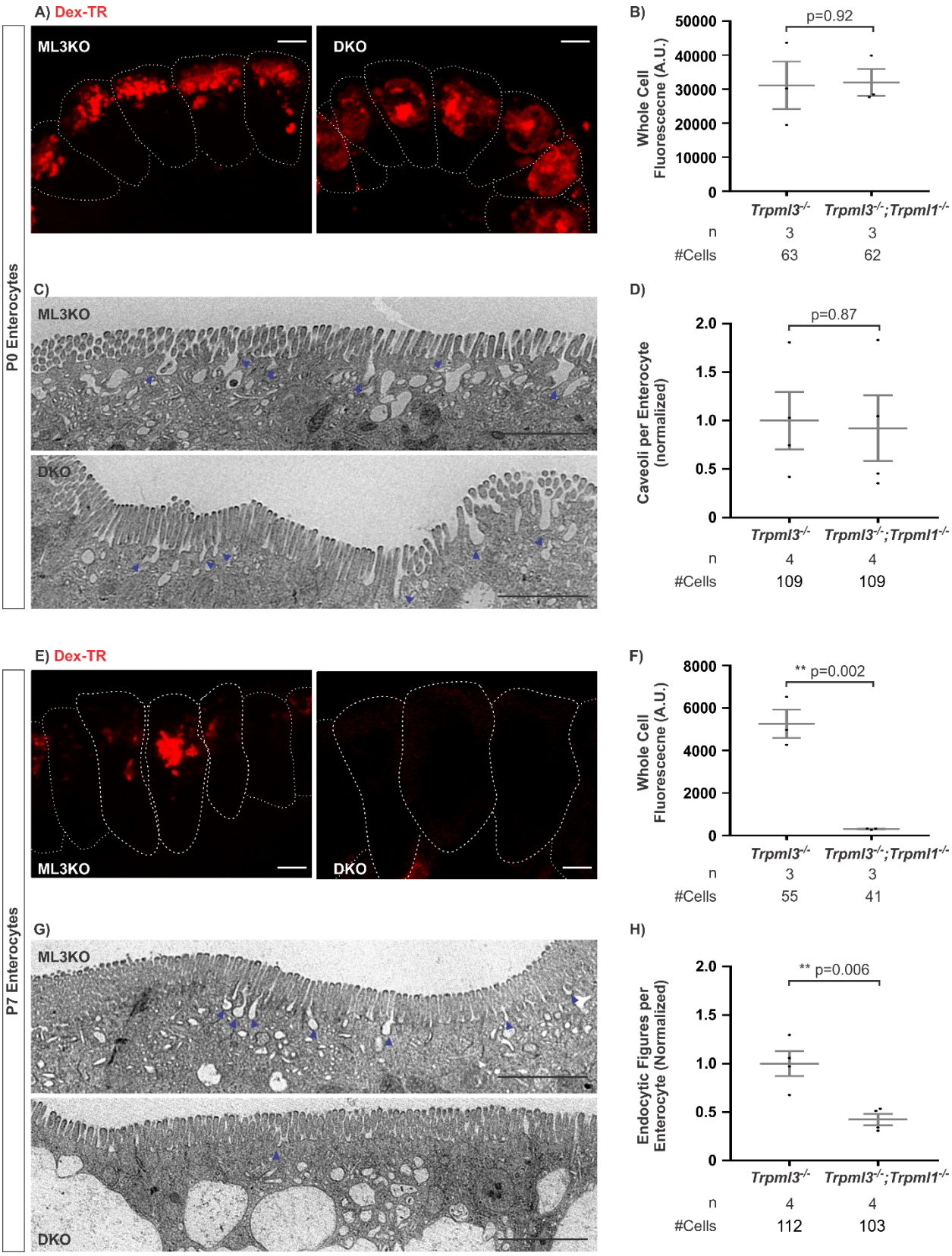
A) Dex-TR
ML3KO
DKO
P0 Enterocytes
C)
ML3KO
DKO
B)
p=0.92
Whole Cell Fluorescecne (A.U.)
50000
40000
30000
20000
10000
0
Trpml3-/-
Trpml3-/-;Trpml1-/-
n 3 3
#Cells 63 62
D)
p=0.87
Caveoli per Enterocyte (normalized)
2.0
1.5
1.0
0.5
0
Trpml3-/-
Trpml3-/-;Trpml1-/-
n 4 4
#Cells 109 109
E) Dex-TR
ML3KO
DKO
P7 Enterocytes
G)
ML3KO
DKO
F)
** p=0.002
Whole Cell Fluorescecne (A.U.)
8000
6000
4000
2000
0
Trpml3-/-
Trpml3-/-;Trpml1-/-
n 3 3
#Cells 55 41
H)
** p=0.006
Endocytic Figures per Enterocyte (Normalized)
2.0
1.5
1.0
0.5
0
Trpml3-/-
Trpml3-/-;Trpml1-/-
n 4 4
#Cells 112 103

**Figure 7. The pathological vacuoles in neonatal enterocytes do not alter endocytosis at P0 but eventually lead to reduced endocytosis by P7.** (**A, E**) Confocal projection image of enterocytes from (**A**) P0 and (**E**) P7 control ML3KO (left panels) and DKO (right panels) pups fed Dextran-Texas Red (Dex-TR) right after birth, 120 minutes prior to fixation. (**C, G**) Representative electron micrographs showing the apical membrane of enterocytes from (**A**) P0 and (**E**) P7 control ML3KO (left panels) and DKO (right panels) pups where endocytic figures are in the process of endocytosis (arrowheads). (**B**) Average cellular levels of endocytosed dextran in P0 enterocytes. Despite the different subcellular distribution of dextran, cells from both genotypes have endocytosed similar amounts of it. (**D**) Average apical-membrane endocytic figures observed in electron micrographs of enterocytes of control ML3KO and DKO littermate pups at P0. Despite the incipient vacuolation of DKO P0 enterocytes (Remis et al., 2014), their rate of apical endocytosis plus exocytosis, as assessed from their number of endocytic figures, do not differ from those of ML3KO controls. (**F**) The quantification of average cellular levels of endocytosed dextran at P7 reveals a significant reduction of dextran uptake in DKO enterocytes compared to ML3KO enterocytes. (**H**) Average apical-membrane endocytic figures observed in electron micrographs of DKO pups is significantly lower than that observed in ML3KO littermates. For each animal, the value used is an average from 10 to 30 enterocytes. For clarity, enterocyte boarder was outlined with dotted line. Average ± SEM's are shown on the plots. Sample sizes (n) and numbers of cells measured are indicated underneath the plots. We used the unpaired Student's t-test based on the number of animals (n).

The normal rates of endocytosis immediately after birth suggested that an increase in endocytosis was not the cause of vacuolation, thus confirming our observations that the pathological vacuoles in DKO enterocytes resulted from of a block in lysosomal scission of the endolysosomal hybrid-organelles (Figure 6). However, the severe vacuolation appeared hours to days later, when vacuoles occupied the vast majority of the enterocyte cytosol (Figure 4, 5). The presence of pathologically enlarged vacuole might interfere with the endocytic process as the enterocyte run out of membrane-bound cargos to undergo further endolysosomal trafficking. To test this hypothesis we assessed endocytosis at P7, when enterocyte vacuolation is severe (Figure 5), by measuring the amount of endocytosed Texas Red-conjugated dextran in enterocytes upon feeding. We found that the amount of luminal dextran endocytosed by enterocytes DKO pups was greatly reduced compared to that of control littermates (Figure 7E, F). We also quantified the density of endocytic figures at the apical plasma membrane of enterocytes, and again detected a great reduction in DKO pups compared to of control littermates (Figure 7G, H). Hence, severely vacuolated enterocytes of DKO pups endocytosed materials from the intestinal lumen at a greatly reduced rate. Given that nutrients such as proteins are uptaken by enterocytes from the intestinal lumen by apical endocytosis, our results explained the findings that DKO pups exhibited severe weight loss (or not enough weight gain), and diarrhea during suckling period (Remis et al., 2014).

### 2.3.4 Mucolipins in human infant enterocytes

Human neonates also have lysosome-rich enterocytes (Grand et al., 1976). Compared to rodents, they appear much earlier during gestation, but are present at birth (Grand et al., 1976). However, to our knowledge no studies have investigated whether human infant enterocytes contain the elaborated mucolipin-endowed endolysosomal system, or whether they may be replaced by lysosome-poor, mucolipin-deficient mature enterocytes. We performed immunohistochemistry for LAMP1 and TRPML3-NT, and detected high levels of apical lysosomes as well as mucolipin 3 in enterocytes from a 2 month and 2 day old patients (Figure 8A, B). These patterns of apical lysosomes and mucolipin 3 in human infant enterocytes are similar to those from the mice (Figure 1-3, 6). In addition, a double-staining of LAMP1 and TRPML3-NT revealed that mucolipin 3 was also lysosomal in enterocytes from a 1.5 month old patient (Figure 8C). We used adjacent sections from the same sample, stained them without primary antibodies, and found no immunoreactivity of either LAMP1 or TRPML3, thus confirming that our staining was specific to LAMP1 and TRPML3 (Figure 8A, B). Our results revealed for the first time that human neonatal enterocytes contained a specialized mucolipin-endowed endolysosomal system.

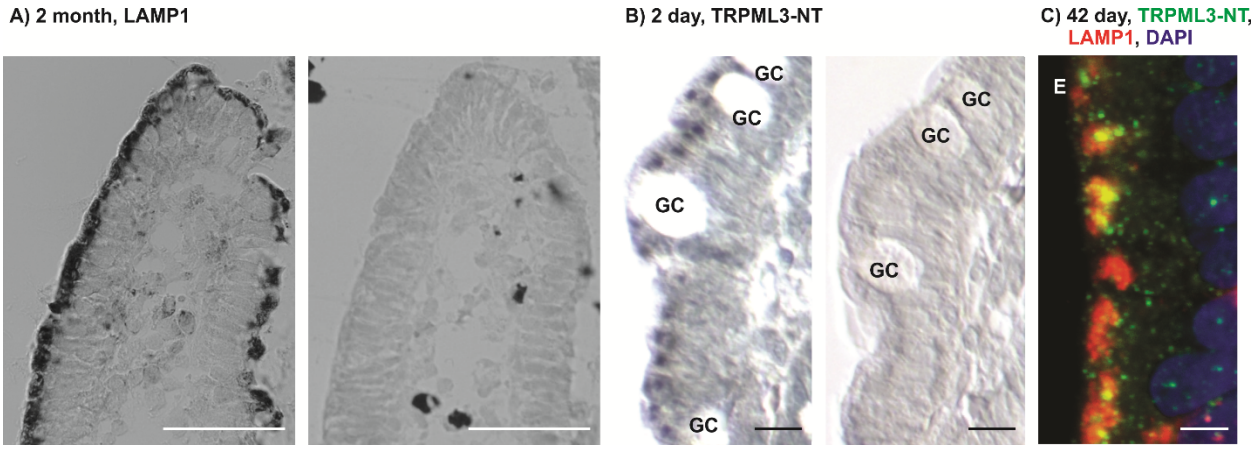


**Figure 8. Human infant enterocytes contain a specialized mucolipin 3-endowed lysosomes.** (**A**) Immunostaining of a lysosomal marker LAMP1 cryosections of human infant ileum (collected 2 months after birth, which had taken place prematurely at 31 weeks of gestation) reveals a high level of lysosomes at the apical side of the enterocytes (left panel). As a negative control, we performed the same immunostaining on an adjacent cryosection without primary antibody (right panel). As in mice, lysosomes accumulate in the apical side of human enterocytes (top half of one villus is shown). (**B**) Immunostaining on adjacent paraffin sections of jejunum from a 2 day old patient with an antibody to mucolipin 3 (TRPML3, left panel) and no primary antibody (negative control, right panel). As in mice (Remis et al., 2014), TRPML3 accumulates in the apical cytoplasm of human enterocytes. GC (goblet cells). (**C**) Double-staining of LAMP1 and mucolipin 3 on a 6 week old intestine reveals that human neonatal enterocytes contain mucolipin 3-endowed lysosomes. Nuclei were counterstained with DAPI. Scale bars are 50 µm (**A**), 10 µm (**B**) and 5 µm (**C**).

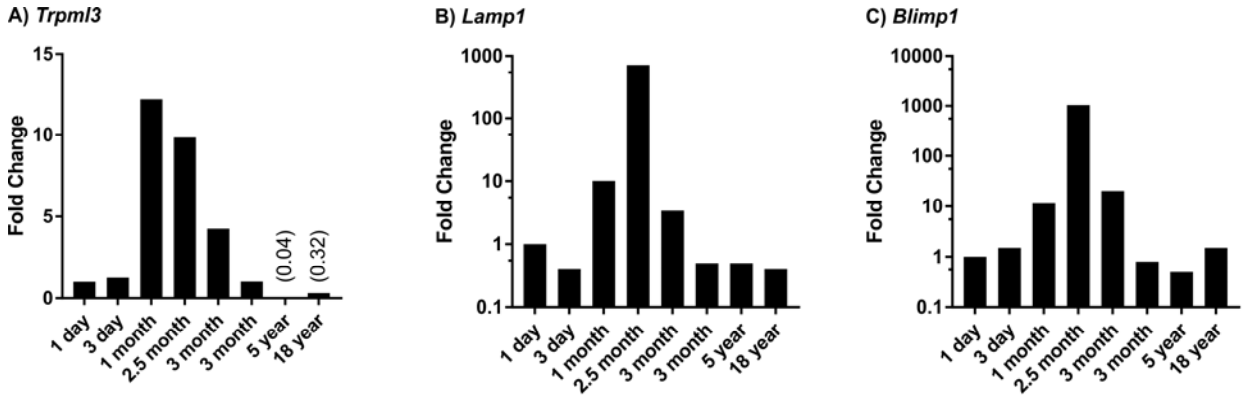


**Figure 9. Human infant intestines are rich in lysosome and mucolipins. A-C**) qRT-PCR showing the relative mRNA level of (**A**) *Trpml3*, (**B**) *Lamp1* (lysosomal membrane protein) and (**C**) *Blimp1* (a transcription factor responsible for development of neonatal enterocyte (Mould et al., 2015) from human small intestine samples. The mRNA level of enterocyte marker *Villin1* was used as a reference for analysis and the relative level of transcripts was normalized to that of the sample from a 1 day-old patient. The relative mRNA levels of *Trpml3*, *Lamp1* and *Blimp1* mRNA level increase greatly in patients at ~1-3 months of age, and subside in older patients (5 and 18 year-old). The "healthy" intestinal samples selected for this study were biopsies from patients without enterocyte pathologies (atresias, ileostomies, non-cancerous intestinal segments from tumor resections or normal intestinal segments from necrotizing enterocolitis patients).

In order to examine the neonatal to "adult-like" transition of human enterocytes, we performed quantitative RT-PCR analysis of *Trpml3* and *Lamp1* mRNA levels in small intestine from human infant (1 day old) to teenage (18 year old) patients to determine when these markers for specialized endolysosomal system subsided in human. We found that *Trpml3* mRNA levels peaked during the age of 1-3 months and subsided after 3 months (Figure 9A). The increase in

*Trpml3* level was a high as ~12 folds in the sample from a 1 month old patient compared to that from a 1 day old patient. Interestingly, we also observed the same pattern of increases in level of the lysosomal marker *Lamp1* among these same patients (Figure 9B). We noticed that the change in *Lamp1* levels was much larger (up to ~720 folds in 2.5 month old patient compared to 1 day old patient) than that of *Trpml3.*

Finally, to add to a small pool of knowledge on human neonatal enterocytes, we also perform quantitative RT-PCR analysis of *Blimp1* which is a transcription factor controlling neonatal enterocyte development and regulating the replacement of neonatal to "adult-like" enterocytes in mice (Muncan et al., 2011; Mould et al., 2015). A recent study reported Blimp1 expression in human embryonic enterocytes and its absence in adult enterocytes (Mould et al., 2015); however, there is no report whether this important transcription factor is present in infant enterocytes and the age by which its expression subsides. Here, we found that *Blimp1* was upregulated around 1-3 months (its peak was observed in 2.5 month old patient at ~1000 folds increase compared to 1 day old patient), and its expression appeared to subside after 3 months of age (Figure 9C).

It is worth to note that these mRNA data were collect from a very few number of samples, and in order to determine the age by which neonatal enterocytes are replaced by "adult-like" ones in human, we require a larger sample size of human infant intestinal samples from various ages.

### 2.3.5 Pathological vacuolation in enterocytes of a rodent model of necrotizing enterocolitis

We hypothesized that some pathologies affecting neonatal enterocytes may be disrupting their specialized endolysosomal system. In fact, histological examination of neonatal (P2) rat with induced NEC (Hunter et al., 2009; Tian et al., 2010; Emami et al., 2012) reveled vacuolated pathology in the enterocytes (Figure 10A). This vacuolation of NEC enterocytes, characteristic of a milder form of NEC (Hunter et al., 2009; Tian et al., 2010; Emami et al., 2012), are strikingly similar to the vacuolated enterocytes of neonatal DKO mice lacking mucolipins 3 and 1 (Figure 10B). Periodic acid-Schiff staining indicated that the vacuolated cell from rat model of NEC were enterocytes and not the mucin-filled goblet cells (Figure 10A), a feature we observed in DKO neonates (Figure 10B). We also detected this vacuolated pathology in human NEC surgical samples at locations where necrosis had not developed—the sample was taken from a location adjacent to the necrotic foci (Figure 10C). While we still need to further confirm the molecular basis of vacuolated pathology among NEC patients and rodent NEC model (e.g. are they endolysosomal in nature? do enterocytes from NEC animals exhibit lower level of endocytosis?), our preliminary data have implicated endolysosomal pathology in this disease for the first time.

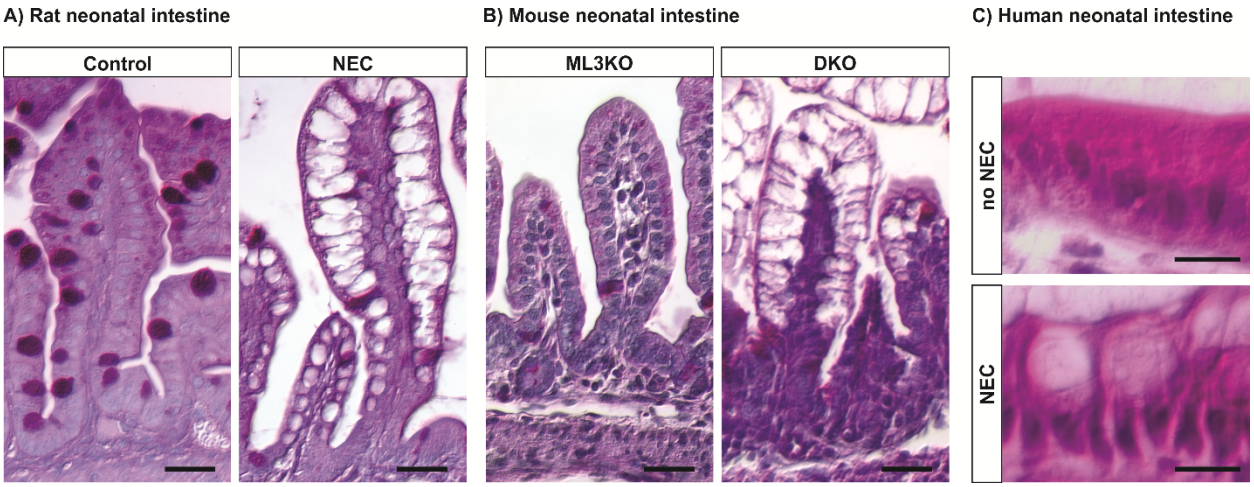


**Figure 10. Human necrotizing enterocolitis (NEC) patient and rodent models of NEC suffer neonatal enterocyte vacuolation resembling that of mucolipins 3 and 1 co-deficient mice.** (**A, B**) Periodic acid-Schiff (PAS) staining of paraffin-embedded sections of neonatal (P2) rat intestines (**A**) reveals vacuolated enterocytes (different from red mucin-labelled goblet cells) in pups with induced NEC (generated as described (Tian et al., 2010), right panel) but not in the control littermate (left panel). (**B**) Vacuolation of DKO pups (right panel), but not control ML3KO littermate controls (**C**), is identical in appearance to that of NEC rat (**A**). (**C**) Hematoxylin and eosin (H&E) staining of paraffin-embedded human intestinal sections of control (2 month old without NEC, upper panel) and NEC (2 week old, lower panel) patients. NEC sample exhibit vacuolated enterocytes resembling those in the rodent NEC model (**A**) and DKO mouse pups (**B**). Scale bars are 50 μm (**A, B**) and 15 μm (**C**).

**2.4 Discussions**

The subcellular defects of MLIV are specific to cell types. While neurons accumulate electron dense bodies with glycosaminoglycans and lipids, epithelial cells tend to display electron lucent vacuoles with a varying amount of fribrillogranullar material and scattered multilamellar membranous whorls (Merin et al., 1975; Tellez-Nagel et al., 1976; Goebel et al., 1982; Folkerth et al., 1995; Bargal and Bach, 1997), very similar to the vacuoles of neonatal enterocytes lacking mucolipins 3 and 1 (Figure 4D, H; 5D, 6). However, the pathological vacuoles in neonatal mice lacking mucolipins do not accumulate glycosaminoglycans, as shown by Periodic Acid Schiff staining (Figure 4H), lipids, polysaccharides nor nucleic acids (Remis et al., 2014)—substances found in the inclusion bodies of neurons from MLIV patients. Nevertheless, what is common to the pathology of all types of cells from MLIV patients is the concentric whorls of membrane, which we also observed in DKO enterocytes (Figure 5D). One important difference is that, while symptoms take months to develop in MLIV patients and mice lacking mucolipin 1 (Bach, 2001; Venugopal et al., 2007; Micsenyi et al., 2009; Geer et al., 2010), the phenotype of mice lacking both mucolipins develops immediately after birth, as their enterocytes severely vacuolate within hours. Hence, these double knockout cells seem to experience a greatly accelerated form of MLIV.

Multiple roles have been proposed for the function of mucolipins in various cell types, either mammalian TRPML1, mammalian TRPML3, or orthologs in other species such as CUP-5 in nematodes, TRPML in flies and MCLN in *Dictyostelium* (Fares and Greenwald, 2001; Puertollano and Kiselyov, 2009; Zeevi et al., 2009; Sun et al., 2011; Lima et al., 2012; Wong et al., 2012). These are letting calcium out of endosomes and lysosomes in order to: 1) regulate endocytosis and/or exocytosis (Reddy et al., 2001; Samie et al., 2013; Miao et al., 2015); 2) favor

the counterionic entry of protons to acidify the lysosomal lumen and thus allow hydrolytic activity (DiCiccio and Steinberg, 2011; Lelouvier and Puertollano, 2011); 3) promote the fusion with autophagosomes and endosomes (Thompson et al., 2007) and 4) facilitate the scission of the resulting endolysosomal hybrid organelle to reform endosomes and lysosomes (Remis et al., 2014; Cao et al., 2017).

Our results in neonatal suckling enterocytes rule out defects in endocytosis or exocytosis (Figure 7) and are not consistent with a defect in lysosomal degradation, since the pathological vacuoles appear largely empty despite their apparent fusion with endosomes and their collection of endocytosed materials (Figures 5). The presence of both endosomal and lysosomal markers in the enlarging pathological vacuoles (Figure 6), the accumulation of endocytosed material normally destined to lysosomes in this pathological vacuoles (Figure 7) are also incompatible with a deficiency in endolysosomal fusion. Instead, all these observations suggest a role of mucolipins in the scission required to disassemble the normally transient hybrid organelles into smaller endosomes and lysosomes. Alternatively, these vacuoles could arise by an increase—rather than a decrease—in the rate of endolysosomal fusion, although that would imply a role of mucolipins in preventing, rather than facilitating, vesicle fusion, a role for which there is no support in the published literature. A block of scission or an increase (but not decrease) in fusion would generate the enlarged endolysosomal vacuoles we observe in neonatal enterocytes (Figure 11). However, it must be noted that the pathological vacuoles of DKO enterocytes are aberrant organelles unlike the hybrid organelles that normally form from the transient fusion of late endosomes and lysosomes, which may not (though this is not known for enterocytes) incorporate the early endosome marker EEA1. For this and other reasons, definitive proof that increased fusion, decreased scission or another subcellular abnormality cause vacuolation is wanting but

beyond the scope of this study, which is limited by the inability of neonatal enterocytes to be cultured and thus for the direct observation of their vesicle dynamics.

The specializations of neonatal enterocytes for the absorption of milk nutrients are critical for neonatal growth and survival. A mutation in the Blimp1 transcriptional repressor, normally expressed in enterocytes until the suckling to weaning transition, results in only mature-like enterocytes and, due to their inability to properly digest milk, growth retardation (failure to thrive) and neonatal mortality (Harper et al., 2011; Muncan et al., 2011; Mould et al., 2015). It may therefore come as a surprise that DKO pups, with their severe enterocyte vacuolation, are fully viable and at all times able to grow, even if at a reduced rate. Several observations may explain why their failure to thrive is partial. First, although proteins in milk are digested in lysosomes, sugars and many fats are not. Lactose, the main sugar in milk, is digested by lactase enzymes at the brush border microvilli membranes into glucose and galactose, which are then absorbed via plasma membrane transporters. The normal microvilli of vacuolated DKO enterocytes (Figure 5 and 7) suggest that they would be able to digest and absorb sugars. Milk fats are largely digested by extracellular lipases in the lumen of the digestive track, taken up by enterocytes for assembly into chylomicrons in the Golgi apparatus and then secreted into the lacteals and hence the lymphatic circulation (Manson and Weaver, 1997; Lindquist and Hernell, 2010). The process does not involve the specialized lysosomes of suckling enterocytes. Indeed, there is no defect in the distribution of fat droplets the lacteals of DKO villi, despite the severe vacuolation of their enterocytes (Remis et al., 2014). Nonetheless, a complete inability of milk protein digestion might be expected to cause lethality or at least cause weight loss. However, because enterocytes are constantly generated (Mayhew et al., 1999; Williams et al., 2015) and the newly differentiated ones, situated at the base of the villi, are not vacuolated (Figure 4), they

should be able to endocytose and digest milk proteins. Even the older, vacuolated enterocytes may be able to digest the limited amounts of milk proteins that have been taken up by endocytosis, as their enlarged vacuoles appeared mostly empty (Figure 5). Instead, the deficiency of vacuolated enterocytes in endocytosis across the apical plasma membrane of DKO pups (Figure 7) suggest a defect in the uptake of proteins from the intestinal lumen. Such a defect can explain their diarrhea symptoms and partial failure-to-thrive, which is characterized by reduced growth but not weight loss or lethality, previously reported (Remis et al., 2014). Finally, the replacement of enterocytes around weaning by mature enterocytes that do not co-express mucolipins and do not vacuolate in their co-absence explains the post weaning growth recovery of DKO mice.

Another implication of our results to MLIV, and to LSDs in general, is that certain nutrients provided by maternal milk are not as much used as energy sources as they are as constituents of the growing brain and retina to properly develop and function (Manson and Weaver, 1997; Lindquist and Hernell, 2010). Hence, some of the neurological and retinal symptoms of MLIV and other lysosomal storage diseases might result from, or at least be aggravated by, defective absorption of milk nutrients during suckling. We suggest that nutrient absorption during suckling be examined for patients with lysosomal disorders, as any potential malnutrition might be avoided with, for example, amino acid-based formula that lacks proteins or parenteral nutrition.

Furthermore, the role of mucolipins in neonatal enterocytes extends beyond MLIV to pediatric intestinal dysfunctions, such as NEC. Here, for the first time, we reported the presence of the specialized mucolipin-endowed lysosomal system in human infant intestine (Figure 8, 9). We also noticed that our vacuolated enterocytes from DKO pups strikingly resembled the

vacuolated pathology of rodent models of NEC, particularly its milder forms (De Plaen et al., 2007; Hunter et al., 2008a, 2009; Tian et al., 2010; Emami et al., 2012) (Figure 10A, B). The presence of this pathology in human NEC surgical samples at locations where necrosis had not developed (a position adjacent to the necrotic foci; Figure 10C) suggested that lysosomal dysfunction could be the cause/or contribute to the etiology of NEC. Although lysosomal alterations in our DKO mouse model would not demonstrate NEC mortality, they would greatly advance our understanding of this disease, of unknown pathogenesis, by implicating the endolysosomal system. It is possible that other factors; for example, immaturity of the endolysosomal system due to premature birth, pathogen-mediated interference, or mutations on genes associated with endolysosomal system (such as *Trpml3*), contribute to an individual's predisposition to NEC.

Hence, it would be advisable to examine the intestines of newborns with intestinal diseases for pathological signs like those here described. These signs would not be detected after weaning but could have long-term, yet avoidable, effects in the patients. Studies are underway to determine the time frame in which infants and children possess neonatal-like enterocytes, and whether intestinal dysfunctions during this period should be treated with specific cares distinct from adult patients. It is possible that medical treatments or interventions designed to treat adult patients might not be appropriate to treat pediatric intestinal diseases.

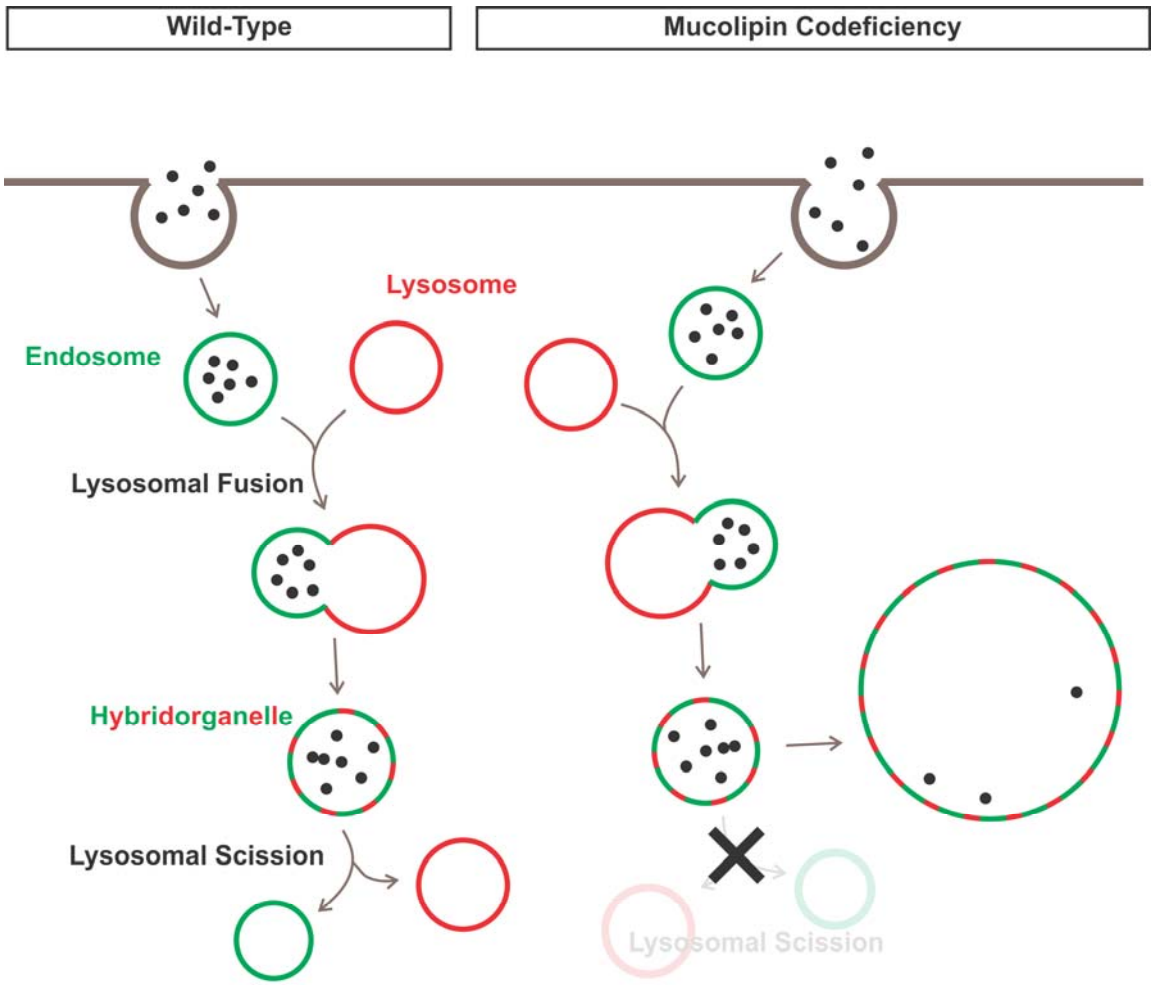


**Figure 11. Proposed model for lysosomal pathology in neonatal enterocytes lacking mucolipins 3 and 1.** In wild-type neonatal enterocyte, maternal nutrients, especially milk proteins, are endocytosed intact into early endosomes, as the stomach is not acidic yet and, therefore, gastric proteases are not active (Henning, 1985; Wilson et al., 1991). Endosomes fuse with lysosomes forming endolysosomal hybrid organelles, where the endocytosed nutrients are intracellular digested. Upon the completion of digestion, the hybridorganelles undergo lysosomal scission occurs to recycle lysosomes and endosomes back to the cytoplasm. In out mouse model lacking mucolipins 3 and 1, the enterocytes contain abnormally enlarged pathological vacuoles at as early as P0. Because these pathological vacuoles were endolysosomal hybridorganelles

(Figure **5**), and there was no increase (or decrease) in endocytosis at P0 (Figure **6A-D**), we deduced the hybridorganelles of enterocytes lacking mucolipins failed to undergo lysosomal scission. With the lack of lysosomal scission, as the endosomes continue to fuse to the hybridorganelled, they continue to increase in size. As the pathological vacuole takes up the entire cytosolic space and endosomes are not replenished, the enterocyte eventually fails to undergo endocytosis of maternal nutrients (by P7, Figure **6E-H**), leading to failure-to-thrive phenotype (Remis et al., 2014). We thus proposed that mucolipins 3 and 1 facilitated lysosomal scission in the neonatal enterocytes.

## 2.5 Materials and methods

### Animals and ethics

All animal care and procedures were in accordance with the *Guide for the Care and Use of Laboratory Animals* published by the National Institutes of Health and were approved by Northwestern University's Institutional Animal Care and Use Committee (Animal Study Protocols: IS00006235, IS00001281, IS00003625). Mice were housed in the barrier rooms of Northwestern University's animal facility. We obtained tissues from either CD1 mice (Charles River), from *Trpml3*$^{-/-}$ (ML3KO) and *Trpml3*$^{+/+}$ littermates with a genetic background ~75% C57BL/6 and ~25% Sv129/Ola (Castiglioni et al., 2011), from *Trpml1*$^{-/-}$ (ML1KO) and *Trpml1*$^{+/+}$ littermates with a genetic background ~75% C57BL/6 and ~25% 129S6 (Venugopal et al., 2007), and from *Trpml3*$^{-/-}$*;Trpml1*$^{-/-}$ (DKO), and littermates with a genetic background of ~75% C57BL/6, ~12.5% Sv129/Ola and ~12.5% 129S6. DKO mouse line was generated by (Remis et al., 2014).

### Human Intestinal Samples

Human intestinal samples were collected and prepared for paraffin or OCT frozen sections or RNA extraction by Dr. Catherine Hunter, M.D., and Dr. Isabelle De Plaen, M.D., Feinberg School of Medicine, Northwestern University. Detailed protocols for tissue processing are described below.

### Antisera Characterization

Our present study used triple controlled immunohistochemistry to determine the tissue and

subcellular expression pattern of mucolipin 3 protein, coded by *Trpml3* gene. We employed antisera raised against N-terminus of TRPML3 (TRPML3-NT). We also compared TRPML3 immunoreactivities to available *in situ* hybridization (ISH) analyses. Finally, we determined which immunoreactivities were absent from the tissues of a ML3KO mouse. See (Castiglioni et al., 2011) for detailed TRPML3 antibody information and prior characterization. Antibodies used in this study included: TRPML3-NT (1:5000 or 1:2000, M7570, Sigma), LAMP1 (1:50, 1D4B-s, Developmental Studies Hybridoma Bank), and early endosome antigen 1 or EEA1 C-15 (1:100, sc-6414, Santa Cruz Biotech).

**Tissue Processing**

We used unfixed tissue for ISH. These tissues were dissected, embedded in OCT and immediately snap frozen in isopentane cooled with dry ice. For fixed tissues, we cardiac perfused the animals with 2% paraformaldehyde, dissected out the intestine, post-fixed for 1 hour in 2% paraformaldehyde, and rinsed 3 times in PBS. We then took the tissue through a sucrose gradient (1 hour each 5%, 10%, 20%) ending with an overnight incubation in 20% sucrose and 50% OCT (Tissue-Tek, Sakura). We mounted the tissue in OCT and froze it on dry ice. For human tissues, the samples were immediately embedded in OCT and frozen on dry ice post-surgery. The frozen tissues were sectioned into 12 μm thickness. We also prepared our own paraformaldehyde fresh from powder. Consistency in fixation was very important as we often saw background autofluorescence that we could ascribe to over or inconsistent fixation.

**Immunohistochemistry**

Signal amplification methods were performed for TRPML3-NT antibodies. We performed

immunohistochemistry using the ABC/DAB (avidin-biotin complex with diaminobenzidine reaction) signal amplification system (PK-6100, Vector) or Tyramide signal amplification (T20922, Invitrogen). Following are brief protocols of our immunohistochemistry techniques as previously described in (Castiglioni et al., 2011; Remis et al., 2014).

ABC+DAB signal amplification. Sections were postfixed for 10 minutes in freshly prepared 2% paraformaldehyde. Antigen retrieval was done by incubating sections in 10mM sodium citrate, pH 6 with 0.25% Triton for 20 min at 92°C and cooling for 30 min at room temperature. Endogenous peroxidase was quenched by incubating in 1% $H_2O_2$, 10% methanol. Sections were blocked for 2 hours in 10% normal goat serum in PBS and incubated with 1:2000 TRPML3-NT in 10% normal goat serum in 0.1% triton + PBS (no azide) overnight at 4°C. The following day, sections were rinsed 4x 10 min in 0.1% triton + PBS and incubated with biotinylated secondary antibody in 10% normal goat serum 0.1% triton + PBS for 1 hr. Sections were then incubated in ABC solution (Vector) for 1 hr, rinsed and incubated with DAB solution (D4293, Sigma) for at least 7 min until tissue turns light brown. Nuclei were counterstained with DAPI (1μM) for 10 min.

Tyramide signal amplification. Sections were postfixed for 10 minutes in freshly prepared 2% paraformaldehyde. Antigen retrieval and peroxidase quenching were done as described above. Sections were block for 1 hour in 1% TSA block solution (Invitrogen). Sections were then incubated with 1:5000 TRPML3-NT in 1% TSA block solution (no azide) overnight at 4°C. On the next day, sections were rinsed 4x 10 min in 0.1% triton + PBS and incubated with secondary antibody in 1% TSA block solution for 1 hour in the dark. We then proceed with tyramide labeling reaction in groups of five or six slides by applying 1:150 tyramide (Invitrogen) working

solution to slide for 10 min at room temperature in the dark. Nuclei were counterstained with DAPI (1μM) for 10 min.

**ImmunoGold labelling of TRPML3-NT**

Intestinal samples were collected, dissected and postfixed overnight at 4°C in 4% paraformaldehyde + 0.5% glutaraldehyde in phosphate buffer (P3619, Sigma). The samples were then embanked in 4% agarose, sectioned into 50 μm thickness using a vibrotome and held in phosphate buffer + 0.1% azide 4°C until needed. Tissues were then processed for aldehyde deactivation by incubating for 30 min in 1% sodium borohydride in PBS. Antigen retrieval was done as described above. Tissues were then rinsed 3x 10 min in phosphate buffer and blocked in 0.3% BSA-c™ (Aurion) in phosphate buffer for 1 hour. Later, tissues were incubated in 1:500 TRPML3-NT in blocking solution for 2 nights at 4°C with agitation. Following primary antibody incubation, tissues were rinsed 3x 10 min in phosphate buffer, and incubated in 1:50 Donkey anti rabbit IgG UltraSmall-Gold (Aurion) in 0.5% BSA-c™ + 0.1% fish gelatin (Aurion) in phosphate buffer for 24 hours at room temperature with agitation. On the following day, tissues were rinsed 3x 10 min in phosphate buffer, 3x 15 min in 2% sodium acetate in phosphate buffer. Silver enhancing step was done by incubating the tissues in 1:1 solution of Aurion reagent A and B (Aurion Silver Enhancing Kit, Aurion) for 20 min, and rinsed 3x 5 min in 2% sodium acetate in phosphate buffer. Gold toning was later performed by immersing tissues in 0.05% gold chloride $HAuCl_4$ for 10 min at 4°C. Tissues were then rinsed 2x 10 min in 0.3% sodium thiosulfate at 4°C, 3x 10 min phosphate buffer, and fixed in 2% glutaraldehyde in phosphate buffer for 30 min.

**In situ hybridization**

We performed ISH on cryosections of snap-frozen, unfixed tissues from CD1, *Trpml3*$^{+/+}$, and ML3KO mice using protocols previously described (Schaeren-Wiemers and Gerfin-Moser, 1993; Duggan et al., 2008; Nagata et al., 2008). Freshly dissected and unfixed tissues were immediately snap frozen by dipping in isopentane cooled to −30°C with dry ice and sectioned (10–12 μm). For ISH, we used two non-overlapping cRNA probes for mouse Trpml3 mRNA (Genbank ID NM_134160). These are a 5' probe, which corresponds to nucleotides 179-723 (from codon 60 at the end of exon 1 to codon 240 at the end of exon 5) and a 3' probe, which corresponds to nucleotides 1005-1594 (from codon 335 in the middle of exon 8 to codon 531 in the middle of exon 12, the last exon).

We PCR amplified these cDNA fragments from mouse inner ear or CVP mRNA and TA-cloned them into vector pCRII. We generated digoxigenin-labeled antisense and sense (control) cRNA probes using the DIG-RNA labeling kit (Roche) according to the manufacturer's instructions. Sections were hybridized with antisense or sense probes as previously described (Schaeren-Wiemers and Gerfin-Moser, 1993; Duggan et al., 2008; Nagata et al., 2008). Sections were mounted for observation. Only cell types that labeled with both the 5' and 3' Trpml3 probes were considered positive for *Trpml3* mRNA.

**Image Acquisition and Analysis**

We acquired images using either a Nikon E600 pan fluorescence microscope (20x 0.75 N.A., 60x 1.4 N.A., or 100X 1.4 N.A. objectives) equipped with a CCD camera (SPOT RC-Slider) or a Zeiss LSM 510 confocal microscope (63x 1.4 N.A. or 100x 1.46 N.A. objectives). Or a Leica

SP5 confocal microscope (63x, 1.4 N.A. objective) When comparing wild type and knockout immunoreactivities, we captured images under identical conditions. In practice, this meant capturing images with identical exposure settings (pan fluorescence) or identical laser and gain settings (confocal). For even illumination, we flat field corrected and white balanced the color (SPOT RC-Slider) camera prior to acquiring DIC images.

Post-acquisition, we identically processed image pairs of wild type tissues and their corresponding knockout controls. This included adjustment for brightness and contrast of all images. We used ImageJ for all post acquisition processing.

**RT-qPCR**

Mouse Samples: RT-qPCR (reverse transcription of RNA followed by quantitative polymerase chain reaction) was performed based on (Castiglioni et al., 2011). Specifically, we used tissues from freshly euthanized animals not cardiac perfused. All tissues were dissected as quickly and as cleanly as possible and immediately snap frozen on dry ice until homogenized in Trizol (Invitrogen). We homogenized all tissues in Trizol using a tissue homogenizer and performed RNA isolation according to the manufacturer's instructions (RNeasy® Plus Micro Kit, Qiagen). RNA concentration was determined by UV absorption ($OD_{260}$). This value helped determine the volume of RNA used per RT reaction, with the goal to reverse transcribe 1 μg of total RNA per reaction. Prior to reverse transcription, we subjected the 1 μg of total RNA to DNaseI treatment (Invitrogen) to eliminate genomic DNA according to the manufacturer's protocol. This DNaseI treated 1 μg of total RNA was then subjected to first strand cDNA synthesis using Superscript III reverse transcriptase (Invitrogen) according to the manufacturer's protocol.

We performed RT-qPCR using a Mastercycler Realplex2 machine (Eppendorf) on ~100 ng (2 µl of a 26 µl RT reaction) of first strand cDNA using SYBR Green PCR Mastermix (Applied Biosystems) in triplicate, according to the manufacturer's instructions. The following primers (IDT) were designed on mouse sequence and used in qPCR: Trpml3ex8f, 5' ATGGAGTTCATCAACGGGTG; Trpml3ex9r, 5' ATAGTTGACGTCCCGAGAAG; 18Sf, 5' TTGACGGAAGGGCACCACCAG; 18Sr,5' GCACCACCACCCACGGAATCG. Melting curve analysis and gel electrophoresis of PCR products indicated single products of the correct size for each primer pair used. In addition, the ML3KO mouse does not contain the binding site for primer ex8f. Prior qPCR analysis (Castiglioni et al., 2011) on ML3KO mice using primers ex8f and ex9r did not detect any product from ML3KO tissue.

Human Samples: RT-PCR was performed using either SYBR® Green. Specifically, we used human samples that were immediately preserved in RNAlater™ Stabilizing Solution (Thermo Fisher) right after the surgery. We homogenized all tissues in Trizol using a tissue homogenizer and performed RNA extraction using RNeasy® Plus Micro Kit (Qiagen) according to the manufacturer's instructions. RNA concentration was determined by UV absorption ($OD_{260}$). This value helped determine the volume of RNA used per RT reaction, with the goal to reverse transcribe 1 µg of total RNA per reaction. We performed first strand cDNA synthesis reaction using iScript™ reverse transcription supermix (Bio-Rad) according to the manufacturer's manual. We then subjected RT-qPCR with 25ng of first strand cDNA using SsoAdvanced™ Universal SYBR® Green Supermix (Bio-Rad) in triplicates on a CFX Connect™ Real-Time PCR Detection System (Bio-Rad) using a 40-cycle protocol. All primers used for qRT-PCR on human samples were designed and pre-mixed to their optimal concentrations by BioRad.

**Tissue Histology**

For frozen sections, tissue was fixed with 4% PFA, washed with PBS, embedded in OCT, snap frozen and sectioned at 8 μm thickness with a cryostat. For human tissues subjected to frozen sectioning, the samples were immediately embedded in OCT and frozen on dry ice post-surgery. For paraffin sections, both human and animal tissues were fixed with 10% neutral buffered formalin, placed in 70% ethanol, dehydrated in increasing series of alcohol, cleared in xylenes or Citrisolv and placed in two subsequent 55°C paraffin baths, embedded and sectioned at 5 μm thickness with a microtome.

Hematoxylin and Eosin staining: Slides containing paraffin sections were deparaffinized and rehydrated with tap water, stained with hematoxylin solution (Sigma) for 90 seconds, washed continuously with running tap water for 2 minutes, placed in distilled water, dehydrated through an alcohol series, dipped 5 times in Eosin (Sigma) bath, washed immediately in 3 baths of 100% ethanol, cleared with Xylenes and coverslipped with cytoseal™ (Thermo Fisher).

Periodic Acid Schiff staining: Slides containing paraffin sections were deparaffinized and rehydrated to tap water, oxidized in 0.5% periodic acid solution for 5 minutes, rinsed in distilled water, placed in Schiff reagent for 15 minutes, washed in lukewarm tap water for 5 minutes, counterstained in hematoxylin solution for 1 minute, washed in tap water for 5 minutes, dehydrated through an alcohol series, cleared with Xylenes and coverslipped.

**Electron microscopy**

A 0.5 cm segment of the distal ileum was dissected in ice-cold PBS, chopped into several smaller

pieces and fixed overnight at 4°C with 2.5% glutaraldehyde in 0.1 M sodium cacodylate buffer (pH = 7.2) [for P0 samples] or 2% PFA plus 2.5% glutaraldehyde in 0.1 M sodium cacodylate buffer [for P5 samples]. Unstained tissues and TRPML3-NT ImmunoGold-labelled 50 μm-thick intestinal sections were stained in 1% $OsO_4$ solution for 1 hour, embedded in resin, placed in beem capsule and baked overnight in 60°C oven. First, sections were cut at 1 μm, stained with 0.5% toluidine blue on a hot plate for 20-30 seconds, rinsed with $dH_2O$ and air dried. Then, specimen block was shaved down, ultra-thin sections cut at 70 nm thickness, placed on a grid, stained for 10 minutes with uranyl acetate and lead citrate, allowed to dry, and imaged using the FEI Tecnai Spirit G2 120kV electron microscope at Northwestern's Nikon Cell Imaging Facility.

**Dextran uptake**

P0 pups were removed from the mother right after birth -prior to receiving any feeding from the mother- while older pups (P6) were removed from the mother and held in a warm chamber for 1 hour. The animals were then fed, 10ul per 1g weight, with commercially available infant formula (Enfamil, 1 scoop per 2 fl oz water, warmed to 37°C.) with Texas Red-conjugated dextran (Life Technologies) at 1mg/ml. For P6 pups, the animals were returned to the mother overnight before dissection at P7. For P0 pups, the animals remained isolated from the mother and kept in 30°C environment for 3 hours before dissection. After the dissection, intestinal tissues were fixed overnight in 4% paraformaldehyde, washed in PBS, dried off excess moisture and snap frozen in OCT using a dry ice-chilled isopentane bath.

We performed immunohistochemistry using the ABC/DAB signal amplification system (Vector) on frozen sections from Dextran-fed animals using the protocol described above with slight

modifications for LAMP1 and EEA1 staining. Specifically, we omitted the antigen retrieval step. For LAMP1, sections were incubated in primary antibody at 1:50 and biotinylated secondary antibody at 1:5000 For this specific staining, DAB with metal enhancer was used, giving dark grey signals rather than brown signals from traditional DAB. For EEA1 staining, 10% donkey normal serum was used. Sections were incubated in primary antibody at 1:100, and biotinylated secondary antibody at 1:200.

In addition, we also performed immunofluorescent staining on these sections for LAMP1 and EEA1 based on the staining described above with modifications. Specifically, we incubated the sections in 1mM glycine for 30 minutes and rinsed 3 times in 1x PBS after post fixation in an attempt to quench some of the autofluorescence caused by aldehyde fixative. We also added a permeabilization step in which the tissues were incubated in 0.1% triton + PBS for 30 minutes. For LAMP1, sections were then incubated in primary antibody at 1:50 and secondary antibody at 1:500 (DyLight 405 Goat anti-rat, Jackson ImmunoResearch) and goat serum was used for blocking step. For EEA1 staining, sections were incubated in primary antibody at 1:100, and secondary antibody at 1:200 (DyLight 405 Donkey anti-goat, Jackson ImmunoResearch). The 405nm signals were pseudocolored green for clearer visualization.

The amount dextran endocytosis was determined by the total intensity of Texas Red fluorescence per cell. To achieve this, z-stack series of images were taken using from frozen sections mounted in Prolong Gold (Invitrogen) without post fixation using Leica SP5 confocal microscope (63x, 1.4 N.A. objective). All confocal laser intensities and exposures remained identical for all samples. The images were taken every 0.5 um for the entire thickness of the frozen section. The

measurement and analysis for the amount of dextran uptake in the enterocytes were done on imageJ using protocols adapted from (Baqui et al., 1998a, 1998b). In brief, Texas Red fluorescence density was individually measured and combined from each optical section spanning the thickness of a single cell. To calculate total fluorescence per cell per optical section, we followed this equation: Corrected total fluorescence per cell = sum of florescence density per cell – (area of selected cell x mean fluorescence of background readings).

**Enteroid Culture**

Live enteroid cultures, derived from adult or P2 intestines, embedded in matrigel were provided by Dr. Jerrold R. Turner, M.D., Ph.D, Harvard Medical School, MA (formerly at University of Chicago). Enteroids were maintained at 37°C in minigut media: DMEM/F12 (#12634010, Life Technologies) + 2mM Glutamax + 100 units/ml Penn/Strep (#15140-148, Invitrogen) + 10 mM Hepes + 1:100 N2 supplement (#AR009, R&D Systems) + 1:50 B27 supplement (#17504044, Invitrogen) (Sato et al., 2009). To detect endocytosis of the cultured enterocytes, enteroids were exposed to Texas Red-conjugated dextran (Life Technologies) at 0.5 mg/ml in minigut media for 3 hours at 37°C prior to rising for 10 min in fresh media and fixation. For immunohistochemistry, individual enteroids were recovered from matrigel by incubating in cell recovery solution (354253, Corning™) on ice for 20 min. Enteroids in suspension were collected by centrifugation at 100G for 1 min. Staining protocol for TRPML3-NT are described above with a light modification. That is, after each step, enteroids were collected by centrifugation at 100G for 1 min, and resuspended with the appropriate solution for the next step of the protocols. After immunohistochemistry, fluorescence-stained enteroids were either mounted whole onto a glass slide or subjected to sucrose gradients for OCT embedding, freezing and cryosectioning.

Cryosections of enteroides were collected onto glass slides and mounted prior to visualization without postfixation.

# CHAPTER 3:

# Mucolipins and Age-Related Hearing Loss

## 3.1 Abstract

Acquired hearing loss is the predominant neurodegenerative condition associated with aging in humans. Although mutations on several genes are known to cause congenital deafness in newborns, few genes have been implicated in age-related hearing loss (ARHL), perhaps because its cause is likely polygenic. Here, we generated mice lacking lysosomal calcium channel mucolipins 3 and 1 and discovered that they suffered a polygenic form of hearing loss. While mucolipin 1 is ubiquitously expressed in all cells, mucolipin 3 is expressed in a small subset of cochlear cells—hair cells (HCs) and marginal cells of the stria vascularis—and very few other cell types. Mice lacking both mucolipins 3 and 1, but not either one alone, experienced hearing loss as early as at 1 month of age. The severity of hearing impairment progressed from high to low frequencies and increased with age, characteristic of ARHL in human. Early-onset of ARHL in these mice was accompanied by outer hair cell (OHC) loss. Adult mice conditionally lacking mucolipins in HCs exhibited comparable auditory phenotypes, thereby revealing that the reason for OHC loss is mucolipin co-deficiency in the HCs and not in the stria vascularis. Furthermore, we observed that OHCs lacking mucolipins contained abnormally enlarged lysosomes aggregated at the apical region of the cell, while other organelles appeared normal. We also demonstrated that these aberrant lysosomes in OHCs lost their membrane integrity through lysosomal membrane permeabilization that led to the release of lysosomal hydrolase cathepsin D into the cytosol, a known cause of cellular toxicity that explains why and how OHCs die, leading to premature ARHL.

## 3.2 Introduction

In the cochlea, sounds are mechanotransduced by hair cells (HCs) of two types, inners (IHCs) and outers (OHCs). While OHCs mechanically amplify sound-induced vibrations of the organ of Corti (Dallos and Fakler, 2002), IHCs signal synaptically to cochlear neurons, communicating auditory information to the brain (Dannhof and Bruns, 1993; Seal et al., 2008). In order for these cells to transduce sounds properly, the stria vascularis maintains a potassium-rich environment in the endolymphatic compartment of the cochlea, which registers a large positive potential (Wangemann, 2006). Damage to sensory, strial and/or neuronal components can lead to hearing impairment. The most prevalent type of deafness is that acquired with age, termed presbycusis or age related hearing loss (ARHL), and its most common cause is death of cochlear HCs, particularly of the more vulnerable OHCs (Ohlemiller, 2006; Liberman, 2017). Because mammalian HCs are not generated after an early developmental period, the deafness caused by their loss is irreversible. But for the same reason cochlear HCs must be remarkably resilient; they withstand constant high-energy demands and mechanical stimulations, and yet many survive for the lifetime of the organism, which in humans can amount for over a century. Hence, identification of genes involved in ARHL could lead to elucidating the molecular mechanisms responsible for HC longevity. Despite its prevalence, only a few genes are known to associate with progressive ARHL (Ohlemiller, 2006) probably because the loss is polygenic. One approach to study polygenic ARHL has been to map the multiple loci contributing to hearing loss observed in certain strains of mice (Noben-Trauth et al., 2003; Noguchi et al., 2006; Ohlemiller et al., 2008; Keller et al., 2011). In an alternative approach, we generated double

knockout mice lacking two genes suspected to function in degeneration of cochlear cells but that, when mutated alone, did not cause deafness.

Mucolipins constitute a group of Transient Receptor Potential (TRP) cation channels present in the membranes of lysosomes and late endosomes. In mammals, there are three mucolipins (also known as TRPML1, 2 and 3), encoded by the genes Mcoln1, 2 and 3 (hereby referred to as Trpml1, 2 and 3) (Montell, 2005; Zeevi et al., 2007; García-Añoveros and Wiwatpanit, 2014). Loss of function mutations in the human Trpml1 gene cause mucolipidosis type IV (MLIV), a lipid storage disease resulting in lysosomal overload and cellular degeneration (Schiffmann et al., 1993; Slaugenhaupt, 2002). *Trpml1*$^{-/-}$ (ML1KO) mice appear normal for the first six to eight months of age, at which time they develop MLIV-like symptoms (motor incoordination, retinal degeneration and loss of body fat) and die within two weeks (Venugopal et al., 2007; Micsenyi et al., 2009). A dominant mutation in the *Trpml3* gene causes deafness and vestibular impairment characterized by HC loss, anatomical malformation of the stria vascularis and reduced endocochlear potential in the varitint-waddler (*Va*) mouse (Cable and Steel, 1998; Di Palma et al., 2002). This gain-of-function mutation resulted in channels with an increased open probability that sustained a constitutive cationic current lethal to cells (Grimm et al., 2007; Kim et al., 2007; Xu et al., 2007; Nagata et al., 2008), which explains the hair cell death and deafness of the Va mice (Nagata et al., 2008; Castiglioni et al., 2011). However, because the *Va* mutation results in constitutively active mucolipin 3 channels, it does not reveal the contribution this channel may make to HCs and hearing, which requires a null mutation lacking functional mucolipin 3.

*Trpml3*$^{-/-}$ (ML3KO) mice display no hearing impairment, nor any other phenotype

examined (Jörs et al., 2010; Remis et al., 2014), prompting the suspicion that there are one or more genes with redundant functions. Two obvious candidates are the remaining mucolipins, *Trpml1* and *Trpml2*. Mucolipin 2 is expressed in immune cells and not in most mucolipin 3-expressing cells, including HCs (Montell, 2005; Zeevi et al., 2007; García-Añoveros and Wiwatpanit, 2014). However, mucolipin 1 is ubiquitous (Bach, 2001; LaPlante et al., 2002; Bach et al., 2005) and thus could act redundantly with mucolipin 3, as shown in neonatal enterocytes, which express high levels of both mucolipins 3 and 1 and have specialized giant lysosomes. These cells were severely vacuolated in mice lacking both mucolipins 3 and 1, but not either one alone. This pathology involved an enlargement of the specialized lysosomes characteristic of neonatal enterocytes (Remis et al., 2014). We reasoned that mucolipins 3 and 1 may also act redundantly in the inner ear.

Here, we generated mice lacking mucolipin 3 and mucolipin 1 in HCs. Mice lacking lysosomal mucolipins 3 and 1 in HCs displayed hearing loss progressing from high to low frequencies and with age. Absence of both mucolipins in OHCs caused enlargement and permeabilization of lysosomes, a known source of cellular toxicity, and OHC degeneration. These results represent a novel polygenic form of ARHL that involves two lysosomal channels and a lysosomal mechanism in the degeneration of OHCs with age.

## 3.3 Results

### 3.3.1 Accelerated age-related hearing loss in mice lacking mucolipins

**Mice lacking mucolipins 3 and 1 experience accelerated ARHL**

In order to examine the role of lysosomal mucolipins in auditory function, we tested the hearing of mice lacking mucolipin 1 (*Trpml1*$^{-/-}$, ML1KO), lacking mucolipin 3 (*Trpml3*$^{-/-}$, ML3KO), and lacking both mucolipins 3 and 1 (*Trpml3*$^{-/-}$;*Trpml1*$^{-/-}$, DKO), by determining their DPOAE and ABR thresholds at high (27 kHz) and low (12 kHz) frequencies. ABRs measure auditory-evoked neural output from the cochlea to the brainstem (Willott, 2006), while DPOAEs reflect OHC function. The latter are measured from the ear canal by presenting a two-tone stimulus (Martin et al., 2006). Adult mice (~P60 - P120) lacking either mucolipin 1 or 3 alone (ML1KO or ML3KO) had comparable ABR and DPOAE thresholds to wild-type animals at both 27 and 12 kHz (Figure 12A-D). However, adult DKO mice had significantly higher ABR and DPOAE thresholds than controls (wild-type, ML1KO and ML3KO), indicating hearing loss (Figure 12A, B). The raised ABR and DPOAE thresholds in DKO mice are similar, a characteristic of OHC dysfunction.The ABR threshold shift for DKO mice is greater at high (27 kHz) frequency (61.61 ± 4.57 dB) than at low (12 kHz) frequency (21.57 ± 3.66 dB; Figure 1A, C). The DPOAE threshold shift is also larger at 27 kHz (at least 43.47 ± 1.40 dB; this is an underestimate because we could not detect thresholds above 90 dB) than at 12 kHz (28.28 ± 2.96 dB) (Figure 12B, D). These data suggest that DKO mice experience hearing loss which progresses from high to low frequencies, a characteristic of ARHL.

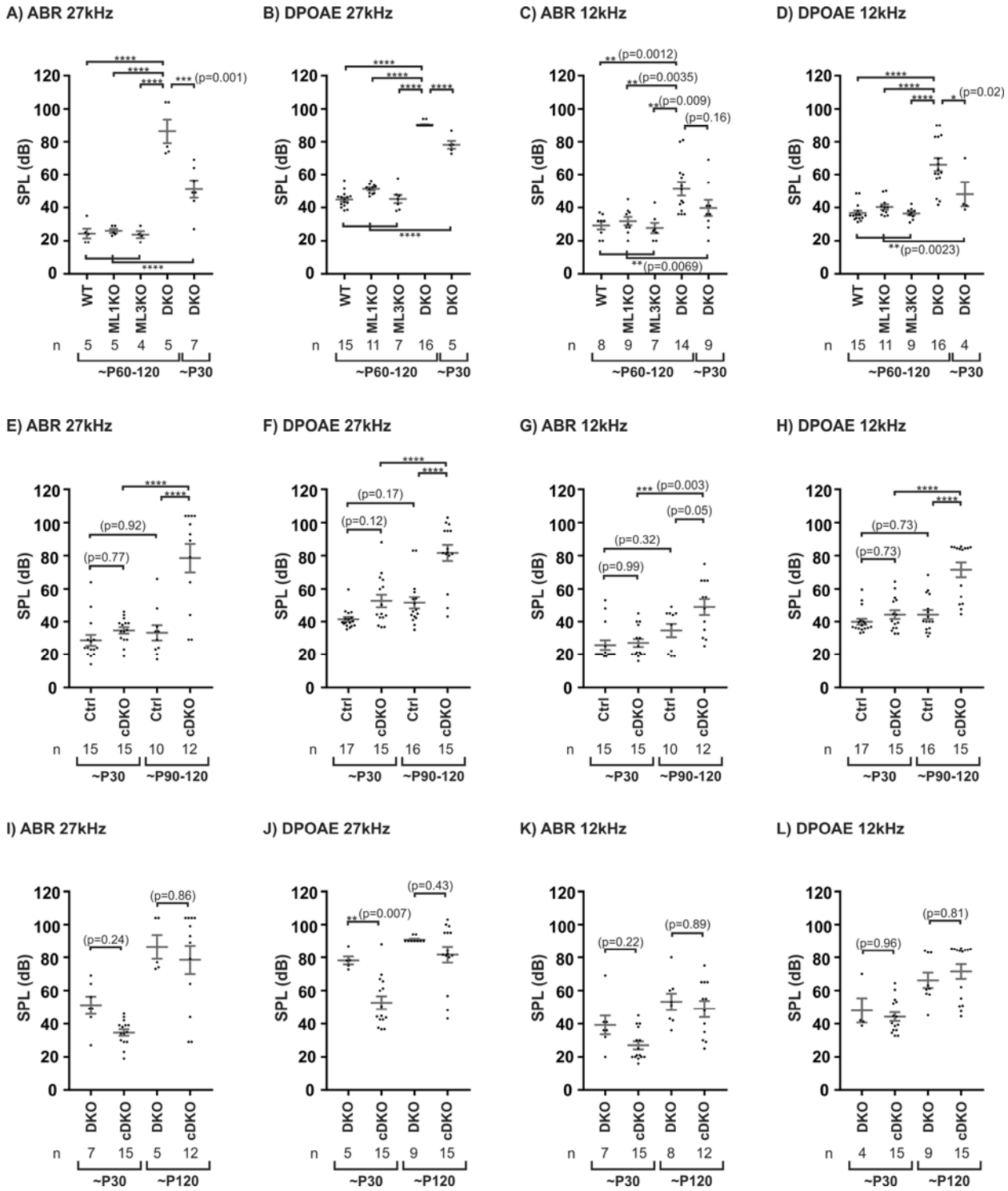


**Figure 12. Co-absence of mucolipins 3 and 1 in HCs, but not either alone, causes age-related hearing loss progressing from high to low frequency. (A-L)** Hearing thresholds at 27

and 12 kHz determined using auditory brainstem responses (ABRs; **A**, **C**, **E**, **G, I, K**) and distortion product otoacoustic emissions (DPOAEs; **B**, **D**, **F**, **H, J, L**) in adult (~P60-120) and juvenile (~P30) mice. (**A, B**) Adult mice lacking both mucolipins 3 and 1 (DKO), but not either alone (ML1KO or ML3KO), have raised ABR (**A**) and DPOAE (**B**) thresholds at 27 kHz compared to wild-type (WT) mice. Juvenile DKO mice (~P30) exhibit somewhat smaller threshold shifts at 27 kHz for both ABR and DPOAE. (**C-D**) Adult DKO mice have a mild hearing loss at 12 kHz indicated by both ABR (**C**) and DPOAE (**D**) threshold shifts. At 12 kHz, juvenile DKO mice have intermediate ABR and DPOAE threshold shifts. (**E-H**) Hearing tests from mice in which mucolipins 3 and 1 are conditionally absent in HCs only (cDKO) indicate that adult cDKO mice (~P120) have raised hearing thresholds at both 27 (**E, F**) and 12 (**G, H**) kHz. Contrary to juvenile DKO mice (**A-D**), juvenile cDKO mice do not exhibit ABR (**E, G**) and DPOAE (**F, H**) threshold shifts at either 27 (**E, F**) or 12 kHz (**G, H**). (**I-L**) Age-matched data (P30 and P120) from (**A-H**) were replotted for statistical comparisons of ABR (**I, K**) and DPOAE (**J, L**) thresholds between DKO and cDKO mice at 27 (**I, J**) and 12 kHz (**K, L**). At P30, while there is no statistical difference of auditory thresholds between DKO and cDKO animals in most cases, except for DPOAE thresholds at 27 kHz (**J**), juvenile DKO mice appeared to consistenly have slightly higher ABR and DPOAE threshold shifts than juvenile cDKO mice. However, by P120, both DKO and cDKO mice exhibit comparable ABR (**I, K**) and DPOAE (**J, L**) thresholds at both at 27 (**I, J**) and 12 kHz (**K, L**). ****, $p \leq 0.0001$.

Juvenile (P30) DKO mice already exhibit some hearing loss which, as in the adult, is more pronounced at 27 than at 12 kHz (Figure 12A-D). ABR threshold shifts of juvenile DKO mice (26.36 ± 3.99 dB at 27 kHz and 9.97 ± 3.82 dB at 12 kHz) are smaller than the threshold shifts of adult DKO mice 61.61 ± 4.57 dB at 27 kHz and 21.57 ± 3.66 dB at 12 kHz) (Figure 12A, C). Similarly, juvenile DKO mice also exhibit DPOAE threshold shifts (31.15 ± 2.64 dB at 27 kHz and 10.23 ± 3.39 dB at 12 kHz), but the loss of sensitivity is again less than in older adult DKO animals (Figure 12B, D). Taken together, our data indicate that mice lacking both mucolipins 3 and 1 suffer an early onset form of ARHL.

**Mucolipin 3 and 1 co-absence in HCs causes ARHL**

In the cochlea, mucolipin 3 is expressed in both auditory HCs and stria vascularis (Castiglioni et al., 2011) (Figure 13), whereas mucolipin 1 is ubiquitous (Bach, 2001; LaPlante et al., 2002; Bach et al., 2005). In neonatal cochleae (P11), mucolipin 3 is expressed in IHCs, OHCs and stria vascularis in a cytoplasmic punctate pattern, consistent with its previously reported lysosomal localization in these cells (Castiglioni et al., 2011). Mucolipin 3 immunoreactivity is primarily located apically in OHCs, but dispersed throughout the IHC cytoplasm (Figure 13A, E). Our results only disagree with this prior report in one aspect: while it was believed that mucolipin 3 disappeared from mature OHCs, we now find that in the mature cochlea (~P120), OHCs maintain mucolipin 3 immunoreactivity, albeit at a lower level that IHCs (Figure 13A). In stria vascularis, mucolipin 3 immunoreactivity appears dispersed at P11 but surround the nuclei of strial marginal cells by P120 (Figure 13B, F), as previously reported (Castiglioni et al., 2011). As a negative control and as evidence that the immunoreactivity was

specific for TRPML3, immunohistochemistry in ML3KO tissues gave no signal above background in either HCs or stria vascularis (Figure 13C, D). The restricted expression of mucolipin 3 in HCs and strial cells suggests that mucolipins could contribute to auditory functions of both HCs and stria vascularis.

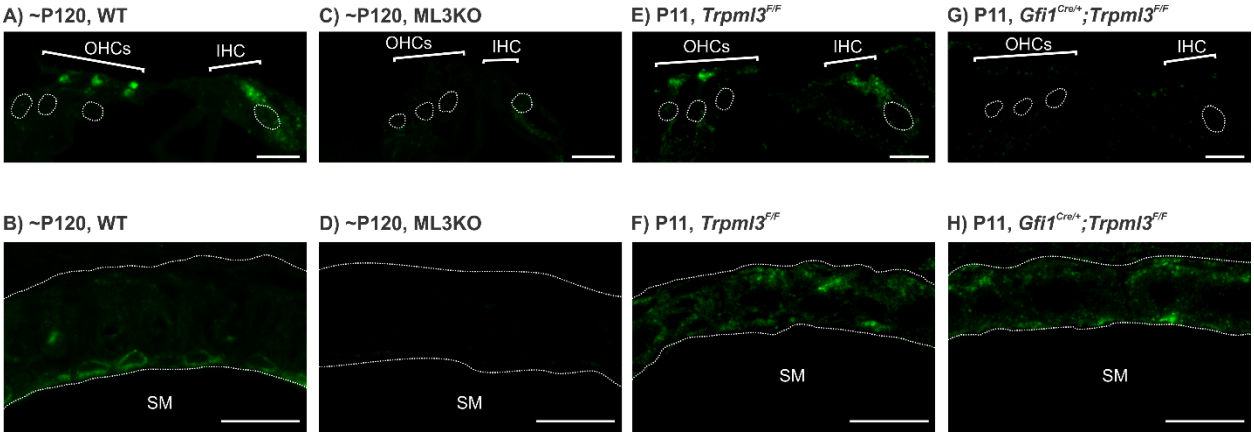


**Figure 13. Mucolipin 3 is localized to HCs and the stria vascularis in both adult and neonatal cochleae.** Immunohistochemistry of the mucolipin 3 carboxyl-terminus (TRPML3-CT) on adult (~P120) (**A-D**) and neonatal (P11) (**E-H**) cochleae. (**A**) TRPML3-CT labels vesicles in both IHCs and OHCs as well as cells of stria vascularis (**B**) in wild-type cochlea. (**C, D**) In ML3KO tissues, there is no TRPML3-CT immunoreactivity detected above the background signals in either HCs (**C**) or stria vascularis (**D**). (**E, F**) Neonatal *Trpml3*$^{F/F}$ HCs express mucolipin 3 in a similar pattern as adult HCs, however, the levels of TRPML3-CT immunoreactivity in P11 OHCs and IHCs are comparable (**E**). Mucolipin 3 appears more dispersed in the P11 stria vascularis (**F**). (**G, H**) There is no TRPML3-CT immunoreactivity detected in *Gfi*$^{Cre/+}$*;Trpml3*$^{F/F}$ HCs (**G**), while its signal is detected in the stria vascularis (**H**). Scale bars are 10µm (**A, C, E, G)** and 20µm (**B, D, F, H**). For clarity, HC nuclei and strial boarder were outlined in top panels. SM, scala media.

Because defects in either HCs (Ohlemiller, 2006; Potter et al., 2016) or in stria vascularis can cause progressive loss of HCs and hearing (Gamp et al., 2003; Knipper et al., 2006; Ohlemiller et al., 2008), accelerated ARHL in DKO mice could be due to the co-absence of both mucolipins 3 and 1 in HCs and/or stria vascularis. In order to determine which cells require mucolipins 3 and 1 to maintain hearing, we used a floxed allele of *Trpml3* (Remis et al., 2014), a complete KO of *Trpml1* (Venugopal et al., 2007) and the hair cell-specific $Gfi1^{Cre}$ line (Yang et al., 2010) to generate mice conditionally lacking both mucolipins 3 and 1 in HCs but not in strial cells ($Gfi1^{Cre/+};Trpml3^{F/F};Trpml1^{-/-}$, cDKO). In the cochlea of these mice, $Gfi1^{Cre}$ ablates *Trpml3* only in auditory HCs (Figure 13E-H), while all cells lack mucolipin 1. Because animals lacking either mucolipin 1 or 3 alone do not experience hearing defects (Figure 12A-D), we grouped together littermate controls for statistical analysis.

Adult (~P120) cDKO mice experienced hearing loss like DKO mice with comparable auditory threshold shifts and frequency dependence (Figure 12). Specifically, ABR threshold shifts among adult cDKO were 45.30 ± 10.31 dB at 27 kHz and 14.32 ± 6.51 dB at 12 kHz (Figure 12H, G). DPOAE threshold shifts for adult cDKO were 30.12 ± 5.91 dB at 27 kHz and 27.23 ± 5.12 dB at 12 kHz (Figure 12F, H). ABR and DPOAE threshold shifts were again more severe at high (27 kHz, Figure 12E, F) than low (12 kHz, Figure 12G, H) frequencies, the same pattern observed in adult DKO mice (Figure 12A-D). Finally, ABR and DPOAE thresholds for ~P120 cDKOmice did not differ from those observed in ~P120 DKO mice (Figure 12I-L). Hence, we concluded that by 4 months of age, co-absence of mucolipins 3 and 1 in HCs was the main cause of the early-onset ARHL observed in our mouse models.

However, we found that juvenile (P30) cDKO mice did not display raised ABR and DPOAE thresholds at either 27 and 12kHz (Figure 12E-H), unlike juvenile DKO mice (Figure 12A-D). While, at P30, cDKO mice had slightly higher average ABR and DPOAE thresholds than their control littermates, this difference was not statistically significant (Figure 12E-H). Although the average hearing thresholds at P30 were higher in juvenile DKO than in cDKO mice, this apparent difference was also not statistically significant in most of cases (the exception being the DPOAE thresholds—but not of ABRs—at 27 kHz) (Figure 12I-L). It is hence not possible for us to conclude with certainty that the levels of hearing and the extents of hearing loss differ at 1 month of age. These apparent discrepancies between juvenile DKO and cDKO mice may be inherent to the variability in hearing at this early age, when hearing loss is beginning to develop. Alternatively, if these differences are real they would reflect only a small contribution of strial mucolipin co-deficiency to hearing loss at early stages. Even if these scenario were true, the strial contribution would be small and transient, as it is no longer detected by 4 months of age.

### 3.3.2 Cochlea degeneration in mice lacking mucolipins

Lysosomal defects in stria vascularis can lead to progressive hearing loss. In particular, in mice mutant for lysosomal LIMP2, the potassium channel KCNQ1 is not localized to the apical membrane of strial marginal cells, and this leads to progressive hearing loss and HC degeneration (Gamp et al., 2003; Knipper et al., 2006). Hence, we examined the stria vascularis of mucolipin co-deficient adult (4 to 4.5 months old) mice. The stria vascularis was of normal thickness and KCNQ1 was properly localized in DKO mice (Figure 14A, B). The lack of an

anatomical phenotype is consistent with the genetic evidence that mucolipins are required in HCs, but not in strial cells, to prevent early-onset ARHL.

On the other hand, we observed a small but consistent increase in OHC (~1.4 fold), but not IHC size, in DKO cochleae, determined by the surface area of HCs just under the cuticular plate (Figure 14C-F). This could be an early sign of OHC dysfunction leading to hearing loss in mice lacking mucolipins 3 and 1 in HCs as cells in the process of dying are often swollen (Trump et al., 1997). These results further suggest that the lack of mucolipins 3 and 1 in HCs, especially OHCs, is likely the primary cause of early-onset ARHL in these mice.

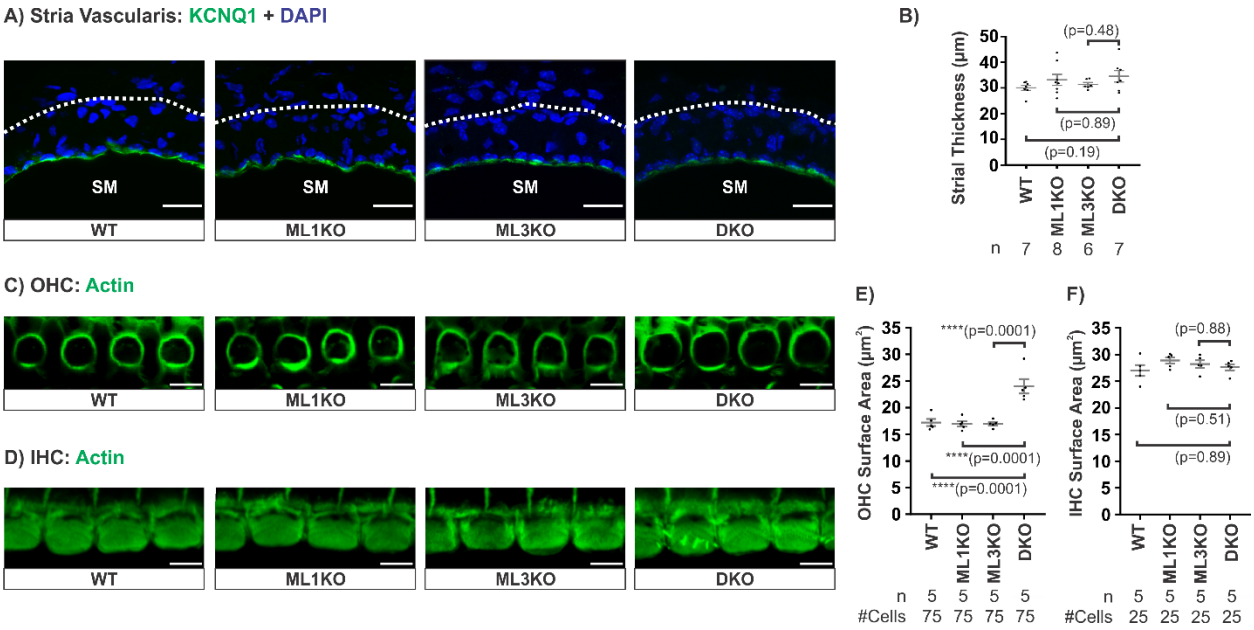


**Figure 14. There is an anatomical defect in OHCs but not in the stria vascularis from cochleae lacking both mucolipins 3 and 1.** (**A**) Immunoreactivity of potassium channel KCNQ1 in the stria vascularis shows that there is no mislocalization of this channel in DKO cochlea compared to WT, ML1KO and ML3KO animals. SM, scala media. (**B**) Quantification of strial thickness indicates that there is no strial degeneration in DKO cochlea. (**C-D**) Actin labeling reveals that OHCs (**C**) but not IHCs (**D**) from DKO cochlea are larger than those of control cochleae. (**E-F**) Quantification of hair cell apical surface area, measured just under the cuticular plate of hair cells from middle turn, confirms that DKO OHCs are larger than the controls. Samples were from 4 - 4.5 month old animals. Scale bars are 20µm (**A**) and 5µm (**C-D**).

**Mucolipin 3 and 1 co-absence in HCs causes OHC degeneration**

The most common cause of deafness and hearing loss is degeneration of OHCs. Hence, we examined the cochleae of adult (~P120) mice subjected to hearing testing. At the cochlear positions associated with 27 and 12 kHz (Müller et al., 2005), there is no IHC loss regardless of genotype (Figure 15). However, there is a high degree of OHC loss in DKO and cDKO cochleae, especially at the basal 27 kHz place, but not in wild-type, ML1KO and ML3KO controls (Figure 15A-E). The level of OHC loss around the 27 kHz position is much greater than around 12 kHz, which is consistent with the greater ABR and DPOAE threshold shifts at 27 kHz (Figure 12). Cytocochleograms also reveal that wild-type, ML1KO and ML3KO mice display a loss of OHCs at the extreme base of the cochlea (Figure 15F). This loss, accompanied by high frequency hearing loss, is a characteristic of the C57BL/6 inbred strain (Parham, 1997; Spongr et al., 1997; Ison et al., 2007). Because all mice tested have a genetic background of C57BL/6 mixed with Sv129 and 129S6, and the ABR and DPOAE thresholds of the ML1KO and ML3KO mice do not differ from those of their wild-type littermates (Figure 15A-D), their loss of OHCs at the extreme base is not attributed to the loss of mucolipins. However, the cytocochleograms of DKO and cDKO mice reveal a much greater OHC loss at more apical positions compared to littermate controls. In addition, the fact that there is no obvious IHC loss in DKO and cDKO mice agrees with their comparably raised DPOAE and ABR thresholds, which are characteristic of OHC dysfunction (Figure 12B-H). This pattern of OHC loss, from high (cochlear base) to low (cochlear apex) frequencies, is consistent with the pattern of hearing loss observed (Figure 12). Finally the extent of OHC loss was virtually identical between DKO and cDKO mice, which

demonstrates that the cause of OHC degeneration is the co-absence of mucolipins 3 and 1 in HCs, and not in strial cells (Figure 15F).

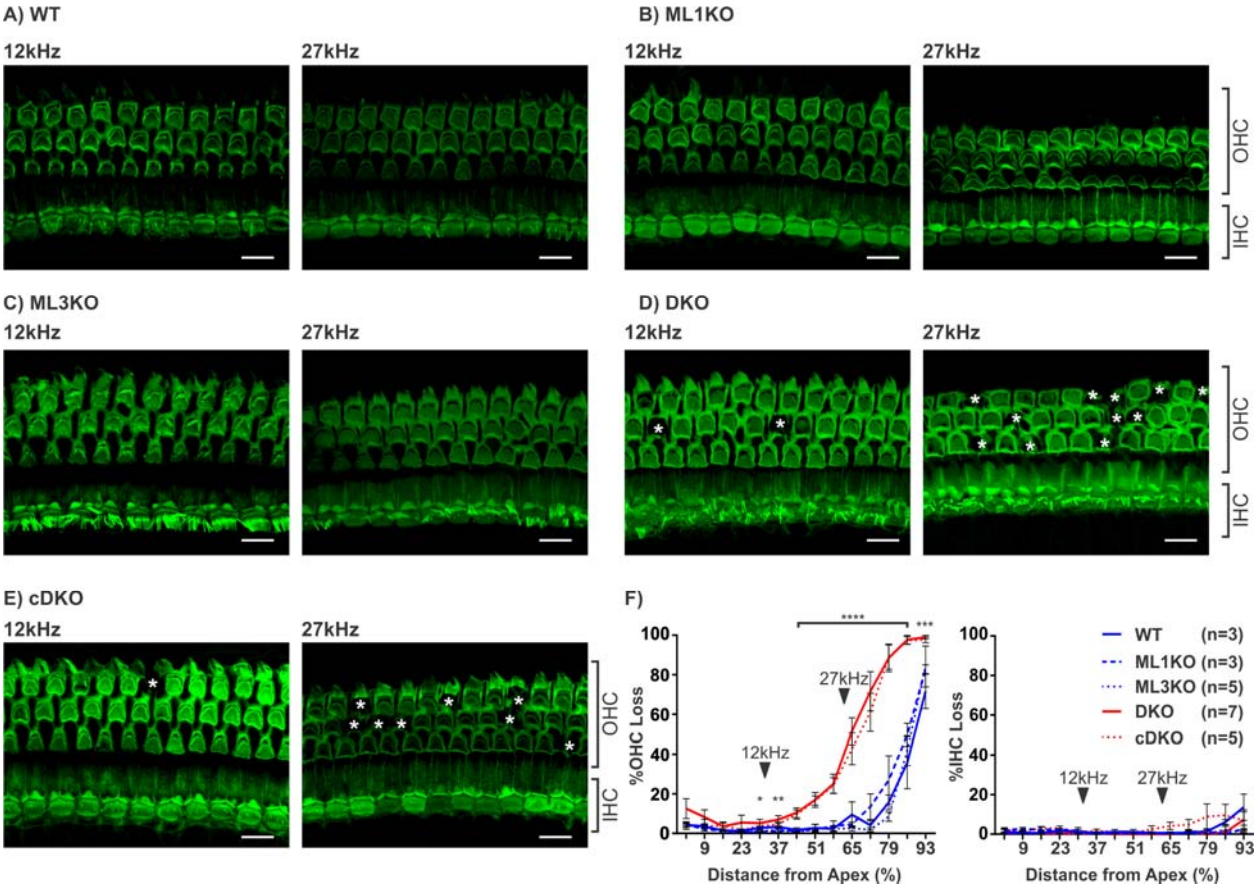


**Figure 15. Age-related hearing loss in animals lacking both mucolipins 3 and 1 is accompanied by OHC death.** (**A-E**) Actin labeling shows hair cells from a whole-mount surface preparation of the adult cochlea (~P120). Cochlear positions transmitting sound at 12 and 27 kHz were calculated using a mouse frequency-place map (Müller et al., 2005). There is no hair cell loss at 12 and 27 kHz positions in WT (**A**), ML1KO (**B**) and ML3KO (**C**) cochleae. However, OHC loss can be observed in DKO (**D**) and cDKO (**E**) cochleae (asterisks). The extent of OHC loss is more severe at the 27 kHz position. No IHC loss was observed at either position. (**F**) Cytocochleograms showing %OHC and %IHC loss along the cochlear spiral for all

genotypes (**A-E**). *, p=0.014; **, p=0.009; ***, p=0.0008; ****, p≤0.0001. Positions corresponding to 12 and 27 kHz are indicated by arrowheads. Scale bars are 10μm.

### 3.3.3 Lysosomal pathology in hair cells lacking mucolipins

**Lysosomes in OHCs lacking mucolipins 3 and 1 are enlarged**

Because mucolipins are lysosomal channels, we examined these organelles using immunohistochemistry for the lysosomal marker LAMP1. First, we found that DKO OHCs have enhanced LAMP1 immunoreactivity compared to control OHCs (Figure 16A, B). When comparing whole-cell LAMP1 fluorescence from immunohistochemistry on frozen cochlear sections, DKO OHCs have ~3.7 fold higher LAMP1 immunoreactivity than those from control cochleae (Figure 15C: wild-type, 6656 AU ± 2561 SEM; ML1KO , 5730 AU ± 2166 SEM; ML3KO , 7721 AU ± 2063 SEM; DKO, 30793 AU ± 6917). This lysosomal enrichment in DKO OHCs was not dependent on their position along the length of the cochlea, as we did not observe differences in LAMP1 staining in OHCs from middle, apical-middle or apical turns (Figure 16D). Hence, to further explore the subcellular basis of ARHL in DKO mice, we consistently examined OHCs from middle cochlear turns, which roughly correspond to 25-75% distance from the cochlear apex, and hence to the area of OHC loss (Figure 15F).

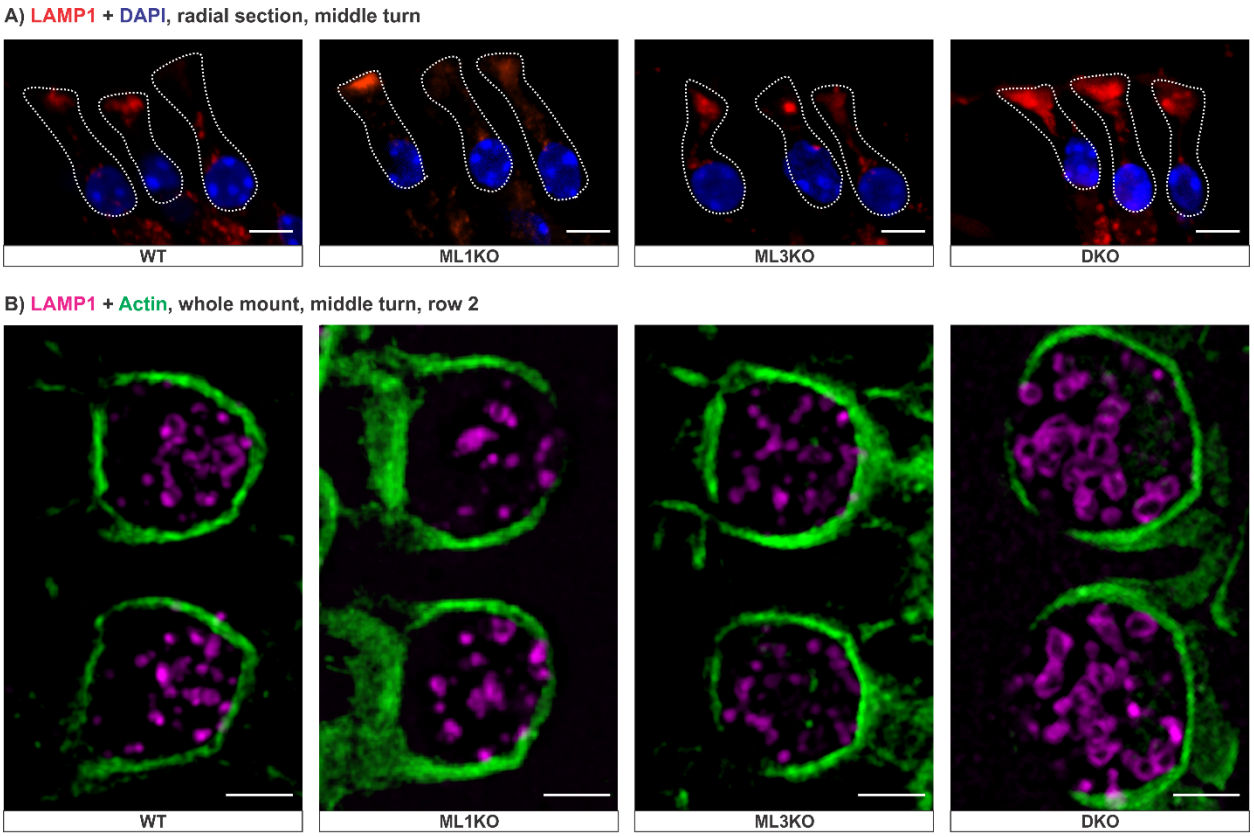
A) LAMP1 + DAPI, radial section, middle turn
WT
ML1KO
ML3KO
DKO
B) LAMP1 + Actin, whole mount, middle turn, row 2
WT
ML1KO
ML3KO
DKO

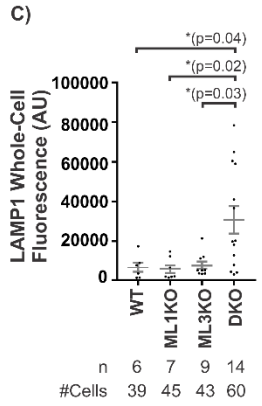
C)
LAMP1 Whole-Cell Fluorescence (AU)
*(p=0.04)
*(p=0.02)
*(p=0.03)
WT
ML1KO
ML3KO
DKO
n 6 7 9 14
#Cells 39 45 43 60

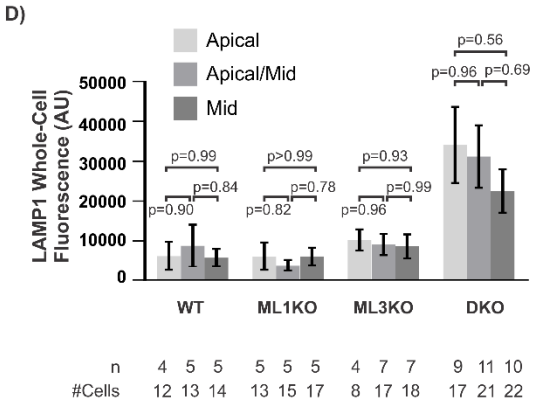
D)
Apical
Apical/Mid
Mid
LAMP1 Whole-Cell Fluorescence (AU)
p=0.90
p=0.99
p=0.84
p=0.82
p>0.99
p=0.78
p=0.96
p=0.93
p=0.99
p=0.56
p=0.96
p=0.69
WT
ML1KO
ML3KO
DKO
n 4 5 5 5 5 5 4 7 7 9 11 10
#Cells 12 13 14 13 15 17 8 17 18 17 21 22

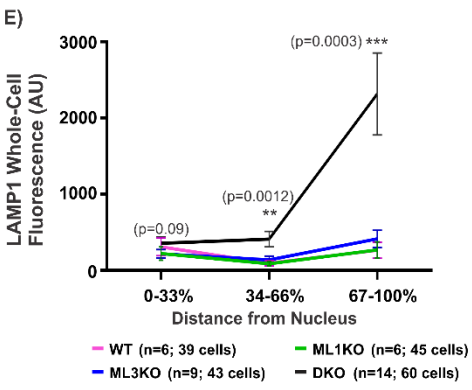
E)
LAMP1 Whole-Cell Fluorescence (AU)
(p=0.09)
(p=0.0012) **
(p=0.0003) ***
0-33%
34-66%
67-100%
Distance from Nucleus
WT (n=6; 39 cells)
ML1KO (n=6; 45 cells)
ML3KO (n=9; 43 cells)
DKO (n=14; 60 cells)

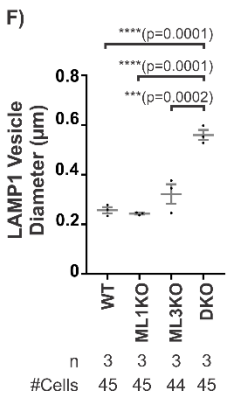
F)
LAMP1 Vesicle Diameter (µm)
****(p=0.0001)
****(p=0.0001)
***(p=0.0002)
WT
ML1KO
ML3KO
DKO
n 3 3 3 3
#Cells 45 45 44 45

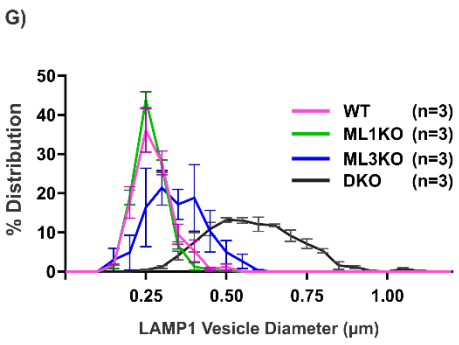
G)
% Distribution
WT (n=3)
ML1KO (n=3)
ML3KO (n=3)
DKO (n=3)
LAMP1 Vesicle Diameter (µm)

**Figure 16. OHCs lacking mucolipins 3 and 1 possess pathologically enlarged lysosomes.** (**A**) Immunoreactivity of LAMP1 (a lysososomal membrane protein) in adult (~P120) OHCs reveals apical accumulation of lysosomes in DKO OHCs but not in those from WT, ML1KO and ML3KO control cochleae. (**B**) Superresolution structured illumination microscopy shows that DKO OHCs, but not the controls, possess enlarged lysosomes as indicated by LAMP1 immunoreactivity. Images illustrated in (**B**) were OHCs from row 2. (**C**) Quantification of total whole-cell LAMP1 fluorescence from (**A**) reveals a significant increase in LAMP1 in DKO OHCs but not in control cochleae. (**D**) LAMP1 whole-cell intensity values used in (**C**) are re-plotted separately based on cochlear position (apical, apical/middle and middle). We observed no difference in OHC LAMP1 intensity between cochlear turns within each genotype. (**E**) LAMP1 intensity values used in (**C**) are re-teplotted binning the apical-basal axis of OHCs in 3 segments based on the % distance from the nucleus. (**F**) By measuring LAMP1 vesicle diameter from images taken from confocal and structured illumination microscopy microscopy, we found that lysosomal diameter of DKO OHCs is ~2.18 fold larger than that from control OHCs. (**G**) A frequency distribution plot of LAMP1 vesicle diameter in all genotypes. Scale bars are 5μm (**A**) and 2μm (**B**). AU stands for arbitrary units of fluorescent intensity.

The lysosomal (LAMP1) increase in DKO OHCs was not homogeneous throughout the cells, but concentrated at their most apical third. At the basal third (0-33% distance from the nucleus) of the cell, DKO OHC contained approximately the same amount of LAMP1 immunofluorescence as controls OHCs (Figure 16E: wild-type, 3086 AU ± 1174 SEM; ML1KO , 2202 AU ± 887 SEM; ML3KO, 2268 AU ± 554 SEM; DKO, 3560 AU ± 851 SEM). There was a slight increase in overall LAMP1 at the middle third (34-66% distance from the nucleus) of DKO OHC (Figure 16E: wild-type, 943 AU ± 384 SEM; ML1KO , 845 AU ± 278 SEM; ML3KO, 1381 AU ± 509 SEM; DKO, 4094 AU ± 1019 SEM). However, there was a striking increase of LAMP1 fluorescence at the apical third portion of DKO OHCs (Figure 16E: wild-type, 2621 AU ± 1087 SEM; ML1KO , 2683 AU ± 1070 SEM; ML3KO, 4119 AU ± 1143 SEM; DKO, 23139 AU ± 5397 SEM).

The increase on LAMP1 immunoreactivity could be due to an increase in LAMP1 protein concentration in lysosome membranes, in the number of lysosomes, or in their size. To more accurately visualize lysosomes in OHCs, we performed LAMP immunohistochemistry on whole-mount surface preparations of the organ of Corti (which affords better preservation of cellular structures that frozen sections) and imaged them with superresolution structured illumination microscopy (SIM). Because LAMP1 localizes to the membrane of lysosomes, we used its immunofluorescence to measure lysosomal size. To facilitate comparisons, we used the same criteria for selection of representative lysosomes for measurements in control and DKO OHCs: 1) we only selected lysosomes that were visibly isolated as the microscope could not resolve objects closer than ~100 nm; and 2) we only measured lysosomal diameter using the optical plane that yielded the largest diameter, since we found lysosomes to be roughly spherical. Our

examinations indicate that lysosomes (LAMP1 positive vesicles) were larger in OHCs from DKO cochleae than those from the controls (Figure 16B). Specifically, lysosomes from DKO OHCs had a 2.18 fold larger diameter than those measured from control OHCs (Figure 16B, F: wild-type, 0.257 ± 0.01 μm SEM; ML1KO , 0.243 ± 0.003 μm SEM, ML3KO , 0.322 ± 0.04 μm SEM; DKO, 0.560 ± 0.02 μm SEM). Increasing lysosomal diameter by 2.18 fold (from wild-type to DKO) would result in a 4.75-fold increase in lysosomal surface area, which accounts for the 4.63-fold increase in LAMP1 immunoreactivity, as it is a lysosomal membrane marker (Figure 16C). Moreover, we found that DKO OHCs not only have larger lysosomes (~0.25 – 0.8μm) but also fewer smaller ones (~0.15 – 0.4 μm), of the size typically found in control OHCs (Figure 16G). Our results suggest that the increase in overall LAMP1 fluorescence observed in mucolipin co-deficient OHCs (Figure 16A, C) is not due to an increase in the number of lysosomes or in the density of LAMP1 protein, but to an increase in the size of the lysosomes.

**Autophagy, mitophagy and pexophagy appear unaltered in mucolipin co-defficient OHCs**

Lysosomal defects have been shown to lead to cytotoxicity in two ways. One is by a failing to degrade damaged organelles (such as mitochondria or peroxisomes) that have become toxic, a process generally performed through autophagy. Another way lysosomes can harm cells is by becoming toxic themselves, a process involving permeabilization of their membranes (Boya and Kroemer, 2008; Oku et al., 2017). Lysosomes harbor within their lumens hydrolytic enzymes that would be harmful if released into the cytosol. We explored whether either of these mechanisms could account for the OHC degeneration caused by mucolipin co-deficiency. Initially we focused on organelles whose dysfunction causes OHC loss: peroxisomes

(Delmaghani et al., 2015) and mitochondria (Chen and Tang, 2014; Seo et al., 2017). These organelles have a limited lifespan and when damaged are removed by lysosomes through the processes of pexophagy and mitophagy. If these processes were impaired, we would expect an increase in the number of such organelles.

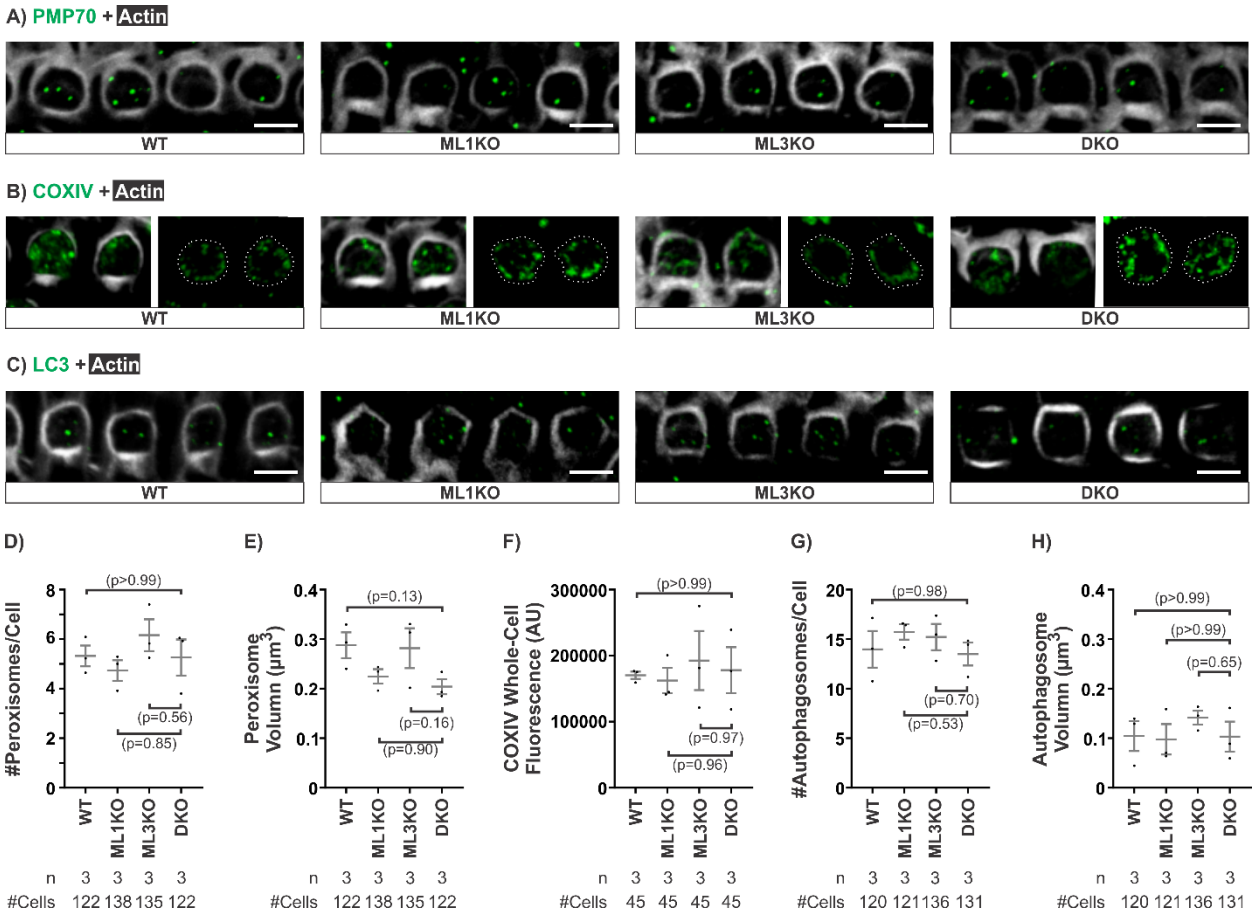


**Figure 17. Enlarged lysosomes in OHCs lacking mucolipins 3 and 1 do not cause defects in lysosomal degradation of damaged organelles.** (**A-C**) Whole-mount cochleae from WT, ML1KO, ML3KO and DKO adult (~P120) animals using different organelle markers: peroxisome (PMP70, **A**) and mitochondria (COXIV, **B**) and autophagosome (LC3, **C**). There is no apparent defect in distributions and numbers of peroxisomes (**A**), mitochondria (**B**) and

autophagosomes (**C**). (**B**) For each genotype, the region below OHC's cuticular plate was shown on the left, and the region at the middle of OHC (an optical section taken from the space between the cuticular plate and the nucleus) was shown on the right. Because there is no actin signal on the basolateral membrane at the region in the middle of OHC, OHC boarder was outlined in white. (**A-C**) Unless otherwise noted, representative images were reconstructed from a projection of 8 confocal optical sections spanding 0.88 μm under the cuticular plate. (**D, E**) The number of peroxisomes per OHC and peroxisomal volume, indicated by PMP70 immunoreactivity, from DKO OHCs are similar to those from controls. **(F**) Whole-cell fluorescence of COXIV did not differ between DKO and control OHCs. (**G, H**) The number of autophagosomes per OHC and autophagosomal volume, indicated by LC3 immunoreactivity, from DKO OHCs are similar to controls. Scale bars are 5μm. AU stands for arbitrary units of fluorescent intensity.

Because dysfunctional and/or damaged peroxisomes can increase sensitivity to noise-induced hearing loss (NIHL) even at neonatal stages (Delmaghani et al., 2015), we used a peroxisomal marker PMP70 to examine whether there was any peroxisomal accumulation or defect in DKO OHCs (Figure 17A, D, E). Both control and DKO OHCs had similar numbers of peroxisomes per cell (Figure 17D: wild-type, 5.32 ± 0.42 SEM; ML1KO, 4.73 ± 0.45 SEM, ML3KO, 6.16 ± 0.64 SEM; DKO, 5.26 ± 0.73 SEM), and the peroxisomes were of similar size (Figure 17E: wild-type, 0.289 ± 0.024 μm3 SEM; ML1KO, 0.225 ± 0.015 μm3 SEM, ML3KO, 0.282 ± 0.040 μm3 SEM; DKO, 0.204 ± 0.01 μm3 SEM). Hence, we did not detect peroxisomal abnormalities in mucolipin co-deficient OHCs.

Because defects in mitochondrial physiology can cause HC death (Fischel-Ghodsian et al., 1997; Chen and Tang, 2014), we examined whether there was any mitochondrial defect in DKO OHCs using antibodies to the mitochondrial cytochrome C oxidase subunit IV (COXIV) (Figure 6B). COXIV immunoreactivity was strong and dense under the OHC's apical cuticular plate and along the basolateral membrane (left panels: COXIV signals at OHC apical portion; right panels: COXIV signals at basolateral membrane from OHC middle portion; Figure 17B). Because mitochondria exist in a range of shapes and sizes from tubular to fragmented (Westermann, 2012), our confocal imaging could not quantify the number of these organelles. We, therefore, examined whole-cell intensity of COXIV immunoreactivity in individual OHCs as an indirect way to determine whether there was mitochondrial accumulation. Similar to the PMP70 immunostaining, we did not detect any difference in COXIV whole-cell fluorescence in DKO OHCs compared to controls (Figure 17F: wild-type, 170385 ± 5483 AU SEM; ML1KO, 162342 ± 19183 AU SEM; ML3KO, 192623 ± 44740 AU SEM; DKO, 178165 ± 34829 AU SEM).

Lysosomes degrade these and other damaged organelles via autophagy, a process in which a double membrane encircles the cellular components to be degraded, forming an autophagosome that fuses with the lysosome. Because defects in autophagy have also been found to promote ARHL and HC degeneration (Fujimoto et al., 2017), we used immunoreactivity to LC3 to visualize autophagosomes. Although LC3 exists in a diffuse cytosolic form, it will coalesce on autophagosome membranes, giving a punctate pattern (Mizushima, 2009). We found that there was no increase or decrease in autophagosomes in DKO OHCs as indicated by the number of LC3 puncta (Figure 17C, G, H). Specifically, both control and DKO OHCs have ~14

autophagosomes per cell (Figure 17G: wild-type, 13.98 ± 1.85 SEM; ML1KO, 15.73 ± 0.78 SEM, ML3KO, 15.22 ± 1.32 SEM; DKO, 13.50 ± 1.16 SEM). We also noted no alteration in the volume of autophagosomes, which is ~0.1μm3 (Figure 17H: wild-type, 0.104 ± 0.030 μm3 SEM; ML1KO, 0.098 ± 0.031 μm3 SEM, ML3KO, 0.141± 0.014 μm3 SEM; DKO, 0.103± 0.030 μm3 SEM).

In conclusion, we detected no aberrant accumulation (or decrease) of autophagosomes, peroxisomes or mitochondria in OHC lacking mucolipins 3 and 1, as would be expected if lysosomes failed to perform the intracellular digestion of damaged organelles.

**Lysosomes in OHCs lacking mucolipins 3 and 1 are permeabilized**

Lysosomal membrane permeabilization can trigger multiple cell death pathways, presumably due to the release into the cytosol of the hydrolytic enzymes normally safely retained within the lumen of the organelle (Brunk et al., 1997; Ono et al., 2003; Boya and Kroemer, 2008; Aits et al., 2015). Because larger lysosomes are more susceptible to lysosomal membrane permeabilization (Ono et al., 2003), we examined lysosomal integrity in OHCs using the galectin 3 assay as an indicator of lysosomal membrane permeabilization (Aits et al., 2015). Galectin 3 is a cytosolic lectin with high binding-affinity to the glycocalyx located on the luminal surface of lysosomes. Because galectin 3 is impermeable to membranes, it does not normally localize to the lumen of lysosomes. However, if the lysosomal membrane is compromised, galectin 3 translocates to the lumen. Indeed, we observed puncta of galectin 3 immunoreactivity in DKO OHCs associated with lysosomes, as indicated by a double-staining of LAMP1 and galectin 3

(Figure 7D), while the galectin 3 signal in control OHCs was cytosolic (Figure 18A-C). In addition, superresolution SIM reveals that galectin 3 is surrounded by the lysosomal membrane marker LAMP1, and, therefore, localized to the lysosomal lumen (Figure 18E).

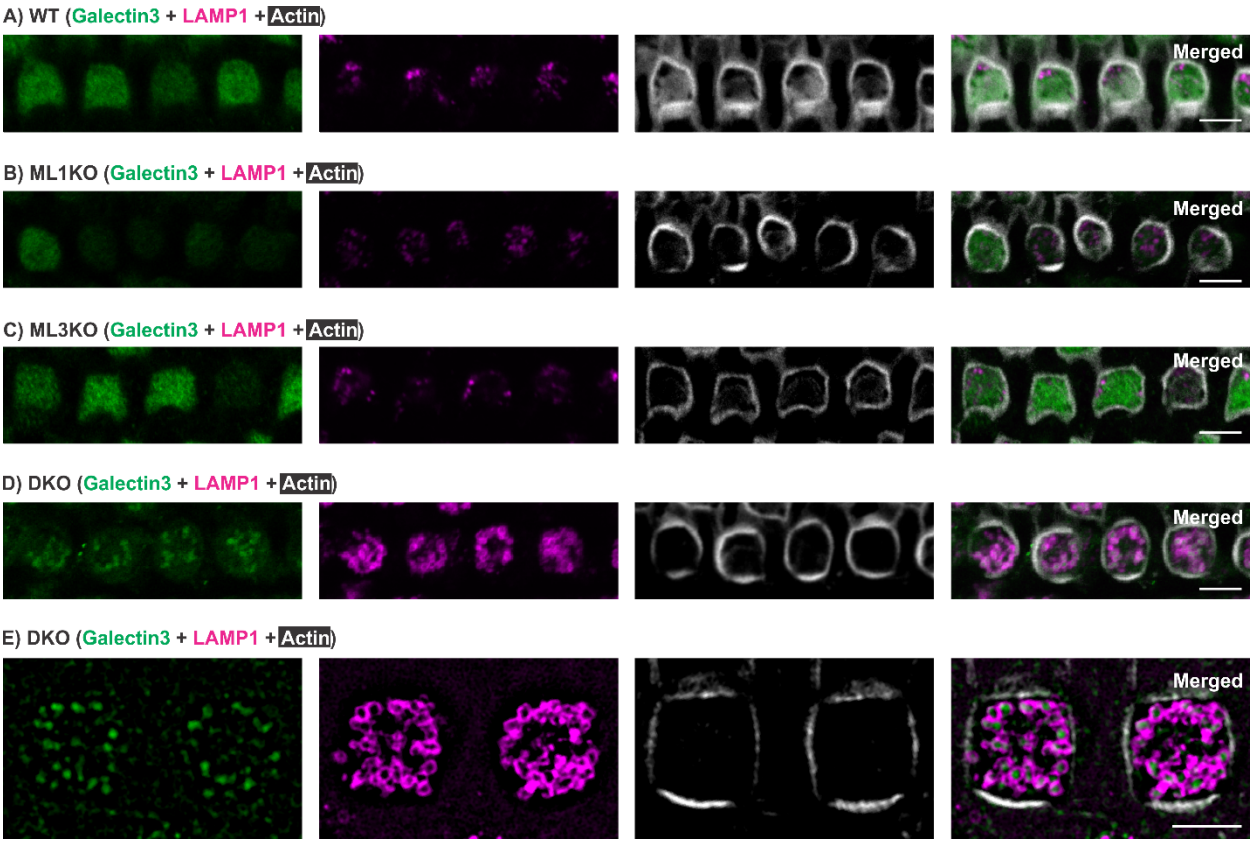


**Figure 18. OHCs lacking mucolipins 3 and 1 exhibit lysosomal membrane permeabilization.** (**A-D**) Immunoreactivity of galectin 3, a membrane-impermeable cytosolic lectin with high affinity for the luminal lysosomal glycocalyx (Aits et al., 2015), and lysosomal associated membrane protein LAMP1 reveal that lysosomal membranes in DKO OHCs are permeabilized. Galectin 3 is cytosolic in WT (**A**), ML1KO (**B**) and ML3KO (**C**) OHCs, and its expression level varied. (**D**) In contrast, galectin 3 immunoreactivity has a vesicular pattern that is associated with LAMP1 signal in DKO OHCs. (**E**) Superresolution structured illumination microscopy shows that galectin 3 is localized to lysosomal lumen. Scale bars are 5µm (**A-D**) and 2µm (**E**).

An expected consequence of lysosomal membrane permeabilization would be the release of hydrolytic enzymes from the lysosomal lumen to the cytosol. In the controls, cathepsin D is localized to the lysosomal lumen, as indicated by its association with LAMP1 immunoreactivity (Figure 19A-C). Conversely, in DKO OHCs, most of the enlarged lysosomes contain undetectable to low levels of cathepsin D (Figure 19D). The absence of cathepsin D in DKO lysosomes is consistent with the presence of galectin 3 in the lysosomal lumen, confirming that the lysosomal membrane is permeabilized in DKO. While we could not detect cathepsin in the cytosol of DKO OHCs, we reason that its vastly larger volume dilutes cathepsin D below the level of detection. Altogether, mucolipin co-deficient lysosomes have permeabilized membranes, a condition known to cause the release of toxic hydrolases into the cytosol (Boya and Kroemer, 2008; Li et al., 2016b; Oku et al., 2017).

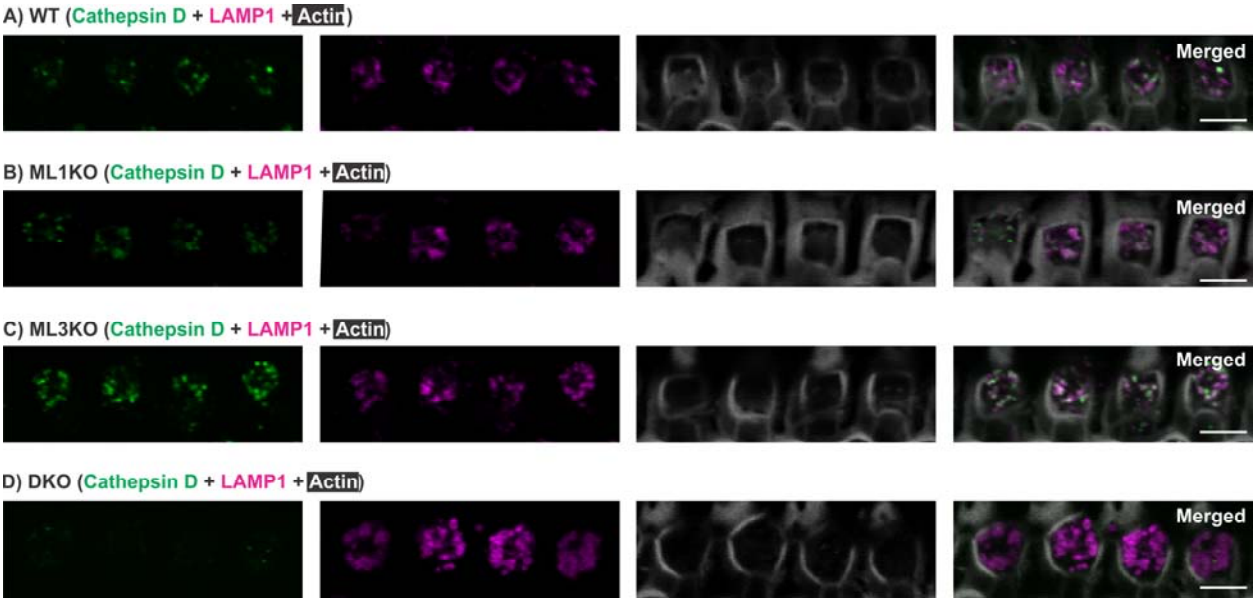


**Figure 19. Upon lysosomal membrane permeabilization, enlarged lysosomes from OHCs lacking mucolipins 3 and 1 contain almost undetectable level of lysosomal cathepsin D.** (**A-D**) Immunoreactivity of cathepsin D and LAMP1 reveal that upon lysosomal permeabilization, DKO lysosomes contain very low levels of cathepsin D. Cathepsin D has a vesicular expression pattern strongly associated with lysosomes in WT (**A**), ML1KO (**B**) and ML3KO (**C**) OHCs. (**D**) In contrast, cathepsin D levels are low or undetectable in DKO lysosomes. Samples were from adult (~P120) animals. Scale bars are 5μm.

**3.4 Discussion**

Although lysosomal defects have been noted to cause hearing loss (Ohlemiller et al., 2002; Heldermon et al., 2007; Schachern et al., 2007), our findings implicate HC lysosomes for the first time in ARHL and HC degeneration. In the case of mucopolysaccharidosis (MPS) I (Schachern et al., 2007) and MPSIIIB (Heldermon et al., 2007), deafness includes loss of both HCs and supporting cells of the organ of Corti. However, because lysosomal vacuolation was not detected in HCs but was found prominently in supporting cells, defective HC lysosomes were not considered the cause of HC degeneration and deafness. These studies, however, did not selectively ablate lysosomal genes in HCs, as we did here to reveal that the source of HC loss was cell autonomous and not due to defects in SCs.

The genetic and subcellular bases of ARHL have proven ardous to uncover (Ohlemiller, 2006; Liberman, 2017). By using transgenic mouse models with co-deficiency of lysosomal mucolipins 3 and 1 in HCs, we found a novel, polygenic cause for early-onset ARHL accompanied by OHC loss. Our findings implicate two new genes, *Trpml1* and *Trpml3*, adding to the exiguous list of genes that participate in the complex pathologies associated with presbycusis. This hearing loss phenotype is polygenic because of the redundancy between *Trpml1* and *Trpml3*. It is unclear why HCs would require both mucolipins to maintain their longevity since there is no hearing phenotype or HC degeneration in mice lacking either mucolipin alone (Jörs et al., 2010). However, this redundancy also occurs in neonatal intestinal enterocytes where a pathology was observed in DKO mice, but not in ML1KO and ML3KO mice (Remis et al., 2014). As with other cases of genetic redundancy, it is possible that mucolipin 3 serves a subtle lysosomal function that we can only detect in the absence of mucolipin 1.

Nonetheless, and although we did not detect any enhanced ARHL even in aged (8 month old) ML3KO mice (data not shown), we should not rule out the possibility that in the much longer lifespan of decades mucolipin 3 deficiency might predispose humans to an earlier onset ARHL.

We previously reported mucolipin 3 expression in IHCs, OHCs and stria vascularis of neonatal cochlea (Nagata et al., 2008; Castiglioni et al., 2011). Our current immumolocalization confirms these studies in almost every aspect, but here we make one correction. Previously, we reported that mucolipin 3 subsided significantly in adult OHCs, but we now demonstrate that mucolipin 3 is expressed in adult OHCs, although at a lower level compared to IHCs (Figure 13A). The discrepancy between the two reports is due to the fact that adult cochlear sections were subjected to a milder antigen retrieval condition than those from neonatal cochlea in Castiligoni et al. (2011)'s study to prevent tissues from detaching from the glass slides, while, here, we used an identical antigen retrieval condition for both neonatal and adult cochlea.

While mucolipin 1 is expressed in lysosomes of all cell types (Bach, 2001; LaPlante et al., 2002; Bach et al., 2005), mucolipin 3 is expressed in only a small subset of cells (Nagata et al., 2008; Remis et al., 2014). This restricted expression suggests that cells expressing mucolipin 3 may have specialized lysosomes. Indeed, mucolipin 3-expressing neonatal intestinal enterocytes have giant lysosomes dedicated to the intracellular digestion of endocytosed proteins from maternal milk (Remis et al., 2014); Mucolipin 3-expressing melanocytes produce melanosomes from specialized pre-melanosomal lysosomes (Raposo and Marks, 2002; Schiaffino, 2010); and marginal cells of the stria vascularis, which also express mucolipin 3 (Nagata et al., 2008), use lysosomes to localize potassium KCNQ1 channels to their apical membranes (Knipper et al., 2006). Hence, it seems reasonable to hypothesize that HCs,

expressing mucolipins 3, may also have specialized lysosomes.

Causes of hearing loss can be: 1) sensory, 2) strial and 3) neuronal (Cheatham et al., 2004; Knipper et al., 2006; Seal et al., 2008; Kim et al., 2013; Flores et al., 2015; Potter et al., 2016). Because mucolipin 3 is not expressed in the spiral ganglia or in the brain (Nagata et al., 2008; Castiglioni et al., 2011; Remis et al., 2014), we excluded the possibility that accelerated ARHL in mice lacking mucolipins was neuronal. To differentiate whether hearing defects in these mice was sensory, strial, or both, we generated mice conditionally lacking both mucolipins 3 and 1 in HCs only (cDKO). We discovered that DKO cochlea do not exhibit any strial deformation, degeneration or misexpression of its important functional protein KCNQ1 (Figure 14A, B). While we cannot rule out the possibility that there might be strial contribution to hearing loss in mice lacking mucolipins, this strial contribution to accelerated ARHL in DKO mice at 1 month of age is likely minimal—while there is a visible trend, the differences are not statistically significant in most cases. In addition, by 4 months of age, cDKO mice exhibited the same extent of hearing loss and OHC loss as DKO mice, which lack mucolipins 3 and 1 in all cells, suggesting that defects in HCs is likely the primary cause of hearing loss due to OHC death in these animals (Figures 12). Hence, our results suggest that mucolipins largely act autonomously in OHCs to maintain their long-term survival and, therefore, hearing.

Our original hypothesis was that HCs have specialized lysosomes for self-repair and maintenance, and hence for their ability to survive in a challenging environment for a very long time (in many cases for as long as the lifetime of the organism). While the loss of OHCs due to mucolipin co-deficiency favored this hypothesis, we found no evidence that in these OHCs the lysosome-mediated repair mechanisms (autophagy, mitophagy and pexophagy) are compromised

(Figure 17). Whereas the hypothesis that HCs contain specialized lysosomes dedicated to a self-repair required for their remarkable longevity is still valid, this is not the reason for OHC loss due to mucolipin co-deficiency. Instead, we reveal another mechanism by which OHC vulnerability may be increased: swelling and permeabilization of lysosomes, which would lead to the release of lysosomal hydrolases into the cytosol (Figure 18, 19). Studies have shown that lysosomal enlargement is a common event preceding cell death, and that enlarged lysosomes are vulnerable to lysosomal membrane permeabilization (Ono et al., 2001, 2003). Lysosomal membrane permeabilization causes leakage of luminal contents into the cytosol, including the smaller of the ~50 types of hydrolytic enzymes (Schröder et al., 2010), which can trigger cell death through apoptosis or necrosis (Boya and Kroemer, 2008; Repnik et al., 2014; Li et al., 2016b). Accordingly, we noted a depletion of cathepsin D, one of the smaller hydrolases, from mucolipin co-deficient lysosomes (Figure 19D). This depletion of cathepsin D does not seem to impair the overall function of the lysosomes (at least in regards to pexophagy, mitophagy and autophagy; Figure 17), presumably because they retain most of their (larger) hydrolases (Schröder et al., 2010; Repnik et al., 2014). Causes of lysosomal membrane permeabilization include osmotic lysis and direct membrane lysis by surfactant activity (Repnik et al., 2014). In our case, lysosomal membrane permeabilization might be due to increased luminal osmotic pressure, as lysosomes lacking mucolipins 3 and 1 are abnormally large (Figure 16).

It is also of interest that lysosomal membrane permeabilization in OHCs lacking mucolipins is not immediately cytotoxic. OHCs survive with permeabilized lysosomes for weeks to months, but in time perish along a base to apical gradient characteristic of OHC loss during ARHL. Hence, the toxic effects of lysosomal enlargement and permeabilization are to enhance

the vulnerability of OHCs, whose degeneration ultimately depends on other factors related to age and position. The weak toxicity resulting from lysosomal permeabilization may be due to the pH dependence of lysosomal hydrolases, as they function best at the low pH of the lysosomal lumen and are much less active at cytosolic pH levels. While most lysosomal hydrolases are inactive at a neutral pH, a family of lysosomal hydrolases, notably cathepsin D, L and S, is known to be active in the cytosol (Lkhider et al., 2004; Vasiljeva et al., 2005; Jiang et al., 2006; Boya and Kroemer, 2008). While cathepsins eventually unfold, losing their hydrolytic properties, their preserved activities, even only for a matter of hours, is sufficient to induce cell death signaling (Turk et al., 2012). Because cathepsin represents a small subset of lysosomal enzymes (Schröder et al., 2010), and lysosomal content accounts for a small portion of total cytoplasmic volume, these lysosomal enzymes, would be diluted in the cytosol of OHCs, rendering their hydrolytic activities gradual and cumulative, thereby leading to progressive OHC denegation in ARHL.

Here we report a novel role of mucolipins that affects lysosomal volume and lysosomal membrane integrity. Although we can only speculate the molecular steps leading to these organelle defects, one possibility is an increased lysosomal osmotic pressure due to cation accumulation (Figure 20). Generally, lysosomes are isosmotic with the surrounding cytoplasm, but with different proportions of solutes, *in vivo* (Lloyd, 1996; Yang et al., 2000), and the imbalance between luminal and cytoplasmic solutes can rapidly cause swelling of the lysosomes due to an osmotic influx of water (Forster and Lloyd, 1988). While mucolipin 3 channels are primarily permeable to $Ca^{2+}$ (Nagata et al., 2008), it is worth noting that mucolipin 1 is also permeable to other cations such as $Fe^{2+}$, $Zn^{2+}$, $Na^{+}$ and $K^{+}$ (Dong et al., 2008; Eichelsdoerfer et al., 2010; Wang et al., 2014). Because both mucolipins 3 and 1 are inwardly rectifying lysosomal

cation channels, their absence would prevent cations from leaving the lysosome. Here, we speculate that upon accumulation of luminal cations in HC lysosomes lacking mucolipins, the osmotic pressure would increase, ultimately leading to lysosomal membrane destabilization and permeabilization (Figure 20).

In summary, we identify a new mechanism by which toxic organelles, in our case lysosomes lacking mucolipins 3 and 1, could lead to premature OHC death and ARHL. We also demonstrate a novel role of mucolipin channels in sustaining lysosomal size and lysosomal membrane integrity. The discovery that mice lacking both lysosomal mucolipins 3 and 1 display accelerated ARHL due to OHC degeneration underscores the importance of lysosomes in long-term HC survival.

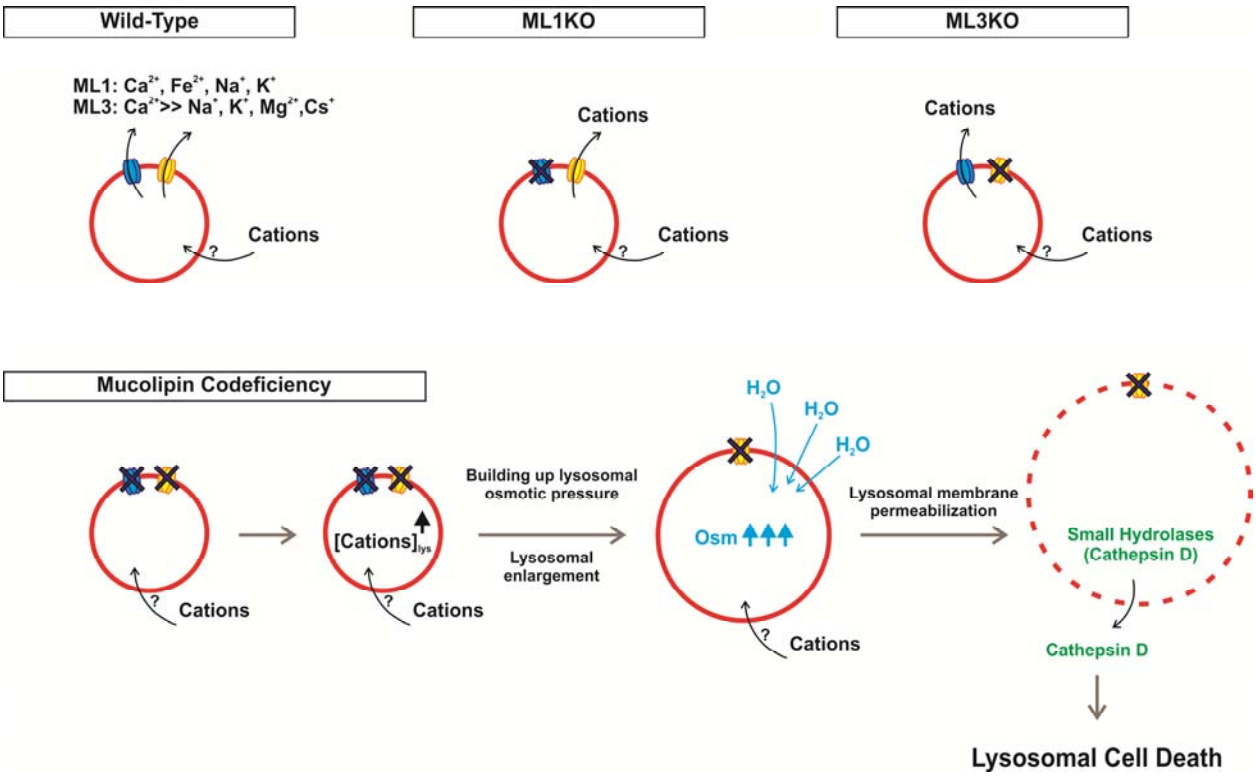


**Figure 20. Proposed model for lysosomal pathology in hair cells lacking mucolipins 3 and 1.** While mucolipin 1 (ML1, blue) channels are non-selectively permeable to $Ca^{2+}$ and other cations such as $Fe^{2+}$, $Zn^{2+}$, $Na^{+}$ and $K^{+}$ (Dong et al., 2008; Eichelsdoerfer et al., 2010; Wang et al., 2014), mucolipin 3 (ML3, yellow) channels are primarily permeable to $Ca^{2+}$ with low permeability to $Na^{+}$, $K^{+}$, $Mg^{2+}$ and $Cs^{+}$ (Nagata et al., 2008; Grimm et al., 2014). We propose that in cochlear outer hair cells (OHCs), lysosomal ionic balance is achieved through mucolipin channels. Because both channels are inwardly rectifying lysosomal cation channels, they function to let cations into the cytosol. We speculate that cations are uptaken into the lysosomes through transporters as they would enter the lysosome against their gradients. In the absence of either mucolipin alone (ML1KO and ML3KO), the remaining mucolipin is sufficient enough to maintain lysosomal ionic balance. However, in mucolipin co-deficient OHCs, majority of cations could not leave the lysosome. Upon accumulation of luminal cations, the osmotic pressure would

increase, resulting in influx of water molecules into the lysosomes and, ultimately, leading to lysosomal enlargement. Enlarged lysosomal enlargement are more susceptible to membrane destabilization and permeabilization, which causes the leakage of small hydrolases, such as cathepsin D, into the cytosol—a known trigger for lysosomal cell death.

## 3.5 Material and Methods

### Ethics

All animal care and procedures were in accordance with the *Guide for the Care and Use of Laboratory Animals* published by the National Institutes of Health and were approved by Northwestern University's Institutional Animal Care and Use Committee (Animal Study Protocols: IS00000593, IS00001281, IS00003625,).

### Animals

Wild-type (WT) and *Trpml1*$^{-/-}$ (ML1KO) mice in this study were littermates generated by mating *Trpml1*$^{+/-}$ x *Trpml1*$^{+/-}$, and had a genetic background of ~75% C57BL/6 and ~25% 129S6 (Venugopal et al., 2007). *Trpml3*$^{-/-}$ (ML3KO) and *Trpml3*$^{-/-}$;*Trpml1*$^{-/-}$ (DKO) were littermates generated by mating *Trpml3*$^{-/-}$;*Trpml1*$^{+/-}$ x *Trpml3*$^{-/-}$;*Trpml1*$^{+/-}$, and had a genetic background of ~75% C57BL/6, ~12.5% Sv129/Ola and ~12.5% 129S6 (Castiglioni et al., 2011; Remis et al., 2014). Finally, mice conditionally lacking mucolipins in hair cells only (*Gfi1*$^{Cre/+}$;*Trpml3*$^{F/F}$;*Trpml1*$^{-/-}$, termed cDKO) and their littermate controls (*Gfi*$^{+/+}$;*Trpml3*$^{F/F}$;*Trpml1*$^{-/-}$, *Gfi*$^{+/+}$;*Trpml3*$^{F/F}$;*Trpml1*$^{+/+}$, *Gfi*$^{+/+}$;*Trpml3*$^{F/F}$;*Trpml1*$^{+/-}$, *Gfi*$^{Cre/+}$;*Trpml3*$^{F/F}$;*Trpml1*$^{+/+}$, *Gfi*$^{Cre/+}$;*Trpml3*$^{F/+}$;*Trpml1*$^{+/+}$ and *Gfi*$^{Cre/+}$;*Trpml3*$^{F/+}$;*Trpml1*$^{+/-}$) incorporated *Gfi1*$^{Cre/+}$ mice with a mixed background of C57BL/6J and 129S6 (Yang et al., 2010), and had an estimated background of ~59% C57BL/6, ~19% Sv129/Ola and ~22% 129S6. Hence, all animals used in this study had a similar genetic background of ~59 to 75% C57BL/6 and 41 to 25% 129 strains. Importantly, regardless of the slight differences in genetic

background, ML1KO mice (littermates of WT) and ML3KO (littermates of DKO) did not differ from WT mice in all aspects examined. Furthermore, cDKO and DKO, although not littermates, had comparable ABR and DPOAE thresholds and virtually identical patterns of hair cell loss. Hence, the slight differences in genetic background did not result in any auditory phenotype, nor did they alter the hearing and hair cell loss phenotype segregating with mucolipin co-deficiency.

**Hearing tests**

During testing, mice of both sexes aged ~P30 and between P60 and P120 were anesthetized with ketamine/xylazine (100 mg/kg; 10 mg/kg, IP) and their body temperature maintained using a heating blanket. Hearing tests were performed on the left ear. Distortion product otoacoustic emissions (DPOAE) were acquired using a custom probe and an in the ear calibration. To determine DPOAE threshold, growth or input-output functions were collected for f2=12 kHz and for f2=27 kHz (where f2=1.2xf1) with the level of f1 being 10 dB higher than f2. These functions were plotted off line and the sound pressure level of f1 that produced a cubic difference tone at 2f1-f2 of 0 dB was defined as threshold. Auditory brainstem responses (ABR) were also acquired to assay auditory nerve activity as well as that in the lower brainstem. For these recordings, subcutaneous needle electrodes were inserted at the vertex and at the mastoid with a referenece electrode in the neck region on the opposite side. ABR thresholds were obtained using short tone bursts of decreasing level (step size=5 dB). Threshold was defined as the level where all ABR waves disappeared into the noise floor. The details of these procedures appear in a previous publication (Cheatham et al., 2014).

**Tissue collection and processing**

For neonatal tissues (younger than P14), the animals were euthanized by decapitation and inner ears dissected in ice cold PBS. For adult tissues (older than P21), the inner ears were dissected following cardiac perfusion with 2% or 4% paraformaldehyde after euthanasia. Tissues collected from both male and female mice were then post-fixed in 2% or 4% paraformaldehyde for 2 hours at room temperature. Adult ears were decalcified either in RDO (Electron Microscopy Sciences) at room temperature for 10 minutes or in 10% (w/v) EDTA, pH 7.3-7.4, at 4°C for at least 24 hours. To prepare frozen sections, the ears were processed and sectioned at 12 μm as described previously (Castiglioni et al., 2011). For whole-mount preparations, the organ of Corti was dissected from the cochlea into one apical, two middle and one basal segment using a whole-mount surface preparation method described previously (Montgomery and Cox, 2016).

**Immunohistochemistry**

Frozen sections were processed as previously described (Castiglioni et al., 2011). The antibodies used for frozen tissue preparation were TRPML3-CT (1:5000, a gift from Dr. Markus Delling, University of California, San Francisco), LAMP1 (1:50, 1D4B-s, Developmental Studies Hybridoma Bank) and KCNQ1 (1:100, sc-20816, Santa Cruz Biotech). For TRPML3-CT immunostaining, the sections were subjected to antigen retrieval by incubating in 10 mM sodium citrate, pH 6 with 0.25% Triton X-100 for 20 minutes at 92°C and cooling for 30 minutes at room temperature prior to blocking, and TRPML3-CT immunoreactivity was detected using a SuperBoost™ tyramide signal amplification kit (B40922, ThermoFisher). Whole-mount organ of

Corti sections were processed for immunohistochemistry as described previously (Delmaghani et al., 2015). The antibodies used for whole-mount preparation were LAMP1 (1:50), LC3 (1:50, ab58610, Abcam), PMP70 (1:100, ab3421, abcam), COXIV (1:100, ab16056, Abcam) and Galectin 3 (1:50, ab58802, Abcam). Nuclei were counterstained with DAPI (1:1000, ThermoFisher) and stereocilia with the filamentous actin probe phalloidin (1:100, ThermoFisher).

**Image acquisition**

For immunohistochemistry on frozen sections, we acquired images on either a Leica SP5 confocal or Nikon E600 pan fluorescence microscope equipped with a Nikon DS-Ri2 camera. For whole-mount preparation, we acquired images on either a Nikon A1 confocal, Nikon A1R+ Confocal or Nikon N-SIM structured illumination super-resolution microscope imaging system using a 100x objective. Three-dimensional renderings of confocal images were generated using NIS Elements AR4.60.00 (Nikon) and Imaris X64 8.4.1 (BitPlane) softwares. Organelle number and volume measurements were performed using built-in analysis functions on Imaris. When comparing controls and mutant immunoreactivities, we captured images with identical settings. Post-acquisition, we identically processed image pairs of control and knockout samples. This included adjustment for brightness and contrast.

**Cytocochleogram construction**

We used the right cochlea, not previously subjected to hearing tests, for cytocochleogram construction. For each cochlea, all 4 segments from a single whole-mount surface preparation were counterstained for stereocilia. Images were captured at 20x, stitched and reconstructed using either MicroSuite FIVE (Olympus Soft Imaging Solutions Corp.) or FIJI (ImageJ). After calculating cochlear length and dividing the cochlea into 7% segments, cytocochleograms were constructed by plotting the average percent HC loss, determined by the absence of stereocilia staining in each 7% segment along the basilar membrane. Cochlear positions corresponding to 12 and 27 kHz were calculated using a mouse frequency-place map (Müller et al., 2005).

**Experimental design and statistical analysis**

For statistical analysis, data were collected from both male and female animals. All statistical tests were performed using Prism software (GraphPad). For consistency, all whole-mount surface preparation measurements were performed on cochlear middle segments, while frozen section measurements were on cochlear middle turns of midmodiolar sections. Average ± SEM are shown in all plots. Data sets were analyzed for significance using a 1-way ANOVA followed by either Tukey's or Dunnett's post-hoc tests or unpaired t-test based on the n = number of animals, and only one ear per animal was used. The statistical comparision of hearing thresholds in ~P30 DKO vs adult WT, ML1KO and ML3KO (Figure 12A-D), as well as the comparisons of hair cell loss in controls (WT, ML1KO and ML3KO) vs both complete and conditional double knockout mice (DKO and cDKO) (Figure 15F), were unpaired t-tests. For all anatomical

examinations and immunostainings, we used cochlea from the ears that were not subjected to hearing tests. The number of cells used to collect individual data are shown on the plots. A 95% confidence interval was used to determine significance ($p<0.05$). All sample size and p values are reported in the figures or the figure legends. All p values lower than 0.0001 are reported as $p < 0.0001$ with **** on the plots; p values higher than 0.99 are reported as $p > 0.99$.

# CHAPTER 4:

# General Discussions

**5.1 Specialized mucolipin-endowed lysosomes**

The studies presented here implicate mucolipins in two very distinct lysosomal functions. Because mucolipin 3 is expressed in a small subset of cells—such as melanocytes, neonatal intestinal enterocytes, auditory HCs and stria vascularis (Nagata et al., 2008; Castiglioni et al., 2011; Remis et al., 2014)—while mucolipin 1 is expressed in all cells (Bach, 2001; LaPlante et al., 2002; Bach et al., 2005), it is not surprising that cells expressing both channels would utilize the specialized mucolipin-endowed lysosomes for their unique features. In fact, cells expressing both mucolipins often have a specialized lysosomal system. For example, melanocytes produce melanosomes from specialized pre-melanosomal lysosomes (Raposo and Marks, 2002; Schiaffino, 2010); and marginal cells of the stria vascularis use lysosomes to localize potassium channels to their apical membranes to maintain strial functions in producing $K^+$-rich endolymph (Knipper et al., 2006). In addition, neonatal enterocytes contain specialized endolysosomal system designated for intracellular digestion of maternal nutrients (Hamosh, 1996; Goodman, 2010). Hence, it is reasonable to hypothesize that the neonatal enterocytes and auditory HCs, expressing both mucolipins 3 and 1, would also utilize specialized mucolipin-endowed lysosomes for their functions.

However, we found that this was only the case in the neonatal enterocytes but not in the auditory HCs. Here, we discovered that both mucolipins 3 and 1 facilitated the scission of endolysosomal hybridorganelles in neonatal intestinal enterocytes upon the completion of milk digestion. However, we found that auditory HCs did not require specialized lysosomes for intracellular degradation of damaged organelles to promote their longevity. In HCs, we found that mucolipins helped maintain lysosomal membrane integrity, and in their co-absence lysosomes become permeabilized, rendering HCs vulnerable to cell death and, therefore, early-

onset ARHL.

It is important to note that mucolipins have also been implicated in multiple aspects of lysosomal functions, and their functions appear to be cell-type dependent. Here, we found that both mucolipins 3 and 1 facilitated lysosomal scission in neonatal enterocytes (Remis et al., 2014); however, a study in macrophages demonstrates that mucolipin 1 facilitates lysosomal fusion to endosomes (Thompson et al., 2007). In addition, studies reported that mucolipins function in lysosomal exocytosis in different cell types. For instance, in a bladder epithelial cell line, mucolipin 3 facilitates lysosomal exocytosis for pathogen expulsion (Miao et al., 2015), while mucolipin 1 regulates lysosomal exocytosis as a part of plasma membrane repair in muscle fibers (Cheng et al., 2014). Our discovery that mucolipins play an indirect role in maintaining lysosomal integrity in auditory HCs has to the growing list of mucolipins' functions.

Here, while we detected lysosomal membrane permeabilization in OHCs lacking mucolipins, we did not perform this assay on the neonatal intestinal enterocytes lacking mucolipins. One very different feature of the inner ear HCs and the intestinal enterocytes is their longevity. While HCs live for years, or decades in human, intestinal enterocytes are replaced with the newly produced cells from the intestinal crypt stem cells every 2-6 days (Mayhew et al., 1999; Williams et al., 2015). While we cannot rule out the possibility that the enlarged endolysosomes in enterocytes lacking mucolipins are permeabilized, we did not observed enterocyte loss in DKO neonatal intestine. Because the toxicity of the damaged permeabilized endolysosomes is likely gradual and cumulative over a long period of time, any cytotoxicity caused by damaged lysosomes would not be rapid enough to induce enterocyte death during the

period of less than a week before the enterocytes are shed and replaced with newly produced ones.

Furthermore, unlike the intestinal enterocytes, HCs do not undergo rapid apical endocytosis. Previously our group showed that cultured hair cells did not undergo endocytosis of fluorescently labeled dextran of various molecular weights (10000 – 70000 MW) and that the nearby supporting cells (dieter cells) instead underwent rapid endocytosis of dextran (unpublished data). We thus concluded that HCs might not rely primarily on apical endocytosis for their functions and, therefore, explored other lysosomal functions in HCs such as autophagy. This result, however, disagrees with previous reports demonstrating high levels of endocytosis in HCs (Meyer et al., 2001; Griesinger et al., 2004). While these studies reported high level of apical endocytosis in HCs, they used a membrane dye FM1-43 as an indication of endocytosis (Meyer et al., 2001; Griesinger et al., 2004). However, without a complete blockage of HC mechanotransduction channels, FM1-43 can enter HCs through these nonselective channels (Meyers et al., 2003) and bind to the lipid-layer of membrane-bound organelles located apically in HCs. The high level of FM1-43 signal at HC apical side can be a result of both endocytosis and FM1-43 labelled organelles, thus giving conflicting interpretations. While we cannot dismiss the possibility that mucolipins facilitate endolysosomal trafficking in HCs, our evidences suggest that HCs do not rely on endolysosomal pathway for their unique functions and features as opposed to the neonatal enterocytes. Our discoveries that mucolipins play very distinct roles in neonatal enterocytes and auditory HCs underscore the notion that mucolipins' roles are cell-type dependent.

**5.2 Genetic redundancy between mucolipins**

Sequence analysis suggests that the three mucolipins, coded by *Trpml* genes, arose from two genome-wide duplication events in deuterostomes (García-Añoveros and Wiwatpanit, 2014). The immediate consequence of the duplication of an existing gene is the creation an identical, redundant copy. Overtime, while each copy could undergo independent mutations, the duplicated genes often retain their sequence similarities, and are functionally conserved (Nowak et al., 1997; Kafri et al., 2009). In fact, this appears to be the case among mucolipins. In *C. elegans*, there is only one copy of mucolipin homolog, *cup-5*, and an expression of either human *Trpml1* or *Trpml3* can rescue MLIV-like phenotypic defects in the *C. elegans cup-5* mutants (Treusch et al., 2004). Because mucolipins can interact with each other in homo- and heteromultimeric fashions *in vitro* to form functional complexes (Venkatachalam et al., 2006; Grimm et al., 2010; Zeevi et al., 2010), it is not surprising that, in cells normally expressing both mucolipins 3 and 1, these channels could substitute for one another.

Here, we found that mice lacking either mucolipin 1 or mucolipin 3 alone were not phenotypically different from wild-type mice in all aspect examined. However, it is unclear why neonatal enterocytes or auditory HCs would require both mucolipins to maintain their functions and survival, respectively, while there is no phenotype in mice lacking either mucolipin alone. Given that the *Trpml3* expression does not increase to compensate for the lack of mucolipin 1 in ML1KO mice (Samie et al., 2009), it may be that mucolipin 1 channels alone are sufficient for normal lysosomal functions, and that mucolipin 3 serves a subtle role that we can only detect in the absence of mucolipin 1.

## 5.3 Future directions

### 5.3.1 Mucolipins and neonatal intestinal enterocytes

Here, we have shown that mucolipins 3 and 1 facilitate lysosomal scission in neonatal enterocytes (Figure 11). In addition, samples from rodent models of NEC and human NEC revealed severely vacuolated enterocytes, a strikingly similar pathology to our DKO mouse lacking both mucolipins 3 and 1, suggesting that dysfunction of this neonate-specific endolysosomal system could be the cause of NEC in human infants. To further investigate the roles of lysosomes in human neonatal enterocyte pathology, we will need more surgical samples, preferably from patients without intrinsic enterocyte pathologies (atresias, ileostomies and tumor resections) to determine the developmental period when human intestines contain lysosome-rich and mucolipin-expressing enterocytes. Although weaning in humans is not sharply defined, as it is in rodents, we expect a gradual decrease in lysosomes and mucolipins from 2 to 11 month, when levels of enzymes abundant in neonatal enterocytes gradually subside (Grand et al., 1976).

Due to limited availability of human neonatal biopsies—both "healthy" and NEC—we could utilize an *ex vivo* enteroid culture system. Intestinal stem cells from epithelial crypt domains can be harvested from freshly obtained surgical samples and cultured, giving rise to three-dimensional cultures that contain a stem cell niche and all the differentiated epithelial cells types, including enterocytes (Mahe et al., 2015; Saxena et al., 2015). The enteroids can be propagated, providing vast supplies of starting materials for transcriptomic and proteomic studies to determine the developmental period when human intestines contain the specialized mucolipin-endowed endolysosomal systems.

Similarly, to explore the possibility that enterocytes from NEC patients might be vacuolated due to lysosomal dysfunctions, we will also need more NEC biopsies. Although

lysosomal alterations would not demonstrate causality in these patients, they would advance our understanding of NEC, which has unknown etiologies, by implicating the endolysosomal system. Future experiments could then be designed to determine whether, for example, immaturity of the endolysosomal system due to premature birth combined with its challenge by postnatal feeding cause NEC, whether pathogen-mediated interference with the endolysosomal system causes vacuolation and necrosis, or whether mutations in genes encoding components of the endolysosomal system (such as *Trpml3*) contribute to a predisposition towards NEC.

### 5.3.2 Mucolipins and age-related hearing loss

Our results implicate HC lysosomes in ARHL. In the absence of mucolipins, HC lysosomes become pathologically enlarged, leading to lysosomal membrane permeabilization and cell death (Figure 20). Although our results did not indicate that HCs utilized lysosomes for self-repair mechanisms though autophagy, we cannot rule out that these lysosomal mucolipins could function in protection or recovery from noise-induced HC damage and hearing loss. HCs are remarkably resilient as they live for years (decades in humans) despite their constant energy demands (high mitochondrial activity) and mechanical insults (Ohlemiller, 2006). Thus, while mucolipins do not contribute to self-repair functions upon aging, they may facilitate self-repair mechanisms upon loud-noise exposure and contribute to protection against noise-related hearing loss.

In order to more directly test a role of mucolipins in HC repair from noise damage, we could induce hearing loss with loud noise, which causes mechanical as well as metabolic stress and damage to HCs, and compare the extent of hearing loss between controls and DKO animals. Exposure to loud noise causes two types of auditory threshold shifts in hearing. Within a day of

exposure, threshold shifts reach their maximum level, but subside by ~7 days and become permanent (Ohlemiller, 2006; Kurabi et al., 2016; Liberman, 2017). The transient component of the auditory threshold shifts is due to reversible damage to the ear, whereas the permanent threshold shifts are due to irreversible damage, including HC death and damage to stereocilia (Ohlemiller, 2006; Kurabi et al., 2016). Although the mechanisms of temporary threshold shift reversibility are unknown, it is reasonable to assume that they involve repair of cellular damage. Hence, an increase of permanent threshold shift among mice lacking mucolipins will be indicative of the failure in repair mechanisms of loud noise-exposed ears.

In addition, further experiments could be designed to subcellularly observe the level of self-repair mechanisms upon noise-exposure in comparison to age-related pathology. While there is no alteration in pexophagy, mitophagy and autophagy in DKO mice upon aging, it is possible that the permeabilized lysosomes of DKO HCs could predispose the animals to defects in these self-repair mechanisms after loud noise exposure.

# REFERENCES

Aits S, Kricker J, Liu B, Ellegaard A-M, Hämälistö S, Tvingsholm S, Corcelle-Termeau E, Høgh S, Farkas T, Holm Jonassen A, Gromova I, Mortensen M, Jäättelä M (2015) Sensitive detection of lysosomal membrane permeabilization by lysosomal galectin puncta assay. Autophagy 11:1408–1424.

Alberts JR, Pickler RH (2012) Evolution and development of dual ingestion systems in mammals: notes on a new thesis and its clinical implications. Int J Pediatr 2012:730673.

Ashmore J (2008) Cochlear outer hair cell motility. Physiol Rev 88:173–210.

Atiba-Davies M, Noben-Trauth K (2007) TRPML3 and hearing loss in the varitint-waddler mouse. Biochimica Et Biophysica Acta-Molecular Basis of Disease 1772:1028–1031.

Bach G (2001) Mucolipidosis type IV. Mol Genet Metab 73:197–203.

Bach G, Cohen MM, Kohn G (1975) Abnormal ganglioside accumulation in cultured fibroblasts from patients with mucolipidosis IV. Biochem Biophys Res Commun 66:1483–1490.

Bach G, Webb MBT, Bargal R, Zeigler M, Ekstein J (2005) The frequency of mucolipidosis type IV in the Ashkenazi Jewish population and the identification of 3 novel MCOLN1 mutations. Hum Mutat 26:591.

Baqui AA, Meiller TF, Chon JJ, Turng BF, Falkler WA (1998a) Interleukin-6 production by human monocytes treated with granulocyte-macrophage colony-stimulating factor in the presence of lipopolysaccharide of oral microorganisms. Oral Microbiol Immunol 13:173–180.

Baqui AA, Meiller TF, Turng BF, Kelley JI, Falkler WA (1998b) Functional changes in THP-1 human monocytic cells after stimulation with lipopolysaccharide of oral microorganisms and granulocyte macrophage colony stimulating factor. Immunopharmacol Immunotoxicol 20:493–518.

Baqui AH, Black RE, Arifeen SE, Hill K, Mitra SN, al Sabir A (1998c) Causes of childhood deaths in Bangladesh: results of a nationwide verbal autopsy study. Bull World Health Organ 76:161–171.

Bargal R, Avidan N, Ben-Asher E, Olender Z, Zeigler M, Frumkin A, Raas-Rothschild A, Glusman G, Lancet D, Bach G (2000) Identification of the gene causing mucolipidosis type IV. Nat Genet 26:118–123.

Bargal R, Avidan N, Olender T, Ben Asher E, Zeigler M, Raas-Rothschild A, Frumkin A, Ben-Yoseph O, Friedlender Y, Lancet D, Bach G (2001) Mucolipidosis type IV: novel MCOLN1 mutations in Jewish and non-Jewish patients and the frequency of the disease in the Ashkenazi Jewish population. Hum Mutat 17:397–402.

Bargal R, Bach G (1997) Mucolipidosis type IV: abnormal transport of lipids to lysosomes. J Inherit Metab Dis 20:625–632.

Boland M (2016) Human digestion--a processing perspective. J Sci Food Agric 96:2275–2283.

Boldrini R, Devito R, Biselli R, Filocamo M, Bosman C (2004) Wolman disease and cholesteryl ester storage disease diagnosed by histological and ultrastructural examination of intestinal and liver biopsy. Pathol Res Pract 200:231–240.

Boya P, Kroemer G (2008) Lysosomal membrane permeabilization in cell death. Oncogene 27:6434–6451.

Brunk UT, Dalen H, Roberg K, Hellquist HB (1997) Photo-oxidative disruption of lysosomal membranes causes apoptosis of cultured human fibroblasts. Free Radic Biol Med 23:616–626.

Buchholz JN, Behringer EJ, Pottorf WJ, Pearce WJ, Vanterpool CK (2007) Age-dependent changes in Ca2+ homeostasis in peripheral neurones: implications for changes in function. Aging Cell 6:285–296.

Cable J, Steel KP (1998) Combined cochleo-saccular and neuroepithelial abnormalities in the Varitint-waddler-J (VaJ) mouse. Hear Res 123:125–136.

Cao Q, Yang Y, Zhong XZ, Dong X-P (2017) The lysosomal Ca(2+) release channel TRPML1 regulates lysosome size by activating calmodulin. J Biol Chem 292:8424–8435.

Casimiro MC, Knollmann BC, Ebert SN, Vary JC, Greene AE, Franz MR, Grinberg A, Huang SP, Pfeifer K (2001) Targeted disruption of the Kcnq1 gene produces a mouse model of Jervell and Lange-Nielsen Syndrome. Proc Natl Acad Sci U S A 98:2526–2531.

Castiglioni AJ, Remis NN, Flores EN, García-Añoveros J (2011) Expression and vesicular localization of mouse Trpml3 in stria vascularis, hair cells, and vomeronasal and olfactory receptor neurons. J Comp Neurol 519:1095–1114.

Chandra M, Zhou H, Li Q, Muallem S, Hofmann SL, Soyombo AA (2011) A role for the Ca2+ channel TRPML1 in gastric acid secretion, based on analysis of knockout mice. Gastroenterology 140:857–867.

Cheatham MA, Goodyear RJ, Homma K, Legan PK, Korchagina J, Naskar S, Siegel JH, Dallos P, Zheng J, Richardson GP (2014) Loss of the tectorial membrane protein CEACAM16 enhances spontaneous, stimulus-frequency, and transiently evoked otoacoustic emissions. J Neurosci 34:10325–10338.

Cheatham MA, Huynh KH, Gao J, Zuo J, Dallos P (2004) Cochlear function in Prestin knockout mice. J Physiol (Lond) 560:821–830.

Cheng X, Shen D, Samie M, Xu H (2010) Mucolipins: Intracellular TRPML1-3 channels. FEBS Lett 584:2013–2021.

Cheng X, Zhang X, Gao Q, Ali Samie M, Azar M, Tsang WL, Dong L, Sahoo N, Li X, Zhuo Y, Garrity AG, Wang X, Ferrer M, Dowling J, Xu L, Han R, Xu H (2014) The intracellular $Ca^{2+}$ channel MCOLN1 is required for sarcolemma repair to prevent muscular dystrophy. Nat Med 20:1187–1192.

Covell WP (1953) Histologic changes in the organ of Corti with intense sound. J Comp Neurol 99:43–59.

Crawley SW, Weck ML, Grega-Larson NE, Shifrin DA, Tyska MJ (2016) ANKS4B is essential for intermicrovillar adhesion complex formation. Dev Cell 36:190–200.

Dallos P, Zheng J, Cheatham MA (2006) Prestin and the cochlear amplifier. J Physiol (Lond) 576:37–42.

Dallos P, Wu X, Cheatham MA, Gao J, Zheng J, Anderson CT, Jia S, Wang X, Cheng WHY, Sengupta S, He DZZ, Zuo J (2008) Prestin-based outer hair cell motility is necessary for mammalian cochlear amplification. Neuron 58:333–339.

Dannhof BJ, Bruns V (1993) The innervation of the organ of Corti in the rat. Hear Res 66:8–22.

De Plaen IG, Liu SXL, Tian R, Neequaye I, May MJ, Han X-B, Hsueh W, Jilling T, Lu J, Caplan MS (2007) Inhibition of nuclear factor-kappaB ameliorates bowel injury and prolongs survival in a neonatal rat model of necrotizing enterocolitis. Pediatr Res 61:716–721.

De Santa Barbara P, van den Brink GR, Roberts DJ (2003) Development and differentiation of the intestinal epithelium. Cell Mol Life Sci 60:1322–1332.

Delmaghani S et al. (2015) Hypervulnerability to Sound Exposure through Impaired Adaptive Proliferation of Peroxisomes. Cell 163:894–906.

Di Palma F, Belyantseva IA, Kim HJ, Vogt TF, Kachar B, Noben-Trauth K (2002) Mutations in Mcoln3 associated with deafness and pigmentation defects in varitint-waddler (Va) mice. Proc Natl Acad Sci U S A 99:14994–14999.

DiCiccio JE, Steinberg BE (2011) Lysosomal pH and analysis of the counter ion pathways that support acidification. J Gen Physiol 137:385–390.

Dong X, Shen D, Wang X, Dawson T, Li X, Zhang Q, Cheng X, Zhang Y, Weisman LS, Delling M, Xu H (2010) PI(3,5)P(2) controls membrane trafficking by direct activation of mucolipin Ca(2+) release channels in the endolysosome. Nat Commun 1:38.

Dong X-P, Cheng X, Mills E, Delling M, Wang F, Kurz T, Xu H (2008) The type IV mucolipidosis-associated protein TRPML1 is an endolysosomal iron release channel. Nature 455:992–996.

Duggan A, Madathany T, de Castro SCP, Gerrelli D, Guddati K, García-Añoveros J (2008) Transient expression of the conserved zinc finger gene INSM1 in progenitors and nascent neurons throughout embryonic and adult neurogenesis. J Comp Neurol 507:1497–1520.

Eichelsdoerfer JL, Evans JA, Slaugenhaupt SA, Cuajungco MP (2010) Zinc dyshomeostasis is linked with the loss of mucolipidosis IV-associated TRPML1 ion channel. J Biol Chem 285:34304–34308.

Emami CN, Chokshi N, Wang J, Hunter C, Guner Y, Goth K, Wang L, Grishin A, Ford HR (2012) Role of interleukin-10 in the pathogenesis of necrotizing enterocolitis. Am J Surg 203:428–435.

Esterberg R, Hailey DW, Coffin AB, Raible DW, Rubel EW (2013) Disruption of intracellular calcium regulation is integral to aminoglycoside-induced hair cell death. J Neurosci 33:7513–7525.

Fares H, Greenwald I (2001) Regulation of endocytosis by CUP-5, the Caenorhabditis elegans mucolipin-1 homolog. Nat Genet 28:64–68.

Fath KR, Burgess DR (1995) Microvillus assembly. Not actin alone. Curr Biol 5:591–593.

Fettiplace R (2017) Hair cell transduction, tuning, and synaptic transmission in the mammalian cochlea. Compr Physiol 7:1197–1227.

Flores EN, Duggan A, Madathany T, Hogan AK, Márquez FG, Kumar G, Seal RP, Edwards RH, Liberman MC, García-Añoveros J (2015) A non-canonical pathway from cochlea to brain signals tissue-damaging noise. Curr Biol 25:606–612.

Folkerth RD, Alroy J, Lomakina I, Skutelsky E, Raghavan SS, Kolodny EH (1995) Mucolipidosis IV: morphology and histochemistry of an autopsy case. J Neuropathol Exp Neurol 54:154–164.

Forster S, Lloyd JB (1988) Solute translocation across the mammalian lysosome membrane. Biochimica et Biophysica Acta (BBA) - Reviews on Biomembranes 947:465–491.

Fridberger A, Flock A, Ulfendahl M, Flock B (1998) Acoustic overstimulation increases outer hair cell Ca2+ concentrations and causes dynamic contractions of the hearing organ. Proc Natl Acad Sci U S A 95:7127–7132.

Gamp A-C, Tanaka Y, Lüllmann-Rauch R, Wittke D, D'Hooge R, De Deyn PP, Moser T, Maier H, Hartmann D, Reiss K, Illert A-L, von Figura K, Saftig P (2003) LIMP-2/LGP85 deficiency causes ureteric pelvic junction obstruction, deafness and peripheral neuropathy in mice. Hum Mol Genet 12:631–646.

García-Añoveros J, Wiwatpanit T (2014) TRPML2 and mucolipin evolution. Handb Exp Pharmacol 222:647–658.

Gates GA, Mills JH (2005) Presbycusis. The Lancet 366:1111–1120.

Geer JS, Skinner SA, Goldin E, Holden KR (2010) Mucolipidosis type IV: a subtle pediatric neurodegenerative disorder. Pediatr Neurol 42:223–226.

Goebel HH, Kohlschütter A, Lenard HG (1982) Morphologic and chemical biopsy findings in mucolipidosis IV. Clin Neuropathol 1:73–82.

Goh LH, How CH, Ng KH (2016) Failure to thrive in babies and toddlers. Singapore Med J 57:287–291.

Gonnella PA, Neutra MR (1984) Membrane-bound and fluid-phase macromolecules enter separate prelysosomal compartments in absorptive cells of suckling rat ileum. J Cell Biol 99:909–917.

Goodman BE (2010) Insights into digestion and absorption of major nutrients in humans. Adv Physiol Educ 34:44–53.

Grand RJ, Watkins JB, Torti FM (1976) Development of the human gastrointestinal tract. A review. Gastroenterology 70:790–810.

Grati M, Schneider ME, Lipkow K, Strehler EE, Wenthold RJ, Kachar B (2006) Rapid turnover of stereocilia membrane proteins: evidence from the trafficking and mobility of plasma membrane Ca(2+)-ATPase 2. J Neurosci 26:6386–6395.

Griesinger CB, Richards CD, Ashmore JF (2004) Apical endocytosis in outer hair cells of the mammalian cochlea. Eur J Neurosci 20:41–50.

Grimm C, Barthmes M, Wahl-Schott C (2014) TRPML3. Handb Exp Pharmacol 222:659–674.

Grimm C, Cuajungco MP, van Aken AFJ, Schnee M, Jörs S, Kros CJ, Ricci AJ, Heller S (2007) A helix-breaking mutation in TRPML3 leads to constitutive activity underlying deafness in the varitint-waddler mouse. Proc Natl Acad Sci U S A 104:19583–19588.

Grimm C, Jörs S, Guo Z, Obukhov AG, Heller S (2012) Constitutive activity of TRPML2 and TRPML3 channels versus activation by low extracellular sodium and small molecules. J Biol Chem 287:22701–22708.

Grimm C, Jörs S, Saldanha SA, Obukhov AG, Pan B, Oshima K, Cuajungco MP, Chase P, Hodder P, Heller S (2010) Small molecule activators of TRPML3. Chem Biol 17:135–148.

Guandalini S (2017) Pediatric Malabsorption Syndromes: Background, Pathophysiology, Epidemiology. Pediatric Malabsorption Syndromes: Background, Pathophysiology, Epidemiology Available at: http://emedicine.medscape.com/article/931041-overview [Accessed November 10, 2017].

Hamosh M (1996) Digestion in the newborn. Clin Perinatol 23:191–209.

Han F, Yu H, Tian C, Chen HE, Benedict-Alderfer C, Zheng Y, Wang Q, Han X, Zheng QY (2012) A new mouse mutant of the Cdh23 gene with early-onset hearing loss facilitates evaluation of otoprotection drugs. Pharmacogenomics J 12:30–44.

Harper J, Mould A, Andrews RM, Bikoff EK, Robertson EJ (2011) The transcriptional repressor Blimp1/Prdm1 regulates postnatal reprogramming of intestinal enterocytes. Proc Natl Acad Sci U S A 108:10585–10590.

Helander HF, Keeling DJ (1993) Cell biology of gastric acid secretion. Baillieres Clin Gastroenterol 7:1–21.

Heldermon CD, Hennig AK, Ohlemiller KK, Ogilvie JM, Herzog ED, Breidenbach A, Vogler C, Wozniak DF, Sands MS (2007) Development of sensory, motor and behavioral deficits in the murine model of Sanfilippo syndrome type B. PLoS ONE 2:e772.

Henning SJ (1981) Postnatal development: coordination of feeding, digestion, and metabolism. Am J Physiol 241:G199–214.

Henning SJ (1985) Ontogeny of enzymes in the small intestine. Annu Rev Physiol 47:231–245.

Hill K, Yuan H, Wang X, Sha S-H (2016) Noise-Induced Loss of Hair Cells and Cochlear Synaptopathy Are Mediated by the Activation of AMPK. J Neurosci 36:7497–7510.

Hirano S, Kataoka K (1986) Histogenesis of the mouse jejunal mucosa, with special reference to proliferative cells and absorptive cells. Arch Histol Jpn 49:333–348.

Hirschberger M, Kleinberg G (1976) Failure to thrive and death in early infancy associated with raised urinary homovanillic and vanillylmandelic acids. Arch Dis Child 51:977–979.

Hoffman EP, Barr ML, Giovanni MA, Murray MF (1993) Lysosomal Acid Lipase Deficiency. In: GeneReviews(®) (Pagon RA, Adam MP, Ardinger HH, Wallace SE, Amemiya A, Bean LJ, Bird TD, Fong C-T, Mefford HC, Smith RJ, Stephens K, eds). Seattle (WA): University of Washington, Seattle.

Hosoyamada T (2006) [Clinical studies of pediatric malabsorption syndromes]. Fukuoka Igaku Zasshi 97:322–350.

Hu J, Li B, Apisa L, Yu H, Entenman S, Xu M, Stepanyan R, Guan B-J, Müller U, Hatzoglou M, Zheng QY (2016) ER stress inhibitor attenuates hearing loss and hair cell death in Cdh23(erl/erl) mutant mice. Cell Death Dis 7:e2485.

Hudspeth AJ (1982) Extracellular current flow and the site of transduction by vertebrate hair cells. J Neurosci 2:1–10.

Hunter CJ, Chokshi N, Ford HR (2008a) Evidence vs experience in the surgical management of necrotizing enterocolitis and focal intestinal perforation. J Perinatol 28 Suppl 1:S14–7.

Hunter CJ, Podd B, Ford HR, Camerini V (2008b) Evidence vs experience in neonatal practices in necrotizing enterocolitis. J Perinatol 28 Suppl 1:S9–S13.

Hunter CJ, Williams M, Petrosyan M, Guner Y, Mittal R, Mock D, Upperman JS, Ford HR, Prasadarao NV (2009) Lactobacillus bulgaricus prevents intestinal epithelial cell injury caused by Enterobacter sakazakii-induced nitric oxide both in vitro and in the newborn rat model of necrotizing enterocolitis. Infect Immun 77:1031–1043.

Ison JR, Allen PD, O'Neill WE (2007) Age-related hearing loss in C57BL/6J mice has both frequency-specific and non-frequency-specific components that produce a hyperacusis-like exaggeration of the acoustic startle reflex. J Assoc Res Otolaryngol 8:539–550.

Jiang H, Sha SH, Forge A, Schacht J (2006) Caspase-independent pathways of hair cell death induced by kanamycin in vivo. Cell Death Differ 13:20–30.

Jörs S, Grimm C, Becker L, Heller S (2010) Genetic inactivation of Trpml3 does not lead to hearing and vestibular impairment in mice. PLoS ONE 5:e14317.

Kafri R, Springer M, Pilpel Y (2009) Genetic redundancy: new tricks for old genes. Cell 136:389–392.

Kazmierczak M, Harris SL, Kazmierczak P, Shah P, Starovoytov V, Ohlemiller KK, Schwander M (2015) Progressive hearing loss in mice carrying a mutation in usp53. J Neurosci 35:15582–15598.

Kim HJ, Gratton MA, Lee J-H, Perez Flores MC, Wang W, Doyle KJ, Beermann F, Crognale MA, Yamoah EN (2013) Precise toxigenic ablation of intermediate cells abolishes the "battery" of the cochlear duct. J Neurosci 33:14601–14606.

Kim HJ, Li Q, Tjon-Kon-Sang S, So I, Kiselyov K, Muallem S (2007) Gain-of-function mutation in TRPML3 causes the mouse Varitint-Waddler phenotype. J Biol Chem 282:36138–36142.

Knipper M, Claussen C, Rüttiger L, Zimmermann U, Lüllmann-Rauch R, Eskelinen E-L, Schröder J, Schwake M, Saftig P (2006) Deafness in LIMP2-deficient mice due to early loss of the potassium channel KCNQ1/KCNE1 in marginal cells of the stria vascularis. J Physiol (Lond) 576:73–86.

Koo B-K, Stange DE, Sato T, Karthaus W, Farin HF, Huch M, van Es JH, Clevers H (2011) Controlled gene expression in primary Lgr5 organoid cultures. Nat Methods 9:81–83.

Kraehenbuhl JP, Bron C, Sordat B (1979) Transfer of humoral secretory and cellular immunity from mother to offspring. Curr Top Pathol 66:105–157.

Kraemer A, Yap AS (2003) Coupling adhesion to actin bundles in the inner ear. Novel functions for novel cadherins. EMBO Rep 4:244–245.

Krivit W, Peters C, Dusenbery K, Ben-Yoseph Y, Ramsay NK, Wagner JE, Anderson R (2000) Wolman disease successfully treated by bone marrow transplantation. Bone Marrow Transplant 26:567–570.

Kujawa SG, Liberman MC (2006) Acceleration of age-related hearing loss by early noise exposure: evidence of a misspent youth. J Neurosci 26:2115–2123.

Kujawa SG, Liberman MC (2009) Adding insult to injury: cochlear nerve degeneration after "temporary" noise-induced hearing loss. J Neurosci 29:14077–14085.

Kurabi A, Keithley EM, Housley GD, Ryan AF, Wong AC-Y (2016) Cellular mechanisms of noise-induced hearing loss. Hear Res 349:129–137.

Ladinsky MS, Huey-Tubman KE, Bjorkman PJ (2012) Electron tomography of late stages of FcRn-mediated antibody transcytosis in neonatal rat small intestine. Mol Biol Cell 23:2537–2545.Lane PW (1972) Two new mutations in linkage group XVI of the house mouse. Flaky tail and varitint-waddler-J. J Hered 63:135–140.

LaPlante JM, Falardeau J, Sun M, Kanazirska M, Brown EM, Slaugenhaupt SA, Vassilev PM (2002) Identification and characterization of the single channel function of human mucolipin-1 implicated in mucolipidosis type IV, a disorder affecting the lysosomal pathway. FEBS Lett 532:183–187.

LaPlante JM, Ye CP, Quinn SJ, Goldin E, Brown EM, Slaugenhaupt SA, Vassilev PM (2004) Functional links between mucolipin-1 and Ca2+-dependent membrane trafficking in mucolipidosis IV. Biochem Biophys Res Commun 322:1384–1391.

Lee MP, Ravenel JD, Hu RJ, Lustig LR, Tomaselli G, Berger RD, Brandenburg SA, Litzi TJ, Bunton TE, Limb C, Francis H, Gorelikow M, Gu H, Washington K, Argani P, Goldenring JR, Coffey RJ, Feinberg AP (2000) Targeted disruption of the Kvlqt1 gene causes deafness and gastric hyperplasia in mice. J Clin Invest 106:1447–1455.

Lelouvier B, Puertollano R (2011) Mucolipin-3 regulates luminal calcium, acidification, and membrane fusion in the endosomal pathway. J Biol Chem 286:9826–9832.

Lev S, Zeevi DA, Frumkin A, Offen-Glasner V, Bach G, Minke B (2010) Constitutive activity of the human TRPML2 channel induces cell degeneration. J Biol Chem 285:2771–2782.

Li J, He Y, Lu Q, Zhang M (2016a) Mechanistic Basis of Organization of the Harmonin/USH1C-Mediated Brush Border Microvilli Tip-Link Complex. Dev Cell 36:179–189.

Li Y, Chen B, Zou W, Wang X, Wu Y, Zhao D, Sun Y, Liu Y, Chen L, Miao L, Yang C, Wang X (2016b) The lysosomal membrane protein SCAV-3 maintains lysosome integrity and adult longevity. J Cell Biol 215:167–185.

Liberman MC (2017) Noise-induced and age-related hearing loss: new perspectives and potential therapies. [version 1; referees: 4 approved]. F1000Res 6:927.

Lima WC, Leuba F, Soldati T, Cosson P (2012) Mucolipin controls lysosome exocytosis in Dictyostelium. J Cell Sci 125:2315–2322.

Lin PW, Nasr TR, Stoll BJ (2008) Necrotizing enterocolitis: recent scientific advances in pathophysiology and prevention. Semin Perinatol 32:70–82.

Lindquist S, Hernell O (2010) Lipid digestion and absorption in early life: an update. Curr Opin Clin Nutr Metab Care 13:314–320.

Lkhider M, Castino R, Bouguyon E, Isidoro C, Ollivier-Bousquet M (2004) Cathepsin D released by lactating rat mammary epithelial cells is involved in prolactin cleavage under physiological conditions. J Cell Sci 117:5155–5164.

Lloyd JB (1996) The taxonomy of lysosomes and related structures. In: Biology of the lysosome (Lloyd JB, Mason RW, eds), pp 1–13 Subcellular Biochemistry. Boston, MA: Springer US.

Mahe MM, Sundaram N, Watson CL, Shroyer NF, Helmrath MA (2015) Establishment of human epithelial enteroids and colonoids from whole tissue and biopsy. J Vis Exp.

Makary CA, Shin J, Kujawa SG, Liberman MC, Merchant SN (2011) Age-related primary cochlear neuronal degeneration in human temporal bones. J Assoc Res Otolaryngol 12:711–717.

Manley GA, Köppl C (1998) Phylogenetic development of the cochlea and its innervation. Curr Opin Neurobiol 8:468–474.

Manson WG, Weaver LT (1997) Fat digestion in the neonate. Arch Dis Child Fetal Neonatal Ed 76:F206–11.

Marcus DC, Wangemann P (2010) Cochlear and vestibular function and dysfunction. In: Physiology and pathology of chloride transporters and channels in the nervous system, pp 425–437. Elsevier.

Martin GK, Stagner BB, Lonsbury-Martin BL (2006) Assessment of cochlear function in mice: distortion-product otoacoustic emissions. Curr Protoc Neurosci Chapter 8:Unit8.21C.

Mason S (1962) Some aspects of gastric function in the newborn. Arch Dis Child 37:387–391.

Maurer J, Heinrich UR, Hinni M, Mann W (1999) Alteration of the calcium content in inner hair cells of the cochlea of the guinea pig after acute noise trauma with and without application of the organic calcium channel blocker diltiazem. ORL J Otorhinolaryngol Relat Spec 61:328–333.

Meyer J, Mack AF, Gummer AW (2001) Pronounced infracuticular endocytosis in mammalian outer hair cells. Hear Res 161:10–22.

Meyers JR, MacDonald RB, Duggan A, Lenzi D, Standaert DG, Corwin JT, Corey DP (2003) Lighting up the senses: FM1-43 loading of sensory cells through nonselective ion channels. J Neurosci 23:4054–4065.

Mayhew TM, Myklebust R, Whybrow A, Jenkins R (1999) Epithelial integrity, cell death and cell loss in mammalian small intestine. Histol Histopathol 14:257–267.

Mburu P, Romero MR, Hilton H, Parker A, Townsend S, Kikkawa Y, Brown SDM (2010) Gelsolin plays a role in the actin polymerization complex of hair cell stereocilia. PLoS ONE 5:e11627.

McConnell RE, Benesh AE, Mao S, Tabb DL, Tyska MJ (2011) Proteomic analysis of the enterocyte brush border. Am J Physiol Gastrointest Liver Physiol 300:G914–26.

McGrath J, Roy P, Perrin BJ (2017) Stereocilia morphogenesis and maintenance through regulation of actin stability. Semin Cell Dev Biol 65:88–95.

Melgar-Rojas P, Alvarado JC, Fuentes-Santamaría V, Juiz JM (2015) Cellular Mechanisms of Age-Related Hearing Loss. In: Free radicals in ENT pathology (Miller J, Le Prell CG, Rybak L, eds), pp 305–333 Oxidative stress in applied basic research and clinical practice. Cham: Springer International Publishing.

Menardo J, Tang Y, Ladrech S, Lenoir M, Casas F, Michel C, Bourien J, Ruel J, Rebillard G, Maurice T, Puel J-L, Wang J (2012) Oxidative stress, inflammation, and autophagic stress as the key mechanisms of premature age-related hearing loss in SAMP8 mouse Cochlea. Antioxid Redox Signal 16:263–274.

Merin S, Livni N, Berman ER, Yatziv S (1975) Mucolipidosis IV: ocular, systemic, and ultrastructural findings. Invest Ophthalmol 14:437–448.

Miao Y, Li G, Zhang X, Xu H, Abraham SN (2015) A TRP channel senses lysosome neutralization by pathogens to trigger their expulsion. Cell 161:1306–1319.

Micsenyi MC, Dobrenis K, Stephney G, Pickel J, Vanier MT, Slaugenhaupt SA, Walkley SU (2009) Neuropathology of the Mcoln1(-/-) knockout mouse model of mucolipidosis type IV. J Neuropathol Exp Neurol 68:125–135.

Montell C (2005) The TRP superfamily of cation channels. Sci STKE 2005:re3.

Montgomery SC, Cox BC (2016) Whole mount dissection and immunofluorescence of the adult mouse cochlea. J Vis Exp.

Mould AW, Morgan MAJ, Nelson AC, Bikoff EK, Robertson EJ (2015) Blimp1/Prdm1 Functions in Opposition to Irf1 to Maintain Neonatal Tolerance during Postnatal Intestinal Maturation. PLoS Genet 11:e1005375.

Moxey PC, Trier JS (1979) Development of villus absorptive cells in the human fetal small intestine: a morphological and morphometric study. Anat Rec 195:463–482.

Müller M, von Hünerbein K, Hoidis S, Smolders JWT (2005) A physiological place-frequency map of the cochlea in the CBA/J mouse. Hear Res 202:63–73.

Muncan V, Heijmans J, Krasinski SD, Büller NV, Wildenberg ME, Meisner S, Radonjic M, Stapleton KA, Lamers WH, Biemond I, van den Bergh Weerman MA, O'Carroll D, Hardwick JC, Hommes DW, van den Brink GR (2011) Blimp1 regulates the transition of neonatal to adult intestinal epithelium. Nat Commun 2:452.

Nagata K, Zheng L, Madathany T, Castiglioni AJ, Bartles JR, García-Añoveros J (2008) The varitint-waddler (Va) deafness mutation in TRPML3 generates constitutive, inward rectifying currents and causes cell degeneration. Proc Natl Acad Sci U S A 105:353–358.

Noben-Trauth K, Zheng QY, Johnson KR (2003) Association of cadherin 23 with polygenic inheritance and genetic modification of sensorineural hearing loss. Nat Genet 35:21–23.

Nowak MA, Boerlijst MC, Cooke J, Smith JM (1997) Evolution of genetic redundancy. Nature 388:167–171.

Ohlemiller KK (2006) Contributions of mouse models to understanding of age- and noise-related hearing loss. Brain Res 1091:89–102.

Ohlemiller KK, Hennig AK, Lett JM, Heidbreder AF, Sands MS (2002) Inner ear pathology in the mucopolysaccharidosis VII mouse. Hear Res 169:69–84.

Oku Y, Murakami K, Irie K, Hoseki J, Sakai Y (2017) Synthesized aβ42 caused intracellular oxidative damage, leading to cell death, via lysosome rupture. Cell Struct Funct 42:71–79.

Ono K, Kim SO, Han J (2003) Susceptibility of lysosomes to rupture is a determinant for plasma membrane disruption in tumor necrosis factor alpha-induced cell death. Mol Cell Biol 23:665–676.

Ono K, Wang X, Han J (2001) Resistance to tumor necrosis factor-induced cell death mediated by PMCA4 deficiency. Mol Cell Biol 21:8276–8288.

Oshikawa T, Baba R, Fujita M (1996) Apical endocytosis of lectins by the absorptive cells of the suckling rat jejunum in vivo. Okajimas Folia Anat Jpn 73:229–245.

Pácha J (2000) Development of intestinal transport function in mammals. Physiol Rev 80:1633–1667.

Piper RC, Luzio JP (2004) CUPpling calcium to lysosomal biogenesis. Trends Cell Biol 14:471–473.

Potter PK et al. (2016) Novel gene function revealed by mouse mutagenesis screens for models of age-related disease. Nat Commun 7:12444.

Puertollano R, Kiselyov K (2009) TRPMLs: in sickness and in health. Am J Physiol Renal Physiol 296:F1245–54.

Raposo G, Marks MS (2002) The dark side of lysosome-related organelles: specialization of the endocytic pathway for melanosome biogenesis. Traffic 3:237–248.

Reddy A, Caler EV, Andrews NW (2001) Plasma membrane repair is mediated by Ca(2+)-regulated exocytosis of lysosomes. Cell 106:157–169.

Remis NN, Wiwatpanit T, Castiglioni AJ, Flores EN, Cantú JA, García-Añoveros J (2014) Mucolipin co-deficiency causes accelerated endolysosomal vacuolation of enterocytes and failure-to-thrive from birth to weaning. PLoS Genet 10:e1004833.

Repnik U, Hafner Česen M, Turk B (2014) Lysosomal membrane permeabilization in cell death: concepts and challenges. Mitochondrion 19 Pt A:49–57.

Rzadzinska AK, Nevalainen EM, Prosser HM, Lappalainen P, Steel KP (2009) MyosinVIIa interacts with Twinfilin-2 at the tips of mechanosensory stereocilia in the inner ear. PLoS ONE 4:e7097.

Rzadzinska AK, Schneider ME, Davies C, Riordan GP, Kachar B (2004) An actin molecular treadmill and myosins maintain stereocilia functional architecture and self-renewal. J Cell Biol 164:887–897.

Samie M et al. (2013) A TRP channel in the lysosome regulates large particle phagocytosis via focal exocytosis. Dev Cell 26:511–524.

Samie MA, Grimm C, Evans JA, Curcio-Morelli C, Heller S, Slaugenhaupt SA, Cuajungco MP (2009) The tissue-specific expression of TRPML2 (MCOLN-2) gene is influenced by the presence of TRPML1. Pflugers Arch 459:79–91.

Sato T, Vries RG, Snippert HJ, van de Wetering M, Barker N, Stange DE, van Es JH, Abo A, Kujala P, Peters PJ, Clevers H (2009) Single Lgr5 stem cells build crypt-villus structures in vitro without a mesenchymal niche. Nature 459:262–265.

Saxena K, Blutt SE, Ettayebi K, Zeng X-L, Broughman JR, Crawford SE, Karandikar UC, Sastri NP, Conner ME, Opekun AR, Graham DY, Qureshi W, Sherman V, Foulke-Abel J, In J, Kovbasnjuk O, Zachos NC, Donowitz M, Estes MK (2015) Human intestinal enteroids: a new model to study human rotavirus infection, host restriction, and pathophysiology. J Virol 90:43–56.

Schachern PA, Cureoglu S, Tsuprun V, Paparella MM, Whitley CB (2007) Age-related functional and histopathological changes of the ear in the MPS I mouse. Int J Pediatr Otorhinolaryngol 71:197–203.

Schaeren-Wiemers N, Gerfin-Moser A (1993) A single protocol to detect transcripts of various types and expression levels in neural tissue and cultured cells: in situ hybridization using digoxigenin-labelled cRNA probes. Histochemistry 100:431–440.

Schiaffino MV (2010) Signaling pathways in melanosome biogenesis and pathology. Int J Biochem Cell Biol 42:1094–1104.

Schiffmann R, Dwyer NK, Lubensky IA, Tsokos M, Sutliff VE, Latimer JS, Frei KP, Brady RO, Barton NW, Blanchette-Mackie EJ, Goldin E (1998) Constitutive achlorhydria in mucolipidosis type IV. Proc Natl Acad Sci U S A 95:1207–1212.

Schröder BA, Wrocklage C, Hasilik A, Saftig P (2010) The proteome of lysosomes. Proteomics 10:4053–4076.

Schuknecht HF, Gacek MR (1993) Cochlear pathology in presbycusis. Ann Otol Rhinol Laryngol 102:1–16.

Seal RP, Akil O, Yi E, Weber CM, Grant L, Yoo J, Clause A, Kandler K, Noebels JL, Glowatzki E, Lustig LR, Edwards RH (2008) Sensorineural deafness and seizures in mice lacking vesicular glutamate transporter 3. Neuron 57:263–275.

Sergeyenko Y, Lall K, Liberman MC, Kujawa SG (2013) Age-related cochlear synaptopathy: an early-onset contributor to auditory functional decline. J Neurosci 33:13686–13694.

Shen D, Wang X, Li X, Zhang X, Yao Z, Dibble S, Dong X, Yu T, Lieberman AP, Showalter HD, Xu H (2012) Lipid storage disorders block lysosomal trafficking by inhibiting a TRP channel and lysosomal calcium release. Nat Commun 3:731.

Shen H, Zhang B, Shin J-H, Lei D, Du Y, Gao X, Wang Q, Ohlemiller KK, Piccirillo J, Bao J (2007) Prophylactic and therapeutic functions of T-type calcium blockers against noise-induced hearing loss. Hear Res 226:52–60.

Shi L, Chang Y, Li X, Aiken S, Liu L, Wang J (2016) Cochlear Synaptopathy and Noise-Induced Hidden Hearing Loss. Neural Plast 2016:6143164.

Shields B, Wacogne I, Wright CM (2012) Weight faltering and failure to thrive in infancy and early childhood. BMJ 345:e5931–e5931.

Siddiqui Z, Osayande AS (2011) Selected disorders of malabsorption. Prim Care 38:395–414; vii.

Slaugenhaupt SA (2002) The molecular basis of mucolipidosis type IV. Curr Mol Med 2:445–450.

Song Y, Dayalu R, Matthews SA, Scharenberg AM (2006) TRPML cation channels regulate the specialized lysosomal compartment of vertebrate B-lymphocytes. Eur J Cell Biol 85:1253–1264.

Spongr VP, Flood DG, Frisina RD, Salvi RJ (1997) Quantitative measures of hair cell loss in CBA and C57BL/6 mice throughout their life spans. J Acoust Soc Am 101:3546–3553.

Steel KP (2002) Varitint-waddler: a double whammy for hearing. Proc Natl Acad Sci U S A 99:14613–14615.

Steinmetz PRH, Aman A, Kraus JEM, Technau U (2017) Gut-like ectodermal tissue in a sea anemone challenges germ layer homology. Nat Ecol Evol 1:1535–1542.

Stelzner M, Helmrath M, Dunn JCY, Henning SJ, Houchen CW, Kuo C, Lynch J, Li L, Magness ST, Martin MG, Wong MH, Yu J, NIH Intestinal Stem Cell Consortium (2012) A nomenclature for intestinal in vitro cultures. Am J Physiol Gastrointest Liver Physiol 302:G1359–63.

Sun T, Wang X, Lu Q, Ren H, Zhang H (2011) CUP-5, the C. elegans ortholog of the mammalian lysosomal channel protein MLN1/TRPML1, is required for proteolytic degradation in autolysosomes. Autophagy 7:1308–1315.

Tellez-Nagel I, Rapin I, Iwamoto T, Johnson AB, Norton WT, Nitowsky H (1976) Mucolipidosis IV. Clinical, ultrastructural, histochemical, and chemical studies of a case, including a brain biopsy. Arch Neurol 33:828–835.

Thompson EG, Schaheen L, Dang H, Fares H (2007) Lysosomal trafficking functions of mucolipin-1 in murine macrophages. BMC Cell Biol 8:54.

Tian R, Liu SX, Williams C, Soltau TD, Dimmitt R, Zheng X, De Plaen IG (2010) Characterization of a necrotizing enterocolitis model in newborn mice. Int J Clin Exp Med 3:293–302.

Tong B, Hornak AJ, Maison SF, Ohlemiller KK, Liberman MC, Simmons DD (2016) Oncomodulin, an EF-Hand Ca2+ Buffer, Is Critical for Maintaining Cochlear Function in Mice. J Neurosci 36:1631–1635.

Treusch S, Knuth S, Slaugenhaupt SA, Goldin E, Grant BD, Fares H (2004) Caenorhabditis elegans functional orthologue of human protein h-mucolipin-1 is required for lysosome biogenesis. Proc Natl Acad Sci U S A 101:4483–4488.

Turk B, Turk D, Turk V (2012) Protease signalling: the cutting edge. EMBO J 31:1630–1643.

Vasiljeva O, Dolinar M, Pungercar JR, Turk V, Turk B (2005) Recombinant human procathepsin S is capable of autocatalytic processing at neutral pH in the presence of glycosaminoglycans. FEBS Lett 579:1285–1290.

Veereman-Wauters G (1996) Neonatal gut development and postnatal adaptation. Eur J Pediatr 155:627–632.

Venkatachalam K, Hofmann T, Montell C (2006) Lysosomal localization of TRPML3 depends on TRPML2 and the mucolipidosis-associated protein TRPML1. J Biol Chem 281:17517–17527.

Venugopal B, Browning MF, Curcio-Morelli C, Varro A, Michaud N, Nanthakumar N, Walkley SU, Pickel J, Slaugenhaupt SA (2007) Neurologic, gastric, and opthalmologic pathologies in a murine model of mucolipidosis type IV. Am J Hum Genet 81:1070–1083.

Vergarajauregui S, Connelly PS, Daniels MP, Puertollano R (2008) Autophagic dysfunction in mucolipidosis type IV patients. Hum Mol Genet 17:2723–2737.

Wakabayashi K, Gustafson AM, Sidransky E, Goldin E (2011) Mucolipidosis type IV: an update. Mol Genet Metab 104:206–213.

Wang W, Zhang X, Gao Q, Xu H (2014) TRPML1: an ion channel in the lysosome. Handb Exp Pharmacol 222:631–645.

Wangemann P (2006) Supporting sensory transduction: cochlear fluid homeostasis and the endocochlear potential. J Physiol (Lond) 576:11–21.

Weiss N (2012) Cross-talk between TRPML1 channel, lipids and lysosomal storage diseases. Commun Integr Biol 5:111–113.

Williams JM, Duckworth CA, Burkitt MD, Watson AJM, Campbell BJ, Pritchard DM (2015) Epithelial cell shedding and barrier function: a matter of life and death at the small intestinal villus tip. Vet Pathol 52:445–455.

Willott JF (2006) Measurement of the auditory brainstem response (ABR) to study auditory sensitivity in mice. Curr Protoc Neurosci Chapter 8:Unit8.21B.

Willott JF, Erway LC (1998) Genetics of age-related hearing loss in mice. IV. Cochlear pathology and hearing loss in 25 BXD recombinant inbred mouse strains. Hear Res 119:27–36.

Wilson JM, Whitney JA, Neutra MR (1991) Biogenesis of the apical endosome-lysosome complex during differentiation of absorptive epithelial cells in rat ileum. J Cell Sci 100 ( Pt 1):133–143.

Winchester B, Vellodi A, Young E (2000) The molecular basis of lysosomal storage diseases and their treatment. Biochem Soc Trans 28:150–154.

Wong ACY, Ryan AF (2015) Mechanisms of sensorineural cell damage, death and survival in the cochlea. Front Aging Neurosci 7:58.

Wong C-O, Li R, Montell C, Venkatachalam K (2012) Drosophila TRPML is required for TORC1 activation. Curr Biol 22:1616–1621.

Xu H, Delling M, Li L, Dong X, Clapham DE (2007) Activating mutation in a mucolipin transient receptor potential channel leads to melanocyte loss in varitint-waddler mice. Proc Natl Acad Sci U S A 104:18321–18326.

Yan D et al. (2013) Mutation of the ATP-gated P2X(2) receptor leads to progressive hearing loss and increased susceptibility to noise. Proc Natl Acad Sci U S A 110:2228–2233.

Yang H, Gan J, Xie X, Deng M, Feng L, Chen X, Gao Z, Gan L (2010) Gfi1-Cre knock-in mouse line: A tool for inner ear hair cell-specific gene deletion. Genesis 48:400–406.

Yang L, Zhang GJ, Zhong YG, Zheng YZ (2000) Influence of membrane fluidity modifiers on lysosomal osmotic sensitivity. Cell Biol Int 24:699–704.

Yang WP, Levesque PC, Little WA, Conder ML, Shalaby FY, Blanar MA (1997) KvLQT1, a voltage-gated potassium channel responsible for human cardiac arrhythmias. Proc Natl Acad Sci U S A 94:4017–4021.

Yu Y-F, Wu W-Y, Xiao G-S, Ling H-Y, Pan C (2016) Protection of the cochlear hair cells in adult C57BL/6J mice by T-type calcium channel blockers. Exp Ther Med 11:1039–1044.

Zeevi DA, Frumkin A, Bach G (2007) TRPML and lysosomal function. Biochim Biophys Acta 1772:851–858.

Zeevi DA, Frumkin A, Offen-Glasner V, Kogot-Levin A, Bach G (2009) A potentially dynamic lysosomal role for the endogenous TRPML proteins. J Pathol 219:153–162.

Zeevi DA, Lev S, Frumkin A, Minke B, Bach G (2010) Heteromultimeric TRPML channel assemblies play a crucial role in the regulation of cell viability models and starvation-induced autophagy. J Cell Sci 123:3112–3124.

Zeigler M, Bargal R, Suri V, Meidan B, Bach G (1992) Mucolipidosis type IV: accumulation of phospholipids and gangliosides in cultured amniotic cells. A tool for prenatal diagnosis. Prenat Diagn 12:1037–1042.

Zhang F, Jin S, Yi F, Li P-L (2009) TRP-ML1 functions as a lysosomal NAADP-sensitive Ca2+ release channel in coronary arterial myocytes. J Cell Mol Med 13:3174–3185.

Zheng J, Shen W, He DZ, Long KB, Madison LD, Dallos P (2000) Prestin is the motor protein of cochlear outer hair cells. Nature 405:149–155.

Zheng QY, Johnson KR, Erway LC (1999) Assessment of hearing in 80 inbred strains of mice by ABR threshold analyses. Hear Res 130:94–107.

# APPENDIX A

## Differentiation of nascent outer hair cells into inner hair cells in the absence of INSM1

## (UNPUBLISHED MANUSCRIPT, awaiting re-submission)

**Differentiation of nascent outer hair cells into inner hair cells in the absence of INSM1**

Teerawat Wiwatpanit[1,*], Sarah M. Lorenzen[1,*], Jorge A. Cantú[1,*], Chuan Zhi Foo[1], Ann K. Hogan[1], Freddie Márquez[1], John C. Clancy[1], Matthew J. Schipma[2], Mary Ann Cheatham[3-4], Anne Duggan[1,#] and Jaime García-Añoveros[1,3-5,#]

[1]Department of Anesthesiology, Northwestern University, Feinberg School of Medicine, Chicago, Illinois 60611, USA

[2]Next Generation Sequencing Core, Northwestern University Feinberg School of Medicine, Chicago, IL, 60611, USA

[3]Department of Communication Sciences and Disorders, Northwestern University, Evanston, IL 60208, USA

[4]Hugh Knowles Center for Clinical and Basic Science in Hearing and its Disorders, Northwestern University, Chicago, IL 60611, USA

[5]Departments of Neurology and Physiology, Northwestern University, Feinberg School of Medicine, Chicago, Illinois 60611, USA

*These authors contributed equally

#Co-corresponding authors

**The mammalian cochlea contains two types of mechanosensory hair cells that play different but critical roles in hearing. Inner hair cells (IHCs), endowed with an elaborate presynaptic apparatus, signal to cochlear neurons and hence communicate sound information to the brain. Outer hair cells (OHCs), equipped for electromotility,**

**mechanically amplify sound-induced vibrations of the organ of Corti, enhancing sensitivity to sound and sharpening tuning[1,2]. Cochlear hair cells are solely generated during development and their death, most often that of OHCs, is the main cause of deafness. OHCs and IHCs, together with supporting cells of the organ of Corti, originate embryonically from the prosensory region of the otocyst, but how the hair cells differentiate into two different types is unknown[3–6]. Here we show that *Insm1*, which encodes a zinc finger protein transiently expressed in nascent OHCs, prevents them from differentiating as IHCs. In the absence of *Insm1* many hair cells born in the position of OHCs switch fates to become IHCs. We first obtained the transcriptomes of immature inner vs outer hair cells and found them to differ from those of the respective mature cell types, indicating that vastly different gene programs underlie their differentiation and their function. We thus identified genes in addition to *Insm1* underlying OHC- as well as IHC-specific development. We then obtained the transcriptomes of immature OHCs with and without INSM1, and found that INSM1 prevents the expression of a subset of early IHC-specific genes in embryonic OHCs. The homeotic cell transformation of OHCs into IHCs in the absence of INSM1 reveals for the first time a mechanism by which these neighboring epithelial cells become different cell types, identifies and narrows the first candidate genes for IHC-specific differentiation, and suggests the evolutionary mechanism by which OHCs arose early in mammalian evolution.**

OHCs express *Insm1* for a brief period, from the onset of their differentiation (E15.5 close to the base of the cochlea) to soon after birth (P2 at the cochlear apex)[7]. In addition, neuronal progenitors delaminating from the otocyst and the resulting spiral ganglion neurons also express

*Insm1* transiently[7]. Because *Insm1* complete knockouts die embryonically by E19.5[8,9], before most of the known differences between OHCs and IHCs appear, we generated a "floxed" allele (*Insm1*$^{F}$) in which one *loxP* site is inserted in the 5'UTR and the other downstream of this single exon gene, so that their recombination will excise the entire coding sequence (Fig 1a and Extended Fig 1). We conditionally ablated *Insm1*$^{F}$ with *Atoh1*$^{Cre}$, which is expressed starting at E13.5, three days prior to the onset of *Insm1* expression, and recombines *loxP* sites in most (92%) cochlear hair cells (HC) and some supporting cells, but not in spiral ganglion neurons[10]. *Atoh1*$^{Cre/+}$*; Insm1*$^{F/F}$ mice displayed ABR threshold shifts that can be accounted for by DPOAE threshold shifts, a form of hearing impairment characteristic of OHC dysfunction (Fig 1b-d). Examination of their organs of Corti revealed that many cells in the position of the OHCs (the outer compartment) lacked multiple characteristics of this cell type and instead displayed those of IHCs. These HCs had apical bundles of long stereocilia like those of IHCs and not the shorter and W-shaped bundles of OHCs (Fig 1e,f); expressed the IHC-enriched calcium buffer calmodulin and lacked the OHC-specific oncomodulin (Fig 1e,f,h); expressed the vesicular glutamate transporter 3 (VGLUT3), required for IHC presynaptic function, and lacked prestin, required for OHC electromotility (Fig 1g); had the flask shape of IHCs rather than the cylindrical shape of OHCs; had nuclei of the same size as those of IHCs instead of the smaller nuclei of normal OHCs (Fig 1i-j). In addition, these nuclei harbored the transcription factor CtBP2 normally expressed in IHCs and not OHCs (Fig 1k), and the cells contained a large number of presynaptic ribbon synapses (12.4 on average, n=14 cells from a mid-apical fragment of the organ of Corti at P21) closer to that characteristic of control IHCs (15.6 on average, n=10 cells from an *Insm1*$^{F/+}$ littermate; all counts from the equivalent mid-apical position) instead of the few typically found in OHCs (2.1 on average, n=28 cells) (Fig 1k). With rare exceptions (like

one cell shown in Fig 1g), most of these abnormal cells displayed all IHC features examined and lacked all those of OHCs, and therefore we termed them oc-IHCs (outer compartment IHCs).

In the complete absence of INSM1 (*Insm1*$^{-/-}$ embryos), *fgf8* mRNA, a marker of embryonic IHCs[11,12], was not expressed in the presumptive OHCs at E16.5[7], a result we confirmed in five additional sections. In total, we detected *fgf8* mRNA in 6/6 IHCs and 0/18 OHCs, in both *Insm1*$^{-/-}$ and *Insm1*$^{+/+}$ littermate controls. In addition, the organs of Corti of these *Insm1*$^{-/-}$ embryos contained the characteristic single row of IHCs plus three rows of OHCs[7], and the presumptive OHCs of *Insm1*$^{GFP::Cre/-}$ embryos, which completely lack the INSM1 protein, express GFP from an active *Insm1* promoter[7]. Hence OHCs, at least as determined by position, expression of *Insm1*$^{GFP::Cre}$ and lack of *fgf8* mRNA, are generated in the absence of INSM1. The oc-IHCs we detect in mature organs of Corti lacking INSM1 appear subsequently, and could be IHCs displaced from their inner compartment to the outer compartment, newly generated IHCs replacing lost OHCs in the outer compartment, or OHCs that misdifferentiated as IHCs. The oc-IHCs were more frequent in the first rather than second and third HC rows of the outer compartment (Extended Fig 2a). However, they were not displaced IHCs, as the IHC row in *Atoh1*$^{Cre/+}$*; Insm1*$^{F/F}$ mice had an arrangement and density of IHCs like that of littermate controls (*Atoh1*$^{Cre/+}$*; Insm1*$^{+/F}$ and *Insm1*$^{F/F}$; Extended Fig 2b). Although during normal development cochlear hair cells are all born during embryogenesis (between E12 and E16[13,14]), early death of hair cells can trigger the generation of new hair cells from proliferating and transdifferentiating supporting cells, a phenomenon limited to the early postnatal days in mice[15–19]. This does not appear to occur in the absence of INSM1, as hair cell density in the outer compartment (normal OHCs plus oc-IHCs) is not altered up to at least P34 (a subsequent lost may occur afterwards)

(Extended Fig 2c,d), whereas oc-IHCs are present well before. Second, postnatally produced hair cells derived from supporting cells initially express their marker SOX2[16–18], whereas none of the hair cells in the outer compartment of *Atoh1*$^{Cre/+}$*; Insm1*$^{F/F}$ examined from P0 to P5 expressed SOX2 (0/95 OHCs at P0 and 0/42 OHCs at P2 and 0/39 OHCs at P5; Fig 2e). Third, some postnatally produced hair cells result from the postnatal proliferation of supporting cells[15–18], yet none of the hair cells in the outer compartment of *Atoh1*$^{Cre/+}$*; Insm1*$^{F/F}$ mice derived from postnatal proliferations as determined by nuclear incorporation of the thymidine analog 5-ethynyl-2′-deoxyuridine (EdU)[20] repeatedly administered from birth to P5 (0/77 OHCs) or P8 (0/40 OHCs) (Fig 2f). Altogether these results indicate that oc-IHCs are not the result of OHCs death followed by replacement from either displaced IHCs or from postnatally generated hair cells. Indeed, we found evidence of oc-IHCs in *Atoh1*$^{Cre/+}$*; Insm1*$^{F/F}$ as early as P0 (Fig 2a-d). Although the characteristic orientation of IHCs vs OHCs is maintained by birth in *Atoh1*$^{Cre/+}$*; Insm1*$^{F/F}$, the disorganization of the OHC rows at the level of the nuclei already revealed alterations in cell shape (Fig 2a). Furthermore, although most differences between IHCs and OHCs develop postnatally, by birth, control animals express neuroplastin preferentially in the stereocilia of OHCs and VGLUT3 selectively in IHCs. By comparison, in *Atoh1*$^{Cre/+}$*; Insm1*$^{F/F}$ many HCs in the outer compartment failed to express (or did so at low levels) neuroplastin (Fig 2b) and many expressed variable levels of VGLUT3 (Fig2c). Finally, the transcription factor BCL11B, which we report later in this study as being selectively expressed in neonatal OHCs (Fig 3e,f), is already missing in many HCs of the outer compartment of *Atoh1*$^{Cre/+}$*; Insm1*$^{F/F}$ mice at P2 (Fig 2d). Hence we conclude that oc-IHCs develop from embryonically generated cochlear outer compartment HCs that misdifferentiate to acquire the features of mature IHCs instead of those of mature OHCs. This change in cell fate represents a homeotic cell transformation of

OHCs into IHCs and reveals that INSM1 is a critical regulator of the OHC vs IHC differentiation switch.

The switch in cell fate takes place in almost half (42.6% ± 10.9 SD; 936 cells counted from organs of Corti collected from 12 mice ages P0 to P46) of outer compartment HCs, while the reminder mature as OHCs. These OHCs that remain untransformed may be accounted for by a variability in the time at which Cre recombines both *Insm1*$^{F}$ alleles in each hair cell. Indeed, we have evidence that a brief expression of *Insm1* is sufficient to evade the phenotypic conversion: *Gfi1*$^{Cre/+}$*; Insm1*$^{F/F}$ mice display almost no oc-IHCs (0.78%; 5/526 OHCs from 2 mice; Extended Fig 3). Since in these mice the onset of Cre recombinase expression coincides with that of *Insm1* (E15.5)[7,21], their nascent OHCs will express *Insm1* for at least several hours. Added to the transient expression of *Insm1*, which subsides in OHCs soon after birth[7], it appears that this gene determines the fate of OHCs during an early and narrow developmental period.

In other developing cell types, INSM1 functions as a transcription factor, either as an activator or as a repressor[22–28]. Hence, we hypothesized that the mechanisms by which *Insm1* directs OHCs to develop differentially from IHCs involves activation of OHC-specific genes or inhibition of IHC-specific genes. In order to test these hypotheses we first determined which genes are expressed in either type of hair cell during differentiation, when *Insm1* is being expressed (Fig 3), and then searched for the genes regulated by INSM1 in developing OHCs (Fig 4). For both approaches we took advantage of the *Insm1*$^{GFP::Cre}$ allele, in which the coding sequence of *Insm1* is replaced by that of a fusion protein between the GFP reporter and the Cre recombinase, thereby serving as a reporter as well as a null allele[7,27]. We generated *Insm1*$^{GFP::Cre/+}$; *Atoh1*$^{A1GFP/+}$*; R26R* $^{tdTomato/+}$ mice, in which all HCs express GFP (starting at E13.5 from

*Atoh1*$^{A1GFP}$ and, in OHCs, from *Insm1*$^{GFP::Cre}$) but only OHCs also express tdTomato following *Insm1*$^{GFP::Cre}$ expression (throughout the cochlea by E18.5[7]; fig 3a,b). We used these mice to sort apart dissociated OHCs and IHCs from neonatal (P0) organs of Corti (obtained with timed pregnancies and corresponding to ~E19.5, the most frequent day of birth for the mouse line used), as in fig 3c. With fluorescent activated cell sorting (FACS) we collected seven separate pools of IHCs (700-1100 cells per pool) and OHCs (2800-3700 cells per pool) and purified their RNAs (~3 ng per IHC pool and 10 to 18 ng per OHC pool). After sorting we extracted total RNA, confirmed by RT-qPCR that it originated mainly from IHCs or OHCs (Fig 3d), and used samples with an RNA integrity number (RIN) >8 for subsequent RNA-seq to obtain for the first time the transcriptomes of separate perinatal IHCs and OHCs (Supplementary table 1). We then analyzed differential gene expression between these developing IHC and OHC transcriptomes (6 sets of each) and identified 922 IHC-enriched genes and 676 OHC-enriched genes (Fig 3e and supplementary tables 1-3). Among these are the 12 genes previously shown (with immunohistochemistry, in situ hybridization or reporter alleles) to be expressed only or preferentially in IHCs or OHCs at embryonic to early postnatal stages[7,11,12,29–32] (Fig 3e), indicating that our approach detects most differentially-expressed genes. The presence of the expected transcripts, however, does not exclude the potential for false positives. Particularly concerning was whether genes with small RNA-seq expression level differences (two-fold or less, such as *Zmat3*), or detected at very low levels in one cell type and not at all in the other (such as *Sox18* and *Msx1*), were truly differentially expressed. Hence we selected 20 transcripts (black squares in Fig 3e), most of them previously uncharacterized, and tested them by TaqMan RT-qPCR for differential expression using as templates the spare (not used for RNAseq) IHC and OHC RNA pools. All 20 genes were confirmed to be differentially expressed, and the

differences in expression levels were similar whether estimated by RNA-seq or RT-qPCR (Fig 3f). We also confirmed differential expression of two additional genes by methods not susceptible to potential artifacts of cell sorting and mRNA detection: *Bcl11b*, whose protein product we detected by immunohistochemistry in E18.5, P0 and P2 OHC (but not IHC) nuclei (Fig 3e inset and Fig 2d); and *Insm2*, whose expression in E17.5 OHCs but not IHCs we detected with an $Insm2^{LacZ}$ reporter mouse line we generated (Fig 3e inset). All the above evidence attests to the low prevalence of false positives among the genes that, based on cell sorting combined with RNA-seq, we estimated as being differentially-expressed between immature IHCs and OHCs.

The transcriptomes of perinatal cochlear hair vs supporting cells have been obtained, but these included a mixture of both OHCs and IHCs[29,30]. Although cell-type specific transcriptomes of mature IHCs and OHCs, obtained with microarray technology, were also reported[33], ours are the first transcriptomes of these cell types prior to maturity, during early differentiation. A comparison among differentiating vs mature IHC- or OHC-enriched genes reveals very little overlap (Fig 3g and supplementary table 4): only 5.9% IHC-enriched and 2% OHC-enriched genes are so at both differentiating and mature stages. These include some known genes characteristic of the mature stage (*Vglut3* and *Otof* in IHCs and *Prestin* in OHCs) but whose expression is incipient at birth. However, the vast majority of the genes preferentially expressed in either cell type during differentiation (like *Insm1*, *Insm2*, *Bcl11b*, Atxn3, Efna5, *Neurod6*, *Sox18* and *Tal1* in OHCs; and *Brip1*, *Dtx3*, *Fgf8*, *Nhs*, *Rin3*, *Zfhx2*, *Zfp324*, *Zfp568*, *Zfp827* and *Zmat3* in IHCs), are not expressed upon maturation, and vice versa. These results reveal that a complex transcriptome, involving hundreds of genes, is transiently active during OHC- and IHC-

specific differentiation. It is in this genetic context that INSM1 directs the differentiation of immature outer compartment HCs into mature OHCs and not IHCs.

Next, in order to explore how INSM1 drives OHC differentiation, we looked for the genes differentially expressed in differentiating OHCs with and without INSM1. We generated litters with both *Insm1*$^{GFP::Cre/+}$ (expressing INSM1 from the wild type allele) and *Insm1*$^{GFP::Cre/-}$ (entirely lacking INSM1 since the *Insm1*$^{-}$ allele deletes its single exon[9]) embryos. Because the complete lack of INSM1 results in embryonic lethality we collected embryos at E18.5, the latest stage at which *Insm1*$^{GFP::Cre/-}$ embryos survive[8,9], and close to the stage (P0/E19.5) at which we had identified the differentiating OHC and IHC transcriptomes. At this stage OHCs have been expressing *Insm1* for approximately one (at the cochlear apex) to three (at the base) days. We then proceeded to dissociate and collect OHCs by FACS from these embryos (three separate pools of OHCs per genotype; Extended Fig 4a-e), extract their RNAs (Extended Fig 4f,g) and process them for RNA-seq to identify and quantify the transcripts expressed by the pools of sorted cells (Fig 4a and supplementary table 5). With stringent statistical conditions (FDR-adjusted p values <0.05), we identified 31 genes (red squares; fig 4a and supplementary table 5) significantly expressed at different levels in *Insm1*$^{GFP::Cre/-}$ vs *Insm1*$^{GFP::Cre/+}$ OHCs. Among these genes, 14 are preferentially expressed in *Insm1*$^{GFP::Cre/+}$ OHCs (upregulated by *Insm1*) and 17 in *Insm1*$^{GFP::Cre/-}$ OHCs (down-regulated by *Insm1*; supplementary tables 6 and 7).

A comparison of the genes regulated in OHCs in the absence of INSM1 (fig 4a and supplementary tables 6 and 7) with those normally enriched in either OHCs or IHCs (from fig 3e and supplementary tables 2 and 3) suggests that *Insm1* is not acting by activating OHC-specific genes but rather by inhibiting IHC-specific genes (supplementary table 8). None of the 14 genes

upregulated by INSM1 in OHCs are enriched in wild type OHCs, whereas 6/17 genes downregulated by INSM1 in OHCs are enriched in wild type IHCs. However, because we worried that FDR-adjustment could exclude genes truly expressed differentially, we also considered the 300 additional genes with a raw p value <0.01 (green squares; fig 4a) as potential targets of *Insm1* regulation. Of the extended list of 146 candidate genes predicted to be upregulated by INSM1 in OHCs (i.e., expressed at higher levels in embryonic OHCs with than without INSM1), only 7 are enriched in wild type OHCs, close to the 4 expected at random (Fig 4b and supplementary table 8). However, of the extended list of 185 candidate genes predicted to be downregulated by INSM1 in OHCs, 36 are enriched in wild type IHCs, considerably more than the 7 expected coincidentally (Fig 4e, supplementary table 8 and extended table 1). By TaqMan RT-qPCR we confirmed the higher expression of 5 of these genes (*Tbx2*, *Nhs*, *Brip1*, *Rin3* and *Lrrn1*) both in OHCs without INSM1 over those with INSM1 as well as in IHCs over OHCs (Fig 4f, 3f and supplementary table 8). Furthermore, the level of enrichment of all of these genes in wild type IHCs (over OHCs) is similar to the level of upregulation in OHCs in the absence of INSM1 (Fig 4f,g and extended table 1). By contrast, most of the genes we identified as differentially expressed in OHCs vs IHCs were not affected by the presence or absence of INSM1 (such as *Prestin* and *Bcl11b* in OHCs and *Vglut3* and *Otoferlin* in IHCs; Fig 4f). The implication is that INSM1 downregulates a small subset of IHC-enriched genes in immature HCs of the outer compartment (which normally mature into OHCs); in the absence of INSM1, those genes are expressed in embryonic outer compartment HCs, which go on to differentiate into mature IHCs instead of OHCs.

At E18.5, OHCs lacking INSM1 have not upregulated most of the early IHC-specific genes and still express the early OHC-specific genes (a few examples are plotted in Fig 4f, including *Vglut3* and *Prestin*), even though many of these cells will subsequently, once differentiated, express all examined IHC features and markers (like VGLUT3) and none of OHCs (like Prestin) (Fig 1e-k). This is consistent with the OHC fate initially specified for outer compartment HCs even in the absence of INSM1. The small set of early IHC-specific genes that are upregulated in embryonic OHCs lacking INSM1 likely represent an early step in the genetic cascade that eventually leads to their complete transformation into IHCs. Since outer compartment HCs expressing these few genes differentiate as IHCs, it follows that these genes are likely required for the IHC differentiation program. Hence, in addition to identifying *Insm1* as a critical gene for the specific differentiation OHC, our results also identify the first candidate genes for executing the specific differentiation of IHCs.

Our results reveal a homeotic transformation of OHCs into IHCs in the absence of INSM1, identifies the genes initially misregulated by ablation of *Insm1*, and provide for the first time a preliminary genetic mechanism for how these two cell types differentiate apart: nascent outer compartment HCs express *Insm1*, which represses (perhaps directly, as a transcriptional repressor, although it could also repress indirectly, via intermediary factors) a small set of early IHC-specific genes and prevents their maturation as IHCs. Interestingly, a similar role may also be played by the nematode ortholog of *Insm1*, *egl-46*, which is also expressed in subtypes of mechanosensory cells: in FLP neurons it prevents the expression of genes characteristic of another type of mechanoensory cell, the light touch receptor neurons[34]; and in HOB it is required for expressing genes that distinguish it from its sister sensory cell, the HOA[35]. However, OHCs

are a new cell type arising in the line leading to mammals and are not evolutionary homologs of the nematode FLP or HOB neurons. The similar roles of *Insm1* and *egl-46* suggest the recurrent utilization of these orthologs for switching sensory cell fates. In fact, the repression by *Insm1* of the IHC-differentiation program in nascent OHCs may not only account for their developmental formation, but also for their evolutionary onset in the mammalian cochlea[36]. It has been proposed that new cell types may arise through the expression in a subset of a pre-existing cell type of a gene that represses its cell-specific differentiation, opening the pathway for an alternative differentiation[37]. In the case of the mammalian organ of Corti, the ancestral cell type is most probably the IHCs, since they share more features with other hair cells than the OHCs; expression of *Insm1* in a subset of these ancestral cells could have led to an alternative differentiation into OHCs.

**Supplementary Information** is available in the online version of the paper at www.nature.com/nature.

**Acknowledgments** The genetically engineered mice were generated with the assistance of the Transgenic and Targeted Mutagenesis Laboratory, partially supported by NIH grant CA60553 to the Robert H. Lurie Comprehensive Cancer Center at Northwestern University. Imaging work was performed at the Northwestern University Center for Advanced Microscopy supported by NCI CCSG P30 CA060553 to the Robert H Lurie Comprehensive Cancer Center. FACS was performed on a BD FACSAria SORP system, purchased through the support of NIH 1S10OD011996-01, at the Flow Cytometry Core Facility supported by Cancer Center Support Grant (NCI CA060553). Next generation sequencing, TaqMan qRT-PCR, RNA quality control and RNAseq analysis were supported by the Northwestern University NUSeq Core Facility. We

thank A. Groves for protocols and advice, D. He for original databases of microarray results, J. Zheng and S. Takahashi for antibodies and protocols, J. Bartles for comments and A. Ahmad for data collection. Work supported by NIH Grants NS044363, DC000089 and DC012483.

**Author Information** Reprints and permissions information is available at www.nature.com/reprints. The authors have no competing interests. Correspondence and requests for materials should be addressed to J.G.A. (anoveros@northwestern.edu) and A.D. (a-duggan@northwestern.edu).

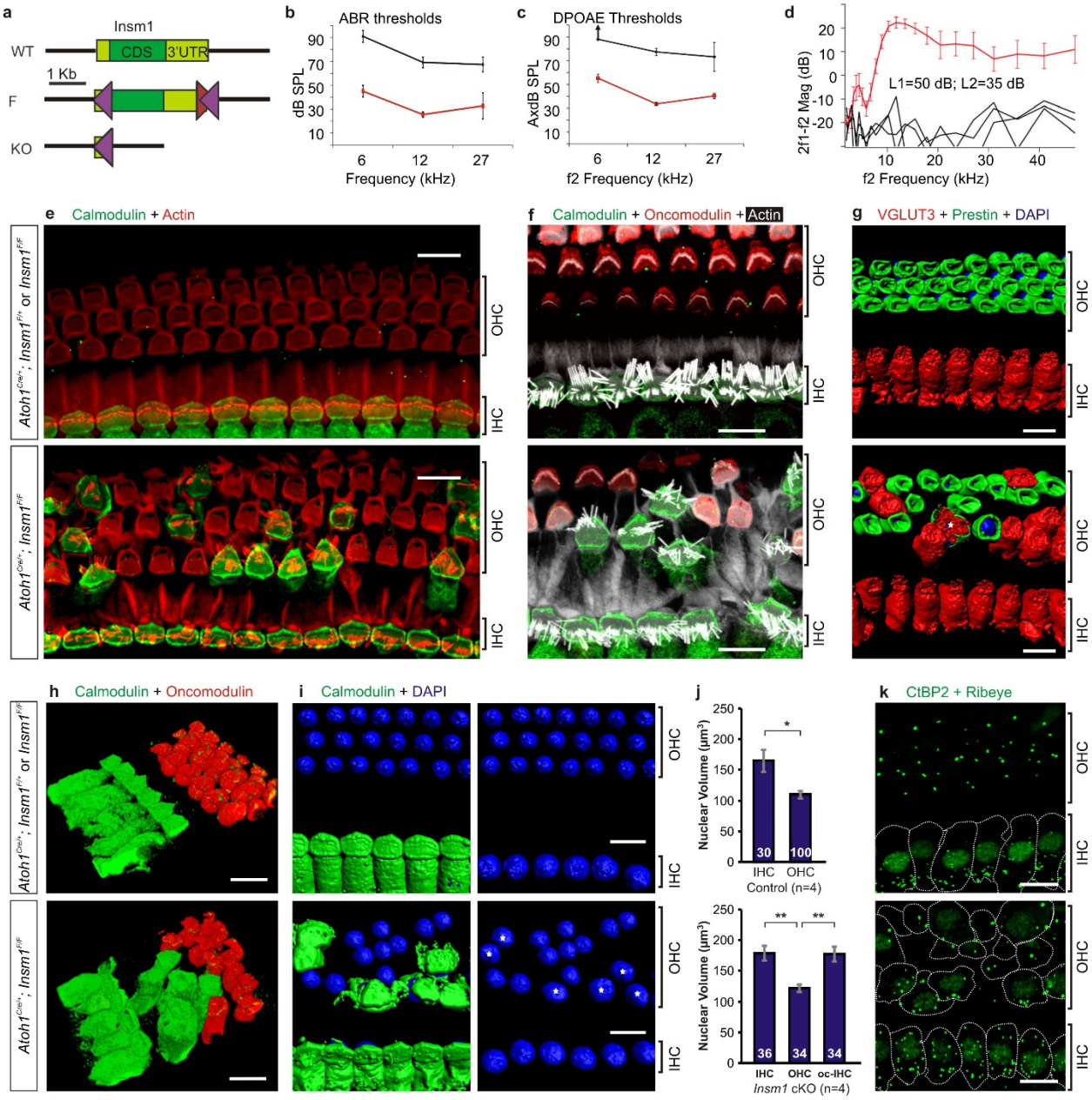


**Figure 1: Conditional ablation of *Insm1* in hair cells causes hearing impairment and the appearance of IHC-like cells in place of OHCs**. **a** Schematic of the wild type (WT), floxed (F) and conditionally deleted (cKO) alleles of *Insm1*. We generated a Floxed (F) allele in which the sole exon of *Insm1* (green rectangle, with the coding sequence (CDS) dark green and the untranslated regions (UTRs) light green) has a *loxP* site (purple triangle) inserted in a poorly-

conserved area of its 5' UTR and another *loxP* site downstream of the *Insm1* gene. Co-expression with Cre recombinase generates an *Insm1* KO allele lacking its CDS and 3'UTR, leaving only part of the 5'UTR. The red triangle represents an FRT site remaining from the targeting strategy. **b-d** Hearing thresholds determined by auditory brainstem responses (ABRs; **b**) and distortion product otoacoustic emissions (DPOAEs; **c**), and iso-input functions for the DPOAE at 2f1-f2 (**d**) of $Atoh1^{Cre/+}$; $Insm1^{F/F}$ mice at age P25 to P31 (black traces; n=5, 3 males + 2 females) and control littermates (red traces; n=8; 4 $Insm1^{F/F}$ to control for potential effects of the *loxP* insertions, and 4 $Atoh1^{Cre/+}$; $Insm1^{F/+}$ to control for any effects of *Atoh1* heterozygosity and *Cre* expression; 6 males + 2 females). ABR threshold shifts may be accounted for by defective DPOAEs, which were either absent or had raised thresholds. The up arrow in **c** indicates that the maximum sound pressure level was not sufficient to reach threshold for f2=6 kHz. **e-l** Immunohistochemistry in whole mount organs of Corti from the mice tested above revealed that the $Atoh1^{Cre}$; $Insm1^{F/F}$ mice had normal IHCs but that many of the OHCs expressed abundant calmodulin but not oncomodulin (**e**, **f**, **h**), had stereocilliary bundles resembling those of IHCs (as revealed with phalloidin labelling of filamentous actin; **e**, **f**), expressed VGLUT3 instead of Prestin (**g**; one rare cell, marked with an asterisk, expressed both), had the cell shape characteristic of IHCs (**h**; marked with asterisks), and had large nuclei like those of IHCs (labelled with DAPI: 4',6-diamidino-2-phenylindole; **i**, **j**). **j** Nuclear volume (average ± SEM) from IHCs, OHCs, and calmodulin-rich HCs in the outer compartment (oc-IHCs). The number of nuclei measured for each cell type are indicated within each bar. Sample size (n) indicates the number of mice from which the nuclei were measured. Student's T-test; $p< 0.05$ (*); $p< 0.01$ (**). **k** Antibodies against CtBP2, which label both the CtBP2 transcription factor expressed in IHC nuclei as well as the synaptic ribbon protein Ribeye (larger cytoplasmic puncta), revealed

CtBP2 in the nuclei of the oc-IHCs, as well as an increase in the number of presynaptic ribbons approaching that of IHCs. Images are from mid-cochlear positions of mice at ages P34 (**e**, **g**, **i**), P46 (**f**, **h**), and P21 (**k**). Controls were *Insm1*$^{F/F}$ (**e**, **g**, **i**) or *Atoh1*$^{Cre}$; *Insm1*$^{F/+}$ (**f**, **j**) littermates. Scale bars are 10μm.

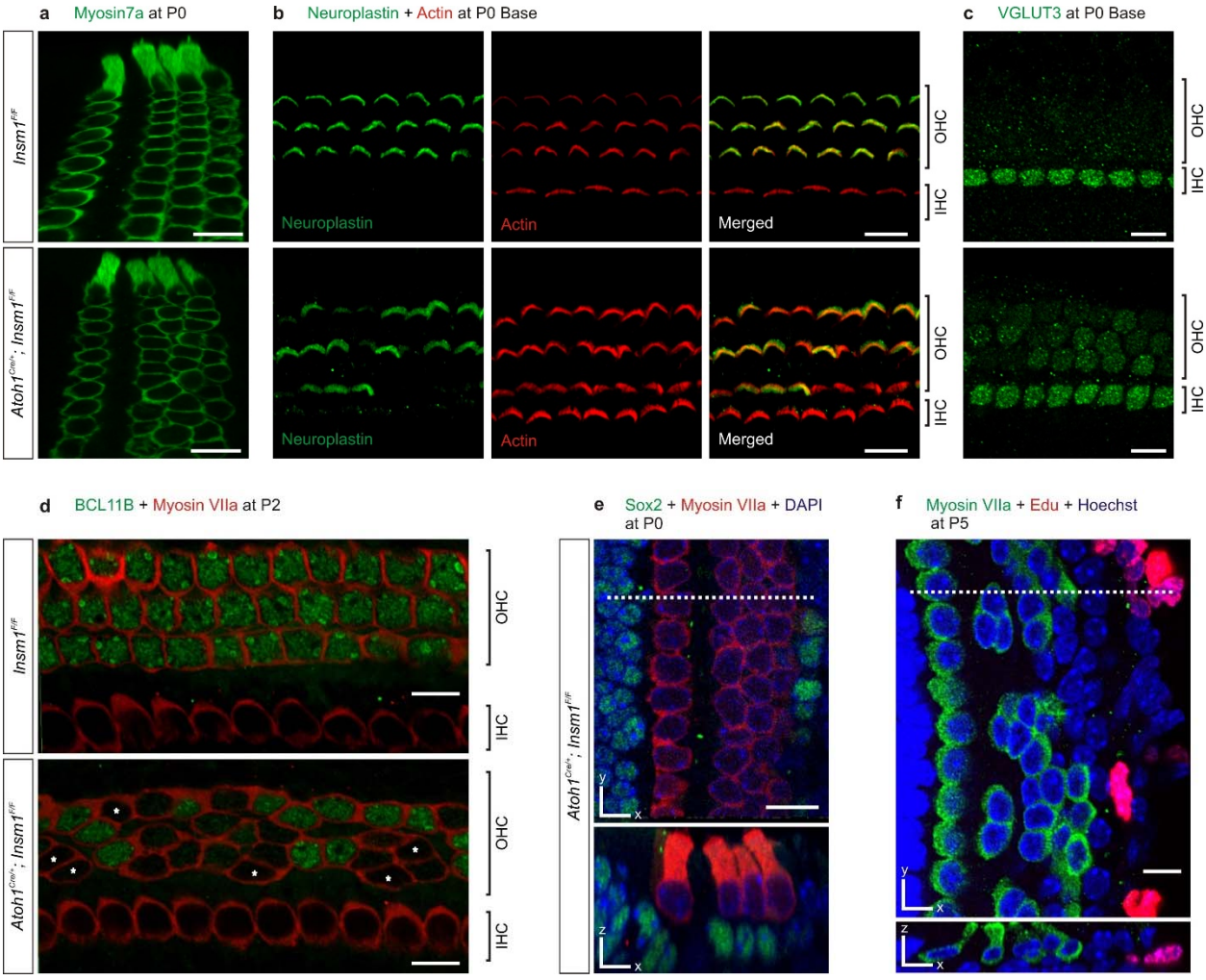


**Figure 2: IHC-like cells in the outer compartment (oc-IHCs) result from OHC misdifferentiation in the absence of INSM1, not from IHC displacement or from supporting cell transdifferentiation. a-f** Immunohistochemistry in organ of Corti whole mounts from mice at P0 and P5. **a** Hair cell marker myosin VIIa revealed that there was no hair cell loss in *Atoh1*$^{Cre/+}$; *Insm1*$^{F/F}$ organ of Corti. Although *Atoh1*$^{Cre/+}$; *Insm1*$^{F/F}$ OHCs at P0 retained their characteristic inclination (opposite to that of IHCs), their cell bodies were disorganized at the nuclear level, as indicated by confocal 3D rendering (optically sliced in the Z and Y planes). **b** All OHCs at the base of cochleae from *Insm1*$^{F/F}$ mice expressed the early OHC-

specific marker neuroplastin (green), localized to stereocilia of OHCs as visualized by the filamentous actin probe phalloidin (red). However, some OHCs at the base of cochleae from *Atoh1*$^{Cre/+}$; *Insm1*$^{Flox/Flox}$ mice lacked or had reduced levels of neuroplastin (**b**); and instead expressed IHC-specific VGLUT3 at varying levels as opposed to the relatively homogenous high level in IHCs (**c**). **d** While BCL11B, an immature OHC-specific transcription factor, was present in all OHCs from *Insm1*$^{Flox/Flox}$ mice, its expression was diminished or undetectable (marked with asterisks) in about half of OHCs from *Atoh1*$^{Cre/+}$; *Insm1*$^{F/F}$ mice at P2. **e** SOX2-immunoreactivity, which labels the nuclei of cochlear supporting cells and, under certain conditions, of hair cells transdifferentiated from them postnatally, was not present in cells of the OHC region in *Atoh1*$^{Cre/+}$; *Insm1*$^{F/F}$ pups. **f** To track postnatal cell proliferation in the organ of Corti, neonatal mice were injected twice daily with EdU from P0 to P5. The lack of EdU in any hair cell from in *Atoh1*$^{Cre/+}$; *Insm1*$^{F/F}$ mice confirmed that these, including oc-IHCs, were not produced from postnatally-dividing supporting cells. Unless otherwise noted, images are from mid cochlear positions. Hair cells were identified by myosin VIIa immunoreactivity, phalloidin, DAPI and Hoechst. Scale bars are 10μm.

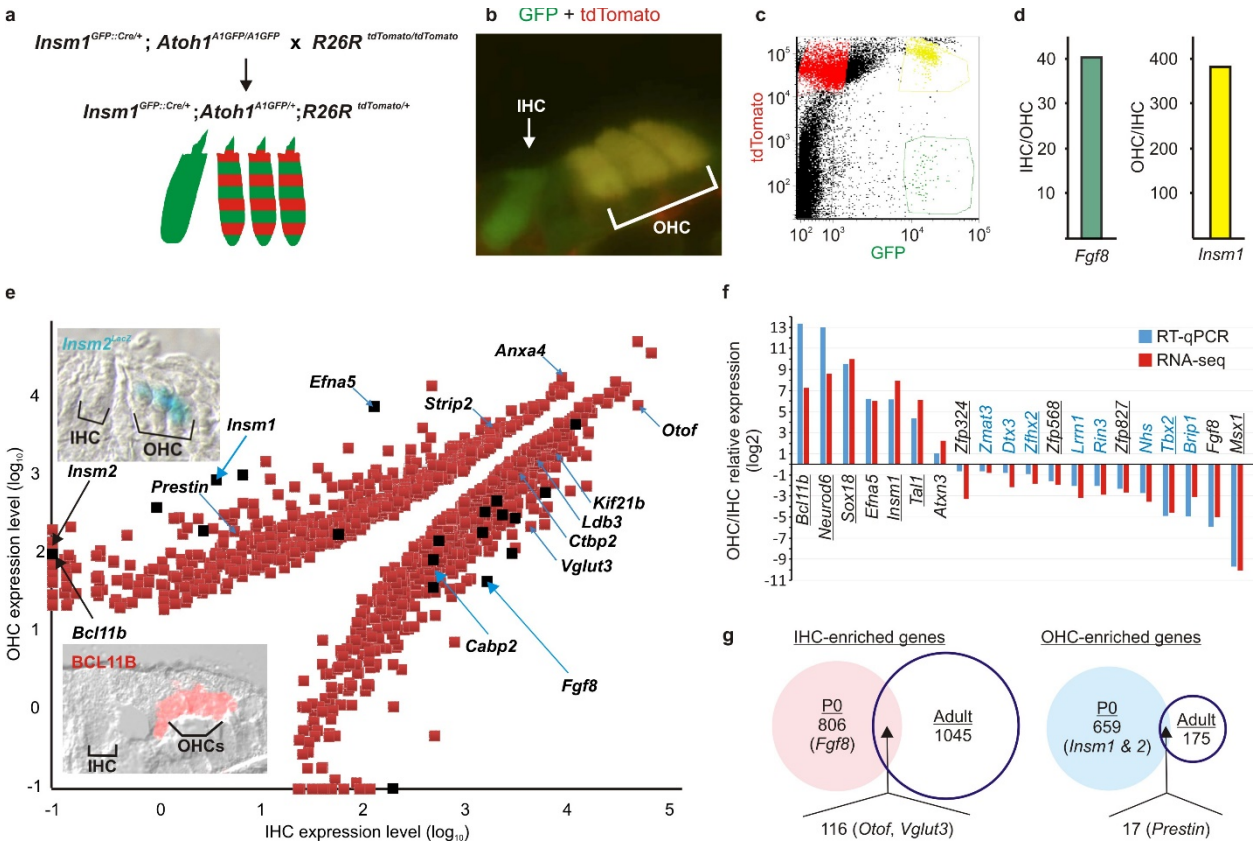


**Figure 3: Genes preferentially expressed in immature IHCs or OHCs. a-d** Strategy for collecting separate pools of perinatal (P0) OHCs and IHCs by fluorescent activated cell sorting (FACS). **a** Genetic strategy for generating pups in which live IHC and OHCs can be fluorescently distinguished (Green, GFP; Red, tdTomato). **b** The resulting *Insm1*$^{GFP::Cre/+}$*; Atoh1*$^{A1GFP/+}$*; R26R*$^{tdTomat0/+}$ mice have IHCs expressing GFP only and OHCs expressing GFP plus tdTomato. Neurons (not seen in this image) express tdTomato but GFP from the *Insm1*$^{GFP::Cre}$ allele has subsided. **c** Cell sorting based on green and red fluorescence separates IHCs (green) from OHCs (yellow) and neurons (red). **d** RT-qPCR for IHC-specific transcript *Fgf8* and OHC-specific transcript *Insm1* confirm that these pools of cells collected are 40x to 380x enriched for IHCs or OHCs, respectively. **e** Logarithmic plot of genes (squares)

preferentially expressed in either IHCs or OHCs based on RNA-seq values. Blue arrows indicate those genes previously known to be HC subtype specific in neonates[7,11,12,29–32]. We additionally confirmed perinatal OHC or IHC-specific expression for *Insm2* with a knock in reporter line (E17.5; top inset), for the *Bcl11b* product by immunohistochemistry (P0; bottom inset), and for *Bcl11b* and 19 more genes (black squares) by TaqMan RT-qPCR (P0). **f** Comparison of fold difference of mRNA expression levels (on a Log2 scale) determined (for genes indicated as black boxes in **e**) by RNA-seq and TaqMan RT-qPCR. Genes encoding transcription factors are underlined. IHC-specific genes inhibited by INSM1 in embryonic OHCs are in blue. **g** Venn diagrams indicating the number of genes enriched in either IHCs or OHCs of neonates vs adults (estimated from[33]). Representative genes are named in parentheses. Although neonatal HCs of either type begin to show expression of some functional markers characteristic of mature cells (*Otoferlin* and *Vglut3* in IHCs and *Prestin* in OHCs), the majority of HC-type specific genes at this early stage differ from those of the mature cells.

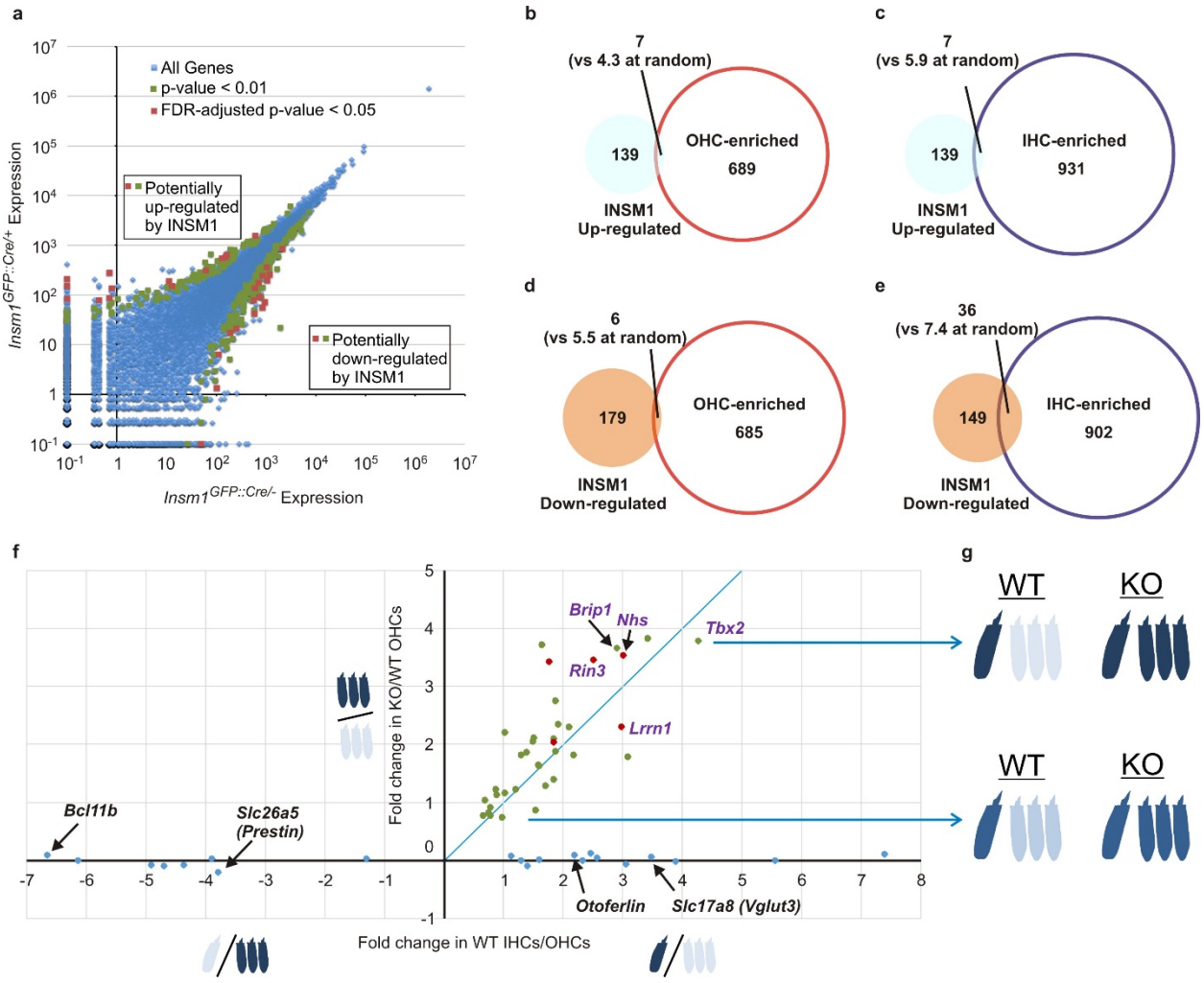


**Figure 4: *Insm1* prevents expression of a subset of immature IHC-specific genes in embryonic OHCs. a** Identification of genes potentially regulated by INSM1 in embryonic to perinatal outer hair cells (OHCs). Plot of average expression levels determined by RNA-seq from E18.5 OHCs expressing (from $Insm1^{GFP::Cre/+}$) or lacking INSM1 (from $Insm1^{GFP::Cre/-}$) (three pools of separately collected OHCs per genotype). In order to plot undetected transcripts (with a value of 0) in this logarithmic scale we arbitrarily assigned them an expression level of $10^{-1}$. However, many genes that appear on this plot as differentially expressed between genotypes are due to unrepresentative values obtained in only one of the three samples. To select transcripts

whose expression differs statistically between genotypes, we used DESeq2[38] and established as cutoff either an FDR-adjusted p-value <0.05 (red squares) or, for a less stringent selection, a raw p-value <0.01 (green squares). Blue diamonds represent all other transcripts. **b-e** Venn diagrams indicating the overlap between IHC or OHC-enriched genes with the genes predicted to be regulated by INSM1 in OHCs. Up and down-regulated genes are those overexpressed in OHCs with or without INSM1, respectively. The expected number of genes that would appear in each of these analyses by random coincidence is shown in parentheses. Only (**e**) reveals a larger overlap than randomly expected, pointing to 36 IHC-specific genes that appear down-regulated by INSM1 in OHCs. **f** Plot of the differential expression of genes in OHCs vs IHCs and OHCs with and without INSM1. Genes are plotted as dots with color-code corresponding to the p-value criteria used in (**a**)**.** Blue dots along the X-axis are examples of the many genes enriched in either IHCs (such as *Otof* and the VGLUT3-encoding *Slc17a8* on the right) or OHCs (such as *Bcl11b* and the Prestin-encoding *Slc26a5* on the left) that are not affected by the presence or absence of INSM1. By contrast, green and orange dots represent the 36 genes that are normally enriched in IHCs and upregulated in OHCs lacking INSM1. Of these, genes whose differential expression was further confirmed by TaqMan RT-qPCR are named in purple. Although the level of differential expression varies from gene to gene (from >2x to ~16x), each gene is upregulated to a similar extent in IHCs (vs OHCs) as in OHCs lacking INSM1 (vs IHCs with INSM1). Hence, INSM1 accounts for the repression (directly or indirectly) of these IHC genes in early OHCs. **g** Graphic interpretation representing one IHC and three OHCs as typically present in cross sections of the organ of Corti. Darker shades of blue indicate higher expression levels.

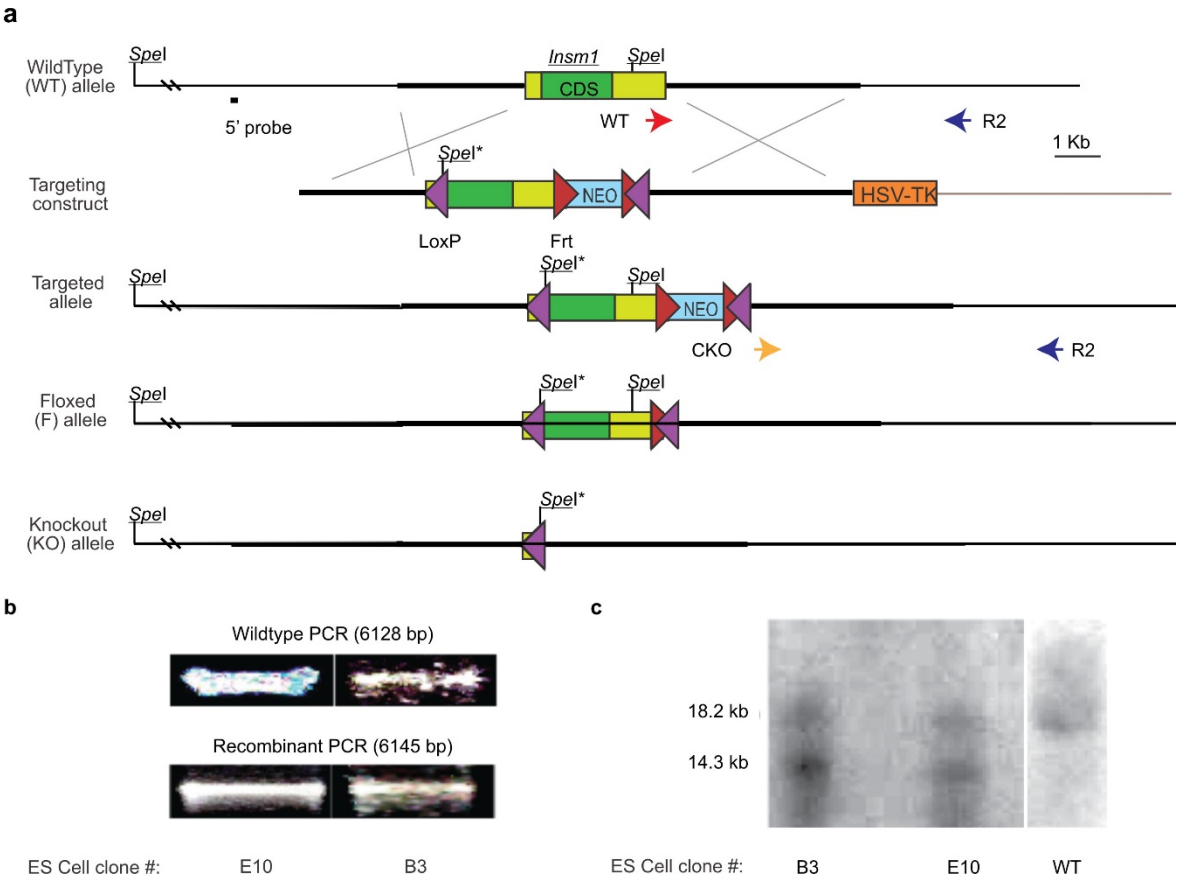


**Extended Figure 1: Generation of a conditional KO allele of *Insm1*. a** We generated a targeting construct in which the sole exon of *Insm1* (green rectangle, with the coding sequence in dark green and the UTRs in light green) has a *loxP* site (purple triangle) inserted in a poorly-conserved area of its 5' UTR and another *loxP* site downstream of the *Insm1* gene. The construct also incorporates a neomycin resistance cassette (NEO, blue) surrounded by *FRT* sites (red triangles) and a Thymidine kinase cassette (HSV-TK; orange), which are used to select for recombination events after gene targeting. **b** We screened a total of 439 clones and identified 5 recombinants (2 are shown) with PCR using primers indicated in (**a**, arrows). Expected sizes for wild type allele using primers WT to R2 is 6163 bp. Expected size for recombinant clones using CKO-Reverse is 6145 bp. **c** Selected ES cell clones were additionally screened for homologous

recombination upstream of the first *loxP* site by Southern blot after digestion with *Spe*I and using the 5' probe indicated in (**a**)[9]. The expected band sizes for wild type and conditional KO alleles are 18,162 bp and 14,333 bp, respectively. From one of these clones (B3) we generated first chimeric mice and then mice with floxed alleles of *Insm1 (*obtained by crossing the chimeras with mice expressing the FlpE recombinase (B6-Tg(CAG-FLPe)36[39], which deleted the NEO cassette flanked by FRT sites). Homozygous *Insm1*$^{F/F}$ mice are viable, demonstrating that the *loxP* insertions do not interfere with the vital functions of *Insm1* and hence may be used for its conditional ablation. Co-expression with Cre recombinase generates an *Insm1* KO allele lacking its entire coding sequence.

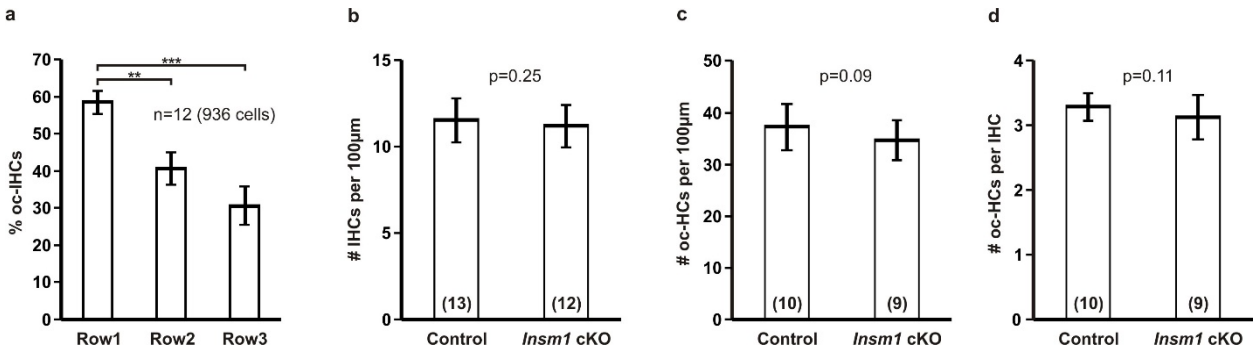


**Extended Figure 2: Densities of IHCs and outer compartment HCs (OHCs and oc-IHCs) in mice conditionally lacking INSM1**. **a** In *Atoh1*$^{Cre/+}$*; Insm1*$^{F/F}$ organs of Corti, inner-like cells in the outer compartment (oc-IHCs) are more frequent in the first row of OHCs (closer to the IHCs) than in the second and third rows. Data obtained from 12 animals (2 males, 3 females and 7 of undetermined sex; 936 cells in total). Student's T-test; ** indicates $p<0.01$; *** indicates $p<0.001$. Error bars indicate SD. **b** *Atoh1*$^{Cre/+}$*; Insm1*$^{F/F}$ mice have the same density of IHCs (11.2 ± 1.2 SD cells per 100 µm along the organ of Corti; n=12) as that of littermate controls (*Atoh1*$^{Cre/+}$*; Insm1*$^{+/F}$ and *Insm1*$^{F/F}$; 11.5 ± 1.3 SD cells per 100 µm; n=13) suggesting that oc-IHCs are not IHCs displaced from the inner to the outer compartment. **c** There is no evidence for loss of OHCs in *Atoh1*$^{Cre/+}$*; Insm1*$^{F/F}$ mice up to P34. Densities of outer compartment hair cells (oc-HCs) do not differ between *Atoh1*$^{Cre/+}$*; Insm1*$^{F/F}$ mice (OHCs + oc-IHCs) and their littermate controls (OHCs only) (34.6 ± 3.8 SD cells per 100 µm along the organ of Corti of *Atoh1*$^{Cre/+}$*; Insm1*$^{F/F}$ mice, n=9; vs 37.3 ± 4.5 SD cells per 100 µm of *Atoh1*$^{Cre/+}$*; Insm1*$^{+/F}$ and *Insm1*$^{F/F}$ littermate controls, n=10). **d** The ratio of outer compartment HCs per IHC do not differ significantly between *Atoh1*$^{Cre/+}$*; Insm1*$^{F/F}$ mice and their littermate controls (3.1 ± 0.3 SD OHCs and oc-IHCs per IHC in *Atoh1*$^{Cre/+}$*; Insm1*$^{F/F}$ mice, n=9; vs 3.3 ± 0.2 SD OHCs per IHC in *Atoh1*$^{Cre/+}$*; Insm1*$^{+/F}$ and *Insm1*$^{F/F}$ littermate controls, n=10). The criteria to identify oc-IHCs in

*Atoh1*$^{Cre/+}$*; Insm1*$^{F/F}$ mice were the presence in the outer compartment of hair cells expressing IHC markers (VGLUT3, high-levels of calmodulin and/or nuclear CtBP2), lacking OHC markers (oncomodulin and/or prestin) and with a shape (determined by myosin VIIa immunoreactivity) like that of IHCs. Mice used for hair cell count were P0-P34.

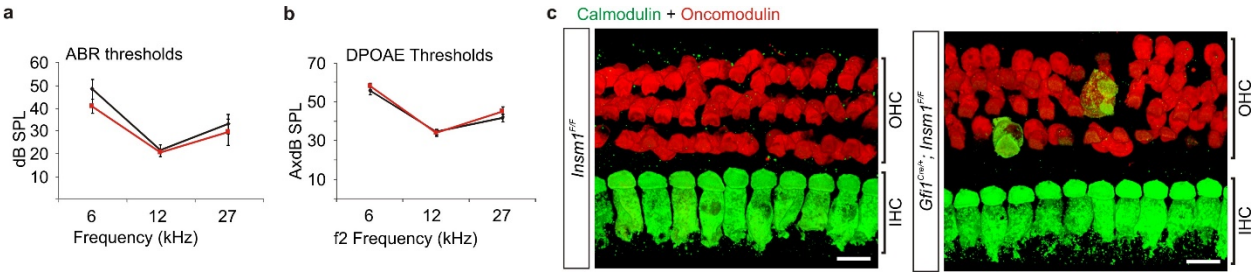


**Extended Figure 3: Conditional ablation of *Insm1* in hair cells using Gfi1-Cre causes no hearing impairment, and results in only very few oc-IHC.** We generated a conditional knockout of *Insm1* in hair cells using Gfi1-Cre in which the expression of cre recombinase coincided with that of *Insm1*. **a-b** Hearing thresholds determined by auditory brainstem responses (ABRs; **a**) and distortion product otoacoustic emissions (DPOAEs; **b**) of $Gfi1^{Cre/+}$; $Insm1^{F/F}$ mice at age P30 to P35 (black traces; n=6, 4 males + 2 females) and control littermates (red traces; n=6; 1 $Insm1^{F/F}$, 1 $Insm1^{F/+}$ and 4 $Gfi1^{Cre/+}$; $Insm1^{F/+}$; 4 males + 2 females). There is no significant difference in ABR and DPOAE thresholds at all frequencies tested between $Gfi1^{Cre/+}$; $Insm1^{F/F}$ mice and their control littermates. **c** Immunohistochemistry in whole mount organs of Corti from P34 mice tested for hearing in (**a-b**) revealed that $Gfi1^{Cre/+}$; $Insm1^{F/F}$ mice had normal IHCs expressing high level of calmodulin. However, very few HCs in the outer compartment also expressed calmodulin at high levels, oncomodulin at low levels, and had a round, flask shape similar to that of IHCs (0.78%; 5/526 OHCs from 2 mice). This result indicates that a brief expression of *Insm1* is sufficient to promote proper OHC differentiation. Scale bars are 10µm.

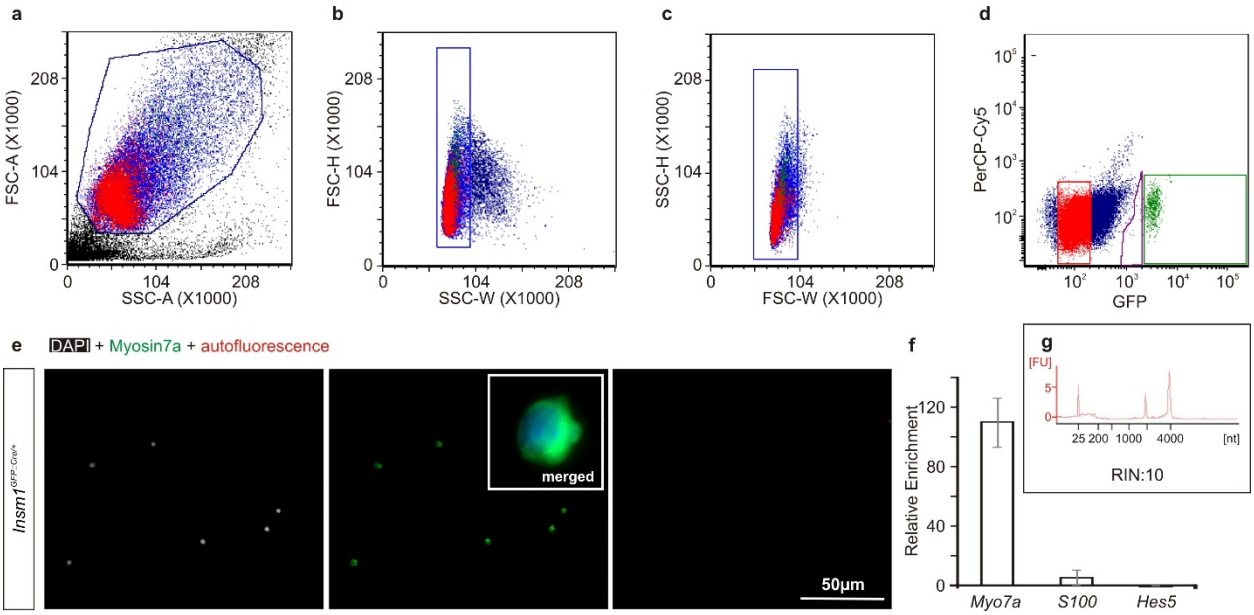


**Extended Figure 4: OHC FACS purification and RNA extraction from an E18.5 *Insm1*$^{GFP::Cre/+}$ embryo. a-c** Forward and side light-scattering are used to exclude dead cells and debris (**a**) and aggregates (≥2 cells) (**b,c**). **d** Live cells are gated in green and red (PerCP-Cy5, to assess autofluorescence) channels to define the GFP+ (green dots) and GFP- (red dots) sorting windows. **e** Myosin VIIa immunoreactivity and DAPI stain of cells collected through cytospinning after FACS confirm that most of the sorted 547 GFP+ cells are hair cells. Inset is a representative merged image of one sorted OHC at high magnification. In this pool, there were no autofluorescent cells collected. **f** RT-qPCR after cell sorting reveals that, compared with GFP- cells, GFP+ cells express HC marker gene *Myo7a* and not the supporting cell marker genes *S100* and *Hes5*. **g** To ensure the quality of the extracted RNA, the RNA Integrity (RIN) score was determined with a BioAnalyzer.

| GeneSymbol | Description | Log2 Fold (IHC/OHC) | Log2 Fold (KO/Het) |
|---|---|---|---|
| Tbx2 | T-box 2 | 4.268712127 | 3.781045749 |
| Smad3 | SMAD family member 3 | 3.417747634 | 3.811200019 |
| Cadps | Ca2+-dependent secretion activator | 3.074283688 | 1.784633146 |
| Nhs | Nance-Horan syndrome (human) | 3.002196896 | 3.53142038 |
| Lrrn1 | leucine rich repeat protein 1, neuronal | 2.974303022 | 2.30112683 |
| Brip1 | BRCA1 interacting protein C-terminal helicase 1 | 2.901240053 | 3.660960043 |
| Rin3 | Ras and Rab interactor 3 | 2.513108025 | 3.45672298 |
| Pcdh1 | protocadherin 1 | 2.161422196 | 1.818043088 |
| Apc2 | adenomatosis polyposis coli 2 | 2.099190868 | 2.291422514 |
| Kcnc3 | potassium voltage gated channel, Shaw-related subfamily, member 3 | 1.912798079 | 2.338575067 |
| Dtx3 | deltex 3, E3 ubiquitin ligase | 1.865571628 | 1.880282934 |
| Spryd3 | SPRY domain containing 3 | 1.862564284 | 2.743476747 |
| Aff3 | AF4/FMR2 family, member 3 | 1.845043179 | 2.038294597 |
| Pacs1 | phosphofurin acidic cluster sorting protein 1 | 1.832624651 | 1.394458382 |
| Car13 | carbonic anhydrase 13 | 1.827719222 | 2.094835081 |
| Dusp27 | dual specificity phosphatase 27 (putative) | 1.76242691 | 3.414558474 |
| Zfhx2 | zinc finger homeobox 2 | 1.691674352 | 1.286663554 |
| Zpld1 | zona pellucida like domain containing 1 | 1.6411418 | 3.711565881 |
| Tmprss7 | transmembrane serine protease 7 | 1.599147043 | 1.620019181 |
| Pgam2 | phosphoglycerate mutase 2 | 1.575650605 | 1.636205885 |
| Rprm | reprimo, TP53 dependent G2 arrest mediator candidate | 1.532495689 | 0.868151806 |
| 5031425E22Rik | RIKEN cDNA 5031425E22 gene (ncRNA) | 1.495402253 | 2.108776135 |
| Tspan17 | tetraspanin 17 | 1.482698362 | 2.049477068 |
| Ercc4 | excision repair cross-complementing rodent repair deficiency, complementation group 4 | 1.375172076 | 1.854772946 |
| Sh3rf1 | SH3 domain containing ring finger 1 | 1.29514406 | 1.80942758 |
| Ccdc97 | coiled-coil domain containing 97 (U2 snRNP) | 1.198411255 | 1.215758186 |
| Ube2o | ubiquitin-conjugating enzyme E2O | 1.011117434 | 2.207289554 |
| Rtn4rl2 | reticulon 4 receptor-like 2 | 1.010799162 | 1.155097332 |
| Midn | midnolin | 0.970785072 | 0.741419419 |
| Slc25a23 | solute carrier family 25 (mitochondrial carrier; phosphate carrier) member 23 | 0.883722615 | 1.130993133 |
| Mtss1 | metastasis suppressor 1 | 0.87139742 | 1.2235249 |
| Zmat3 | zinc finger matrin type 3 | 0.770401976 | 0.765415982 |
| Khsrp | KH-type splicing regulatory protein | 0.767132201 | 0.905293493 |
| Pcdh7 | protocadherin 7 | 0.739379511 | 0.8103131 |
| Cux1 | cut-like homeobox 1 | 0.687360724 | 1.033773092 |
| Lrrc8b | leucine rich repeat containing 8 family, member B | 0.645140674 | 0.771487757 |

**Extended Table 1: Immature IHC-enriched genes upregulated in immature OHCs lacking INSM1.** The fold differential expression of IHCs respect to OHCs and of OHCs without INSM1

(from *Insm1*$^{GFP::Cre/-}$ mice, referred to as KO) with respect to OHCs with INSM1 (from *Insm1*$^{GFP::Cre/+}$, referred to as Het) are indicated as Log2 values.

**Supplementary Table 1: RNAseq values for IHCs and OHCs collected from newborn pups (corresponding to E19.5).** The names of each of the examined genes is given in the *GeneSymbol* column the gene product briefly described in the Description column, the chromosomal location in the *Location* column, and the genome strand in the *Strand* column. Columns *IHC-1* to *OHC-6* display the RNAseq values (normalized gene counts) for each of 6 separate pools of IHCs and OHCs, and columns *Ave IHC* and *Ave OHC* display the average values for each cell type. The *Status* column indicates whether there are enough reads to confidently perform the differential expression test (OK) or not (Low). Out of all 23337 genes examined, 13001 were expressed at sufficient levels in either OHCs or IHCs (OK). The differential expression between IHCs and OHCs is given in Log2 values under the *Change (Log2)* column and its standard error is given in the *Std Err* column. These differential expression values were obtained using DESeq2, which makes sdjustments based on the abundance of the transcripts. The statistical analyses values are listed in the *Test Statistic*, *p-value* (unadjusted) and *p-FDR* (False Discovery Rate-adjusted p values) columns. Genes are ordered from top to bottom according to the statistical strength FDR-adjusted p values) of the differential expression. The *Significant* column indicate whether the differential expression is deemed significant ("yes" for FDR-adjusted p <0.05 and "no" otherwise). Based on this analysis, 1629 genes appear to be differentially expressed between IHCs and OHCs at P0.

**Supplementary Table 2: Genes with significantly higher expression levels in immature IHCs than OHCs.** Genes are ordered from top to bottom according to the statistical strength (FDR-adjusted p values) of the differential expression. Columns are labelled as in Supplementary Table 1.

**Supplementary Table 3: Genes with significantly higher expression levels in immature OHCs than IHCs.** Genes are ordered from top to bottom according to the statistical strength (FDR-adjusted p values) of the differential expression. Columns are labelled as in Supplementary Table 1.

**Supplementary Table 4: Comparison of specific transcriptomes of IHCs or OHCs at differentiating vs mature stages.** Lists of neonatal IHC- and OHC-enriched genes were obtained from supplemental tables 2 and 3 and based on RNAseq data, respectively. The lists of mature IHC- and OHC-enriched genes were calculated from microarray data[33]. These lists were used to generate the Venn diagrams in figure 3g.

**Supplementary Table 5: RNAseq values for OHCs collected from E18.5 embryos with (*Insm1*$^{GFP::Cre/+}$) or without (*Insm1*$^{GFP::Cre/-}$) INSM1.** Columns *GFP/+ OHC-1* to *GFP/- OHC-3* display the RNAseq values (normalized gene counts) for each of 3 separate pools of OHCs from *Insm1*$^{GFP::Cre/+}$ or *Insm1*$^{GFP::Cre/-}$ embryos, and columns *Ave GFP/+ OHC* and *Ave GFP/- OHC* display the average values (used for the fig 4a plot of expression levels for each genotype). All other columns are labelled as in Supplementary Table 1. Genes are ordered from top to bottom based on the statistical strength (FDR-adjusted p values given in column *p-FDR*) of their differential expression. Out of all 23337 genes examined, 12505 were detected at sufficient levels in OHCs at E18.5 (OK values in the *Status* column).

**Supplementary Table 6: Genes expressed at higer levels in E18.5 OHCs lacking INSM1 (*Insm1*$^{GFP::Cre/-}$) compared to those expressing it (*Insm1*$^{GFP::Cre/+}$), potentially down-regulated by INSM1.** Columns are labelled as in Supplementary Table 5. Genes are ordered from top to bottom based on the statistical strength (FDR-adjusted p values, column *p-FRD*) of

their differential expression. Genes were selected based on an FDR-adjusted p<0.05 (in red in column *p-FRD* and corresponding to red squares in fig 4a) or, additionally, an unadjusted p< 0.01 (in green in column *p-value* and corresponding to green squared in Fig 4a).

**Supplementary Table 7: Genes expressed at higher levels in E18.5 OHCs with INSM1 (*Insm1*$^{GFP::Cre/+}$ compared to those lacking it (*Insm1*$^{GFP::Cre/-}$), potentially up-regulated by INSM1.** Columns are labelled as in Supplementary Table 5. Genes are ordered from top to bottom based on the statistical strength (FDR-adjusted p values, column *p-FRD*) of the differential expression. Genes were selected based on an FDR-adjusted p<0.05 (in red in column *p-FRD* and corresponding to red squares in fig 4a) or, additionally, an unadjusted p< 0.01 (in green in column *p-value* and corresponding to green squared in Fig 4a).

**Supplementary Table 8: Genes predicted to be regulated (up or down) by INSM1 in E18.5 OHCs that also appear to be preferentially expressed in P0 (corresponding to E19.5) OHCs or IHCs.** The listed genes correspond to overlaps in the venn diagrams of figs 4b-e. The "GeneSymbol" column names all genes, color coded with respect to the statistical value of their differential expression between *Insm1*$^{GFP::Cre/+}$ and *Insm1*$^{GFP::Cre/-}$ OHCs as in Fig 4a (the most significant in red and the others in green). Column "INSM1 Regulation" indicated whether the genes were enriched in *Insm1*$^{GFP::Cre/+}$ (Up regulated) or *Insm1*$^{GFP::Cre/-}$ (Down regulated) OHCs. For five of these genes (*Tbx2*, *Nhs*, *Lrrn1*, *Brip1* and *Rin3*; named with purple font in Fig 4f) the differential expression was confirmed by TaqMan RT-qPCR (ratios of expression in OHCs without vs with INSM1 are given in columns "KO/Het RT-qPCR Analysis").

# APPENDIX B

## TRPML2 and Mucolipin Evolution

**TRPML2 and mucolipin evolution**

Jaime García-Añoveros[1,2,3,*] and Teerawat Wiwatpanit[4]

Departments of [1]Anesthesiology, [2]Physiology and Neurology, [3]The Hugh Knowles Center for Clinical and Basic Science in Hearing and Its Disorders, and [4]Driskill Graduate Program in the Life Sciences, Northwestern University, Chicago, IL 60611, USA.

*Corresponding author (anoveros@northwestern.edu).

Keywords: Mucolipin, Mcoln, Mcoln2, TRPML, TRPML2, endosome, lysosome, lymphocyte, ion channel, channel evolution, adaptive immunity.

**Abstract**

The TRPML2 protein, encoded by the *Mcoln2* gene, is one of the three mucolipins (TRPML1-3), a subset of the TRP superfamily of ion channels. Although there are no thorough studies on the cellular distribution of TRPML2, its mRNA appears to be largely restricted to lymphocytes and other immune cells. This contrasts with the ubiquitous expression of TRPML1 and the limited but diverse expression of TRPML3, and clearly suggests a specialized role for TRPML2 in immunity. Localization studies indicate TRPML2 is present in lysosomes (including the specialized lysosome related organelle that B-lymphocytes use for processing of the antigen-bound B-Cell Receptor), late endosomes, recycling endosomes and, at a much lower level, the plasma membrane. Heterologously-expressed TRPML2, like TRPML1 and/or TRPML3, forms ion channels that can be activated by a gain-of-function mutation (Alanine to Proline in the fifth transmembrane domain, close to the pore) that favors the open state, by a transient reduction of extracellular sodium followed by sodium replenishment, by small chemicals related to sulfonamides, and by PI(3,5)P2, a rare phosphoinositide that naturally accumulates in the membranes of endosomes and lysosomes and thus could act as a physiologically-relevant agonist. TRPML2 channels are inwardly rectifying and permeable to $Ca^{2+}$, $Na^{+}$ and $Fe^{2+}$. When heterologoulsy co-expressed, TRPML2 can form heteromultimes with TRPML1 and TRPML3. In B-lymphocytes, TRPML2 and TRPML1 may play redundant roles in the function of their specialized lysosome. Although the specific subcellular function of TRPML2 is unknown, distribution and channel properties suggest roles in calcium release from endolysosomes, perhaps to regulate vesicle fusion and/or subsequent scission, or to release calcium from intracellular acidic stores for signaling in the cytosol. Alternatively, TRPML2 could function in the plasma

membrane and its abundance in vesicles of the endocytic pathway could simply be due to regulation by endocytosis and exocytosis. The *Mcoln2* gene is closely downstream from and in the same orientation as *Mcoln3* in the genomes of most jawed vertebrates (from humans to sharks) with the exception of pigs, *Xenopus tropicalis* and ray-finned fishes. The close homology of TRPML2 and 3 (closer to each other that to TRPML1) suggests that *Mcoln2* and *Mcoln3* arose from unequal crossing over that duplicated a common ancestor and placed both gene copies in tandem. These genes would have come apart subsequently in pigs, Xenopus and the ancestor to ray-finned fishes. All jawed vertebrates for which we have thorough genomic knowledge have distinct *Mcoln1, 2 and 3* genes (except ray-finned fishes which, probably due to the whole genome duplication in their common ancestor, have two *Mcoln1*-like genes and two *Mcoln3*-like genes, although only one *Mcoln2* gene). However, the available genomes of invertebrate deuterostomes (a sea urchin, lancelet and two tunicates) contain a single mucolipin gene that is equally distant from the three vertebrate mucolipins. Hence, vertebrate mucolipins arose through two rounds of gene duplication (the first one likely producing *Mcoln1* and the ancestor to *Mcoln2* and *3*) at some time between the onset of craniates and that of jawed vertebrates. This is also the evolutionary period during which adaptive immunity appeared. Given the restricted expression of TRPML2 in immune cells, this evolutionary history suggests a functional role in the adaptive immunity characteristic of vertebrates.

This review on TRPML2 updates and revises a previous review article on the same topic from our group (Flores and Garcia-Añoveros, 2011) and shall supersede it.

**1. Gene splizing, location and evolution**

The TRPML2 protein (also known as Mucolipin 2), the product of the *Mcoln2* gene (also known as *Trpml2*), is one of three vertebrate isoforms (TRPML1-3) of the mucolipin family of Transient Receptor Potential (TRP) cation channels. Their name derives from its paralog mucolipin 1, which is mutated in mucolipidosis type IV, a lysosomal disease. *Mcoln2* was molecularly identified when the *varitint-waddler* mouse mutations, which cause deafness and pigmentation defects, was identified in the adjacent *Mcoln3*. The *Mcoln2* gene maps to human chromosome I (1p22.3) and mouse chromosome 3 (3qH2), very closely downstream (21 and 8 kb, respectively) of *Mcoln3*.

In most tetrapod genomes (35 species) for which there is enough sequence information, as well as in the genome of their closest living relative (the coelacanth *Latimeria chalumnae*), *Mcoln2* is closely downstream of *Mcoln3* and in the same strand (hence "direction"). Two exceptions are an amphibian (*Xenopus tropicalis*) and the pig (*Sus scrofa*). In the frog *Mcoln3* is in the syntenic region (that is, surrounded by the same genes as in most genomes) whereas its *Mcoln2* has translocated to a new genomic location. However, in the 8 available genomes of ray-finned fishes, *Mcoln2* and *Mcoln3* genes are no longer closely linked (in three species–medaka, stickleback and tetraodon–*Mcoln2* is in the same chromosome as *Mcoln3*, but upstream and at a much greater distance, with many other genes in between). The conservation of the close linkage between *Mcoln2* and *Mcoln3* in most tetrapods plus coleacanth (36/38 genomes) might suggest an evolutionary pressure, such as a shared regulation of expression, to keep both genes together. However, both genes display very different patterns of expression (see below) and our unpublished *in situ* hybridization (ISH) experiments reveal no alteration of *Mcoln2* expression in

*Mcoln3* KO mice. Hence, although possible, there is presently no additional evidence favoring a co-regulatory mechanism for *Mcoln2* and *Mcoln3*. Quite likely, their close linkage has prevented their separation in most evolutionary lineages. Another question to be resolved is how the *Mcoln2* and *Mcoln3* became linked. The one cartilaginous fish genome (that of the elephant shark *Callorhinchus milii*) contains genes for all three mucolipins (Figure 1), and the partial genomic assembly available as of the writing of this article reveals that in this genome, as in most tetrapods and coelacanth, *Mcoln2* is closely downstream of *Mcoln3* (Byrappa Venkatesh, personal communication). This close linkage, their same orientation and their high homology (more similar to each other than to *Mcoln1*) suggests that both genes arose from a duplication through ectopic recombination (unequal crossing over), which generates paralogous genes in tandem, but in that case two genes would have separated in the lineage leading to ray-finned fishes.

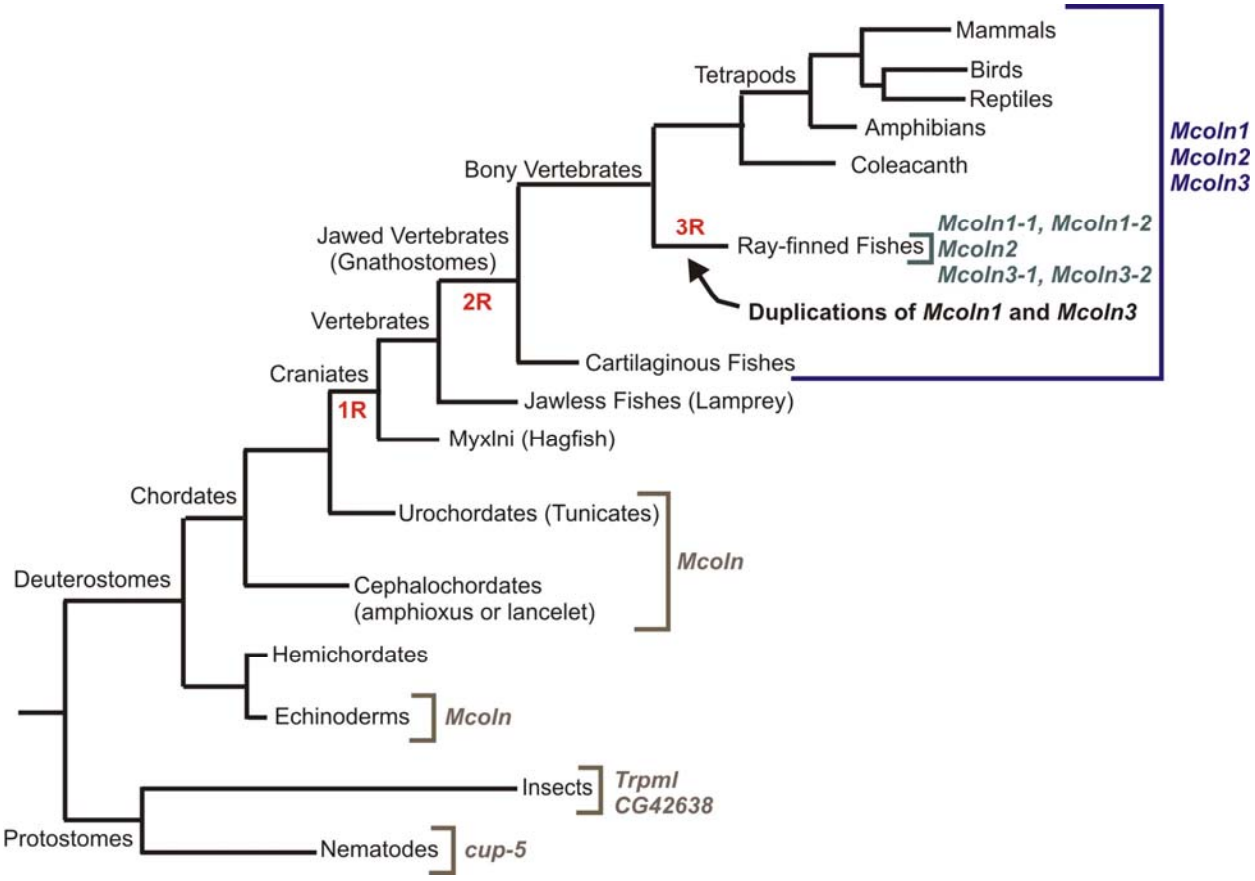


**Figure 1.** Cladogram indicating which genes encoding TRPML proteins (also termed mucolipins) are present in the genomes of different animal groups, which reveals the likely evolutionary period when *Mcoln1*, *2* and *3* originated through duplication (sometimes between the onset of craniates and that of jawed vertebrates). *Trpml* and *CG42638* are the two mucolipin genes in *Drosophila melanogaster* and *cup-5* is the sole mucolipin gene in *Caenorhabditis elegans*. The information regarding mucolipin genes was inferred from a dendrogram assembled in e!Ensembl (http://uswest.ensembl.org/index.html) and from individual searches of *Mcoln* orthologs in the genomes of the sea urchin *Strongylocentrotus purpuratus* (an echinoderm), the lancelet *Branchiostoma floridae* (a cephalochordate) and the elephant shark *Callorhinchus milii*

(a cartilaginous fish). The three presumed whole genome duplications in deuterostomes are indicated as 1R, 2R and 3R.

While nearly all vertebrates sequences thus far seem to contain genes for all three mucolipins (including mucolipin 2), invertebrates of the deuterostome branch (the sea urchin *Strongylocentrotus purpuratus*, which is an equinoderm, the lancelet *Branchiostoma floridae*, which is a cephalochordate, and the tunicates *Ciona intestinalis* and *C. savigni*, which are urochordates) seem to have a single *Mcoln* gene which is equally distant to *Mcoln1, 2* and *3* (Figure 1). Hence, at some time between the onset of craniates and that of jawed vertebrates (tetrapods, coelacanth, ray-finned fishes and cartilaginous fishes, aka Gnathostomes), duplications of an ancestral *Mcoln* gene must have produced all three *Mcoln* paralogs. Completion of the lamprey genome, currently underway, would help further clarify the evolutionary onset of the three vertebrate mucolipins. Based on all the evidence above described, we hypothesized that one of the two presumed whole genome duplications in the evolutionary line leading to jawed vertebrates (1R or 2R; Figure 1) gave rise to *Mcoln1* and an *Mcoln2/3* ancestor, which in a subsequent duplication (likely to be local rather than whole genome) generated (also prior to the appearance of jawed vertebrates) the adjacent *Mcoln2* and *Mcoln3* genes. This evolutionary analysis shall override the one we previously published (Flores and Garcia-Anoveros, 2011), which was based in incomplete genome data and resulted in some suggestions about Mucolipin evolution that are no longer tenable.

A third whole genome duplication (3R) is believed to have occurred in the common ancestor to ray-finned fishes (Figure 1). Accordingly, their genomes contain two close paralogs of *Mcoln1* and *Mcoln3*. However, only one *Mcoln2* is present in each of their genomes (Figure

1). The genomic rearrangements and gene loss that followed this whole genome duplication may explain the separation of *Mcoln2* and *Mcoln3* genes in this lineage.

The evolutionary history of *Mcoln3* and *Mcoln2* is curiously similar to that of the *Tmem138* and *Tmem216* genes, which are closely linked in tandem in the genomes of the elephant shark, coelacanth and most tetrapods but have come apart in the branch leading to ray-finned fishes (in which the 3R whole genome duplication has also similarly resulted in two *Tmem138*-like genes but only one of *Tmem216* gene) as well as in *Xenopus tropicalis* (Venkatesh et al., 2013). Perhaps more significant is the similarity between the evolutionary onset (between the ancestor to craniates and that of jawed vertebrates) and selection of the *Mcoln2* (Figure 1) and that of adaptive immunity (Flajnik and Kasahara, 2010), as it suggests a role of TRPML2 in this cell-based form of immunity characteristic of vertebrates.

The mouse *Mcoln2* gene generates at least two transcripts and polypeptides that result from alternative first exons: TRPML2sv (short, 2384 bp mRNA and 538 residue protein; NM_001005846) and TRPML2lv (long, 2418 bp mRNA and 566 residue protein; NM_026656 vs). The first exon of TRPML2sv does not code for protein, whereas the first exon of TRPML2lv encodes the additional 28 amino acids to the amino-terminus of TRPML2lv. Human *Mcoln2* generates only one mRNA and protein of 566 amino acids, the same size as mouse TRPML2lv (Samie et al., 2009).

**2. Gene expression and protein localization**

By RT-PCR, Trpml2 mRNA was detected in multiple organs of human (lung, trachea,

stomach, colon, mammary glands, and peripheral blood lymphocytes with lower levels in kidney, thymus, testis, and uterus and lowest levels are seen in spleen, adipose tissue and thyroid) and mouse (kidney, thymus, trachea, colon, and adipose tissue with lower levels in lung, liver, pancreas, and testis) (Grimm et al., 2010). However, this technique is overly sensitive and not quantitative, and it may well reveal expression levels that are non-physiological (such as that produced by "leaky" transcription). By quantitative RT-qPCR expression of both alternative mRNAs of mouse Trpml2 were also detected in multiple organs (all those examined). However, expression of the long Trpml2lv transcript was very low in all organs, and expression of the short Trpml2sv transcript was very low in most. Comparatively high expression levels were only detected in thymus and spleen (with lower but still above average levels in kidney and stomach) (Samie et al., 2009). We performed *in situ* hybridization (ISH) with two non-overlapping probes to separate segments on mouse *Trpml2* mRNA on sections of adult mouse organs as well as sagittal sections of newborn mouse pups, and found consistent expression only in thymus and spleen (Natalie Remis and JG-A, unpublished results). By contrast, ISH with probes to the ubiquitous Trpml1 labeled all organs while probes to the more restricted Trpml3 labeled several organs (unpublished results and (Castiglioni et al., 2011)). Hence, while it is possible that Trpml2 mRNA is expressed at very low levels (below detection for ISH) ubiquitously, it is certainly expressed at high levels on cells of thymus and spleen, which suggest expression in lymphoid cells. This is further supported by the source of most Trpml2 cDNA clones (spleen, bone marrow, thymus, and hematopoietic progenitors) (http://www.informatics.jax.org/searches/estclone_report.cgi?_Marker_key=52259&sort=Tissue at Mouse Genome Informatics) as well as by RT-PCR detection of Trpml2 mRNA in B cells, T cells, primary splenocytes, and mastocytoma and myeloma cell lines (Lindvall et al., 2005).

Interestingly, the levels of Trpml2 (but not Trpml3) mRNA were higher in thymus, spleen and kidney of *Mcoln1*1 KO than of wild type mice (Samie et al., 2009), which suggests that the expression of both genes is coordinated in some way and that TRPML2 might be able to compensate for the lack of TRPML1 in these tissues.

In summary, while TRPML1 is ubiquitous and TRPML3 expressed by discrete but diverse cell types, expression of TRPML2 seems highly restricted to lymphocytes and other cells of the immune system.

Although electrophysiological recordings clearly indicate that, when heterologously expressed, some TRPML2 channel localizes to the plasma membrane (Dong et al., 2008; Grimm et al., 2012; Lev et al., 2010; Samie et al., 2009; Zeevi et al., 2010) protein localization studies reveal that most TRPML2, similarly to TRPML1 and TRPML3, localizes to late endosomes and lysosomes (Karacsonyi et al., 2007; Song et al., 2006; Venkatachalam et al., 2006; Zeevi et al., 2009). Tagged TRPML2 heterologously expressed in HEK cells, B-lymphocytes and HeLa cells accumulated at vesicular structures that co-labeled with markers of lysosomes (Lysotracker, Lamp 3 and Rab 11) and late endosomes (CD63) but not with markers of ER (ER-YFP), Golgi (GFP-Golgin 160; GGA3-VHSGAT-GFP), early endosomes (Rab5, EEA1), late endosomes (Rab7-HA) or secretory vesicles (Rab8) (Karacsonyi et al., 2007; Song et al., 2006; Venkatachalam et al., 2006). Immunoreactivities with antibodies raised against TRPML2 co-localized with the lysosomal marker Lamp1 in untransfected HEK cells, although the specificity of these immunoreactivities has not been demonstrated and there is no confirmation by other means that HEK cells express TRPML2 endogenously (Zeevi et al., 2009). In addition to lysosomes, heterologously expressed, tagged TRPML2 has also been localized in HeLa cells to

plasma membrane and tubular endosomes of the Arf6 (GTPase ADP-ribosylation Factor 6) pathway, which are recycling endosomes. TRPML2 co-localizes with CD59 and MHCI, which are also markers of these endosomes, and inhibition of TRPML2 with shRNAs or with a dominant negative isoform of TRPML2 inhibited the recycling of CD59 from these sorting endosomes back to the plasma membrane (Karacsonyi et al., 2007). However, inhibition of clathrin coated endocytosis by co-expression with full length AP180 (a protein that binds clathrin and causes it to be distributed into a lattice-like pattern thereby preventing clathrin-coated pit formation and clathrin-mediated endocytosis), or with the dominant-negative isoform of Dynamin (Dyn1aK44A, which is incapable of binding GTP) resulted in accumulation of TRPML2 at the plasma membrane instead of lysosomal membranes (Venkatachalam et al., 2006). These studies suggested that TRPML2 may be internalized from the plasma membrane through clathirin-coated endocytosis but that once in endosomes it may participate in endosome recycling back to the plasma membrane through the Arf6 pathway.

A problem with the TRPML2 localization studies is that most of them are performed with heterologous overexpression and in cells that do not endogenously express it or have been severely altered through "immortalization" into cell lines. Ideally, these studies would be performed in cells directly obtained from a living organism and that endogenously express TRPML2 (like lymphocytes) with antibodies that recognize endogenous TRPML2 and a control for their specificity (such as a *Mcoln2* KO).

**3. The channel protein including structural aspects**

Like all members of the TRP family, TRPML2 polypeptides are predicted to have their amino-and carboxy-termini in the cytosol, span the membrane six times (with the S1 to S6

domains) and loop in and out of the membrane from the extracellular space by a pore domain situated between S5 and S6. Like all mucolipins, TRPML2 exhibits a large extracellular or luminal loop (~210 amino acids in mouse and human TRPML2) between S1 and S2 (Puertollano and Kiselyov, 2009). Although little mutagenesis has been performed in TRPML2, mutagenesis in the other two mucolipins clearly suggest that this large extracellular loop, though distant from the pore in primary sequence, participates in gating the channel.

**4. Interacting proteins**

Co-immunoprecipitation and FRET analysis demonstrated that heterologously co-expressed, tagged TRPMLs can associate with one another in all combinations (Grimm et al., 2010; Venkatachalam et al., 2006). Others found that TRPML2 co-precipitated with TRPML1/3, albeit with low efficiency, since only 5-6% of the available TRPML2 co-immunoprecipitated with TRPML1 or TRPML3 (Curcio-Morelli et al., 2010; Zeevi et al., 2009). Finally, heterologous expression revealed that TRPML2 with a of a dominant-negative mutation (DD458/459KK) interacted with and suppressed membrane currents generated by dominant gain-of-function mutations (equivalent to the A419V mutation that was shown to increase channel open probability in the *varitint-waddler* mouse (Grimm et al., 2007; Nagata et al., 2008; Xu et al., 2007)) in TRPML1, 2 and 3, whereas the equivalent dominant-negative mutation in any of the three mucolipins interacted with and inhibited the dominant gain-of-function Va-like mutation (A369P) in TRPML2 (Zeevi et al., 2010). These interactions seemed to specifically occur among mucolipins, as none of them co-immunoprecipitated with the more distant TRPM8

(Zeevi et al., 2010). Hence, TRPML2 can form homomultimers as well as heteromultiomers with TRPML1 and/or TRPML3.

Heterologous co-expression of TRPML2 and TRPML3 results in co-localization in Lamp3-positive lysosomes (Venkatachalam et al., 2006) and co-expression of TRPML2 and TRPML1 in B-lymphocytes results in co-localization in Lysotracker-positive lysosomes (Song et al., 2006). In human skin fibroblasts, immunoreactivities with antibodies raised to TRPML1, 2 and 3, co-localize with one another in Lamp1-containing lysosomes, although again it is unclear whether these immunoreactivities represented endogenous TRPML proteins (Zeevi et al., 2009). The co-localization of TRPML2 with TRPML1 appears to be limited to lysosomes, indicating that TRPML2 may have overlapping function with TRPML1. In support, shRNA mediated knockdown of TRPML2 leads to the appearance of abnormal lysosome storage bodies reminiscent of lysosomes seen in ML-IV patients (Zeevi et al., 2009). In summary, TRPML2 can interact with TRPML1 and TRPML3 in lysosomes or late endosomes, although this interaction may be limited and represent a small fraction of the total TRPML2 protein. Hence, although TRPML2 might heteromultimerize with TRPML1 and 3, it likely also forms channels without these subunits.

The heat shock cognate protein of 70 kDa (Hsc70) interacts with the first, large extracellular (or intraluminal, for the vast majority of channels that are in vesicular rather than plasma membranes) loop of TRPML1. HSC70 also co-immunoprecipitates with TRPML2 and TRPML2, although it is unresolved whether this is due to direct binding or to binding to TRPML1 subunits that are heteromultimerized with TRPML2 and or 3. In any case, this interaction would physiologically only occur in the lumen of the lysosomes. Hsc70 participates

in the translocation of cytosolic proteins into the lysosome for degradation, and for this role its presence seems to be required in both the cytosol and the lysosomal lumen. Hence, it was proposed that an interaction between mucolipin channels and intraluminal Hsc70 could facilitate the importation of cytosolic proteins for lysosomal degradation, a process referred to as chaperone mediated autophagy (Venugopal et al., 2009).

**5. A biophysical description of the channel function, permeation and gating**

Even though most TRPML2 probably localizes to the intracellular membranes of endosomes and lysosomes, heterologously expressed TRPML2 results in whole cell recording, and hence some of it must localize to the plasma membrane. Heterologously-expressed TRPML2 at the plasma membrane has been activated with gain-of-function mutations that favor the open state (Grimm et al., 2007; Lev et al., 2010; Samie et al., 2009; Zeevi et al., 2010), alterations in extracellular pH (Dong et al., 2008; Lev et al., 2010), transient reduction of extracellular sodium (Grimm et al., 2012), some synthetic small molecules (Grimm et al., 2012), and the phosphoinositide PI(3,5)P2 (Dong et al., 2010). These recordings demonstrated that TRPML2 mediates inward currents at negative potentials and no outward currents at positive ones, the same inward rectification of TRPML3 and TRPML1 (Grimm et al., 2007; Nagata et al., 2008; Xu et al., 2007) and hence a characteristic of mucolipins. Ion substitution experiments and reversal potentials revealed that the mutated TRPML2 channel is permeable to $Ca^{2+}$, $Na^{+}$ and $Fe^{2+}$ (Dong et al., 2008), which led to the suggestion that TRPML2, like TRPML1, could transport iron from the lumen of endosomes and lysosomes into the cytosol.

The mutation used to generate constitutive activation of TRPML2 generated an A369P substitution in the fifth transmembrane domain (S5). This mutation mimicked the equivalent (A419P) substitution in TRPML3 caused by the *varitint-waddler* mutation, which constitutively activates the channel (Grimm et al., 2007; Nagata et al., 2008; Xu et al., 2007). In HEK293 cells, TRPML2(A369P) but not wild type TRPML2, generated currents and calcium overload. However, heterologous expression of the wild type human TRPML2 in *Drosophila* S2 (Schneider) cells produced currents. The reasons for this constitutive activity are unknown.

Thus far, three small chemical compounds previously found in a screen for agonists of TRPML3 (Grimm et al., 2010) have also been found to activate wild type TRPML2 heterologously expressed in HEK293 cells (Grimm et al., 2012). These are SF-21 (4-chloro-N-(2-morpholin-4-ylcyclohexyl)benzenesulfonamide), SF-41 (1-(2,4-dimethylphenyl)-4-piperidin-1-ylsulfonylpiperazine), and SF-81 (4,6-dimethyl-3-(2-methylphenyl)sulfonyl-1-propan-2-ylpyridin-2-one). These compounds are synthetic and it is unclear whether similar compounds exist in living organisms that might act as natural agonists of TRPML2 and TRPML3.

Another stimulus shown to trigger currents in cells heterologously-expressing wild type TRPML2 is the transient lowering of extracellular sodium followed by the replenishment of sodium or other permeant cations (Grimm et al., 2012), a maneuver that was previously found to activate TRPML3 (Grimm et al., 2010; Kim et al., 2007). However, it is unclear whether these ionic changes occur in a natural setting, and thus whether this form of channel activation bears physiological relevance.

The presence of TRPML2 in endosomes and lysosomes suggest potential physiological evidence to two other channel activators, pH and PI(3,5)P2. The lumen of these organelles is characterized by a low pH, and thus its effect on the constitutively-active TRPML2(A369P) were explored. However, the results obtained were opposite, and while one report found that lowering the pH from 7.2 to 4.6 increased inward currents (Dong et al., 2008), another study reported that lowering the pH from 7.5 to 6.0 reduced the currents by 25% (Lev et al., 2010). The reasons for this difference are unknown. Activation of wild type TRPML2 was also achieved by PI(3,5)P2, a rare phosphoinositide that is specifically found in endosome and lysosome membranes (Dong et al., 2010). This led to the suggestion that activation of mucolipins in endosomes and lysosomes would cause a release of calcium from their lumen into the surrounding cytosolic space that could trigger their fusion or, if already fused, their scission.

Single channel recordings of TRPML2 have only been reported once from artificial lipid bilayers that incorporated TRPML2 protein that had been previously translated in mammalian cells or *in vitro* (Curcio-Morelli et al., 2010).The single channel properties thus obtained were a small conductance (7.44 pS for TRPML2 and 10.2 pS for TRPML3), as well as partial permeability to anions for both channels. These single channel properties differ from the single channel conductance (50 to 70 pS) and permeability to cations of TRPML3 expressed in the plasma membrane of mammalian cells (Nagata et al., 2008) and are uncharacteristic of TRP channels. Because artificial lipid bilayers are not a physiological environment and the properties, the single channel properties of TRPML2 should be corrected or confirmed by recordings from patches of biological membranes.

**6. Physiological functions in native cells, organs, and organisms.**

We do not know the function of TRPML2, which is not surprising given the lack of *Mcoln2* KO mice, of human diseases with mutations on *Mcoln2*, and of the lack of targeted inhibition (by specific antagonists, RNA interference or cell culture-based gene targeting) in cells (such as lymphocytes) that clearly express TRPML2 endogenously. However, heterologous expression of GFP::TRPML2 or GFP::TRPML1 (in which GFP is tagged at the carboxy-terminus of the mucolipins) caused an enlargement or clumping of the lysosomes in these cells quite reminiscent of the pathological vacuolation of lysosomes in MLIV patients. This pathology was not generated by KO of the *Mcoln1* gene in these cells (*Mcoln2* could not be targeted) nor by heterologous expression of TRPML2::GFP or TRPML1::GFP (in which GFP is tagged at the amino-terminus of the mucolipins). A reasonable (although not exclusive) interpretation of these results was that TRPML1 and TRPML2 function redundantly in these cells and that the C-terminus-tagged mucolipins act as dominant negatives. If these assumptions are correct, expression of these constructs would be revealing the effects of interfering with endogenous TRPML1 and TRPML2 function in the lysosomes of B-lymphocytes, which are specialized in the processing of the internalized, antigen-bound B Cell Receptor (Song et al., 2006). This does not reveal the precise role or roles of TRPML2 in lysosomal function but, as for the other mucolipins, reasonable hypothesis include calcium release from endosomes and/or lysosomes to regulate vesicle fusion or scission, calcium release from intracellular acidic stores for signaling purposes, and release of iron or other metals from organelles into the cytosol (Cheng et al., 2010). Alternatively, the abundance of TRPML2 in intracellular membranes could be due to

regulation of its levels in the plasma membrane through endocytosis and exocytosis, and hence its physiological role could take place in the plasma membrane.

Regardless of its subcellular function, the restricted expression of TRPML2 in immune cells, its co-localization with CD59 and the major histocompatibility complex class I (MHC-I) (Karacsonyi et al., 2007) and its presence in and effects on the specialized lysosomes of B-lymphocytes (Song et al., 2006) all point to roles in adaptive immunity. This is further suggested by our evolutionary analysis, which shows that both adaptive immunity (Flajnik and Kasahara, 2010) and the *Mcoln2* gene (Figure 1) arose at about the same time in the deuterostome lineage and remain present is the same extant vertebrate species.

**References**

Castiglioni, A.J., N.N. Remis, E.N. Flores, and J. Garcia-Anoveros. 2011. Expression and vesicular localization of mouse Trpml3 in stria vascularis, hair cells, and vomeronasal and olfactory receptor neurons. *The Journal of comparative neurology* 519:1095-1114.

Cheng, X., D. Shen, M. Samie, and H. Xu. 2010. Mucolipins: Intracellular TRPML1-3 channels. *FEBS Lett*

Curcio-Morelli, C., P. Zhang, B. Venugopal, F.A. Charles, M.F. Browning, H.F. Cantiello, and S.A. Slaugenhaupt. 2010. Functional multimerization of mucolipin channel proteins. *Journal of cellular physiology* 222:328-335.

Dong, X.P., X. Cheng, E. Mills, M. Delling, F. Wang, T. Kurz, and H. Xu. 2008. The type IV mucolipidosis-associated protein TRPML1 is an endolysosomal iron release channel. *Nature* 455:992-996.

Dong, X.P., D. Shen, X. Wang, T. Dawson, X. Li, Q. Zhang, X. Cheng, Y. Zhang, L.S. Weisman, M. Delling, and H. Xu. 2010. PI(3,5)P(2) controls membrane trafficking by direct activation of mucolipin Ca(2+) release channels in the endolysosome. *Nature communications* 1:38.

Flajnik, M.F., and M. Kasahara. 2010. Origin and evolution of the adaptive immune system: genetic events and selective pressures. *Nature reviews. Genetics* 11:47-59.

Flores, E.N., and J. Garcia-Anoveros. 2011. TRPML2 and the evolution of mucolipins. *Advances in experimental medicine and biology* 704:221-228.

Grimm, C., M.P. Cuajungco, A.F. van Aken, M. Schnee, S. Jors, C.J. Kros, A.J. Ricci, and S. Heller. 2007. A helix-breaking mutation in TRPML3 leads to constitutive activity underlying deafness in the varitint-waddler mouse. *Proc Natl Acad Sci U S A* 104:19583-19588.

Grimm, C., S. Jors, Z. Guo, A.G. Obukhov, and S. Heller. 2012. Constitutive activity of TRPML2 and TRPML3 channels versus activation by low extracellular sodium and small molecules. *The Journal of biological chemistry* 287:22701-22708.

Grimm, C., S. Jors, S.A. Saldanha, A.G. Obukhov, B. Pan, K. Oshima, M.P. Cuajungco, P. Chase, P. Hodder, and S. Heller. 2010. Small molecule activators of TRPML3. *Chem Biol* 17:135-148.

Karacsonyi, C., A.S. Miguel, and R. Puertollano. 2007. Mucolipin-2 localizes to the Arf6-associated pathway and regulates recycling of GPI-APs. *Traffic* 8:1404-1414.

Kim, H.J., Q. Li, S. Tjon-Kon-Sang, I. So, K. Kiselyov, and S. Muallem. 2007. Gain-of-function mutation in TRPML3 causes the mouse Varitint-Waddler phenotype. *The Journal of biological chemistry* 282:36138-36142.

Lev, S., D.A. Zeevi, A. Frumkin, V. Offen-Glasner, G. Bach, and B. Minke. 2010. Constitutive activity of the human TRPML2 channel induces cell degeneration. *The Journal of biological chemistry* 285:2771-2782.

Lindvall, J.M., K.E. Blomberg, A. Wennborg, and C.I. Smith. 2005. Differential expression and molecular characterisation of Lmo7, Myo1e, Sash1, and Mcoln2 genes in Btk-defective B-cells. *Cell Immunol* 235:46-55.

Nagata, K., L. Zheng, T. Madathany, A.J. Castiglioni, J.R. Bartles, and J. Garcia-Anoveros. 2008. The varitint-waddler (Va) deafness mutation in TRPML3 generates constitutive, inward rectifying currents and causes cell degeneration. *Proc Natl Acad Sci U S A* 105:353-358.

Puertollano, R., and K. Kiselyov. 2009. TRPMLs: in sickness and in health. *Am J Physiol Renal Physiol* 296:F1245-1254.

Samie, M.A., C. Grimm, J.A. Evans, C. Curcio-Morelli, S. Heller, S.A. Slaugenhaupt, and M.P. Cuajungco. 2009. The tissue-specific expression of TRPML2 (MCOLN-2) gene is influenced by the presence of TRPML1. *Pflugers Arch* 459:79-91.

Song, Y., R. Dayalu, S.A. Matthews, and A.M. Scharenberg. 2006. TRPML cation channels regulate the specialized lysosomal compartment of vertebrate B-lymphocytes. *Eur J Cell Biol* 85:1253-1264.

Venkatachalam, K., T. Hofmann, and C. Montell. 2006. Lysosomal localization of TRPML3 depends on TRPML2 and the mucolipidosis-associated protein TRPML1. *The Journal of biological chemistry* 281:17517-17527.

Venkatesh, B., V. Ravi, A.P. Lee, W.C. Warren, and S. Brenner. 2013. Basal vertebrates clarify the evolutionary history of ciliopathy-associated genes Tmem138 and Tmem216. *Molecular biology and evolution* 30:62-65.

Venugopal, B., N.T. Mesires, J.C. Kennedy, C. Curcio-Morelli, J.M. Laplante, J.F. Dice, and S.A. Slaugenhaupt. 2009. Chaperone-mediated autophagy is defective in mucolipidosis type IV. *Journal of cellular physiology* 219:344-353.

Xu, H., M. Delling, L. Li, X. Dong, and D.E. Clapham. 2007. Activating mutation in a mucolipin transient receptor potential channel leads to melanocyte loss in varitint-waddler mice. *Proc Natl Acad Sci U S A* 104:18321-18326.

Zeevi, D.A., A. Frumkin, V. Offen-Glasner, A. Kogot-Levin, and G. Bach. 2009. A potentially dynamic lysosomal role for the endogenous TRPML proteins. *J Pathol* 219:153-162.

Zeevi, D.A., S. Lev, A. Frumkin, B. Minke, and G. Bach. 2010. Heteromultimeric TRPML channel assemblies play a crucial role in the regulation of cell viability models and starvation-induced autophagy. *Journal of cell science* 123:3112-3124.

# APPENDIX C

## Mucolipins and Postpartum Uterine Involution

# Mucolipins and Postpartum Uterine Involution

## Introduction

The mammalian female reproductive tract is an organ challenged with constant cellular changes. The ovaries and uterus coordinate in response to hormonal cues, which in turns affect the uterine tissue arrangement during estrus cycle and pregnancy. After parturition, the uterine tissue repairs itself, regressing its size while creating new cell population in order for the system to resume its normal cycle and be able to support another pregnancy (Kiracofe, 1980; Salamonsen, 2003; Choi et al., 2012). A failure to regenerate and repair the uterine endometrial tissue after parturition can compromise the overall reproductive health and limit future fertility for females wishing for another pregnancy. Many studies propose that lysosomes might play a major role in regulating the normal cycling of the uterus and its postpartum recovery as there is an accumulation of heterogeneous lysosomes during early postpartum period recovery which subsides late postpartum (Anton et al., 1969; Henell et al., 1983; Bijovsky and Abrahamsohn, 1992). Whether lysosomes regulate uterine tissue remodeling through digestion of apoptotic debree, autophagosomes or extracellular matrix remains unclear.

**Results**

Whether lysosomes regulate uterine tissue remodeling through digestion of apoptotic debree, autophagosomes or extracellular matrix remains unclear. However, studies on rodent uterus report the accumulation of heterogeneous lysosomes during early postpartum period (Anton et al., 1969; Henell et al., 1983; Bijovsky and Abrahamsohn, 1992). We observed an increase of *Trpml1* and *Trpml3* transcript levels around postpartum day (PPD) 1-3, and their expression levels subsided to that of non-pregnant level by PPD10 (Figure 1). The change in *Trpml1* levels appeared subtle with its peak of ~2 folds at PPD2 (Figure 1A). On the contrary, *Trpml3* level increases up to ~13 folds compared to non-pregnant uterus at PPD3 (Figure 1B). The level *Trpml3* similarly subsided by PPD10 (Figure 1B).

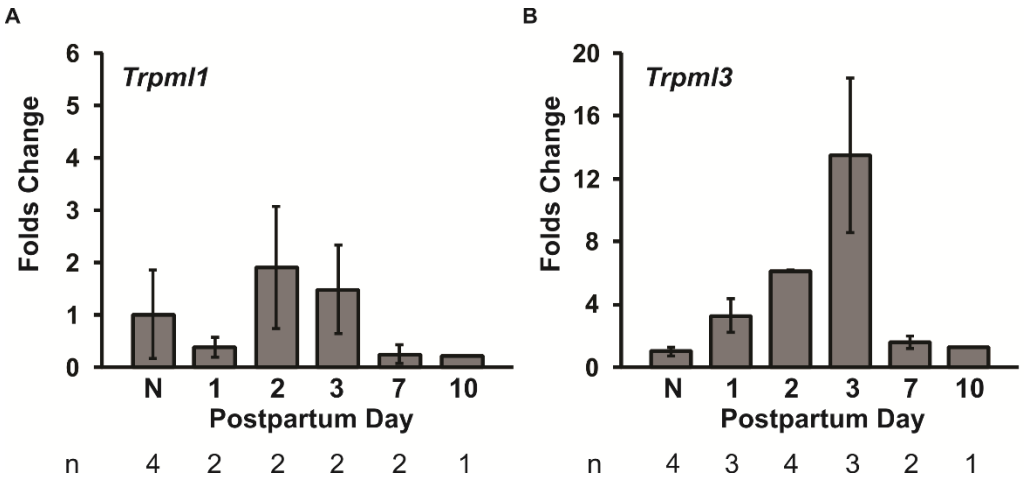


**Figure 1. *Trpml3* is upregulated in early postpartum uteri.** (A) There is no obvious trend of changing expression level of uterine *Trpml1*. (B) Uterine Trpml3 transcript level is upregulated at early postpartum stages with its peak at PPD3. By PPD10, Trpml3 transcript level decreased to that of non-pregnant level. N = non-pregnant.

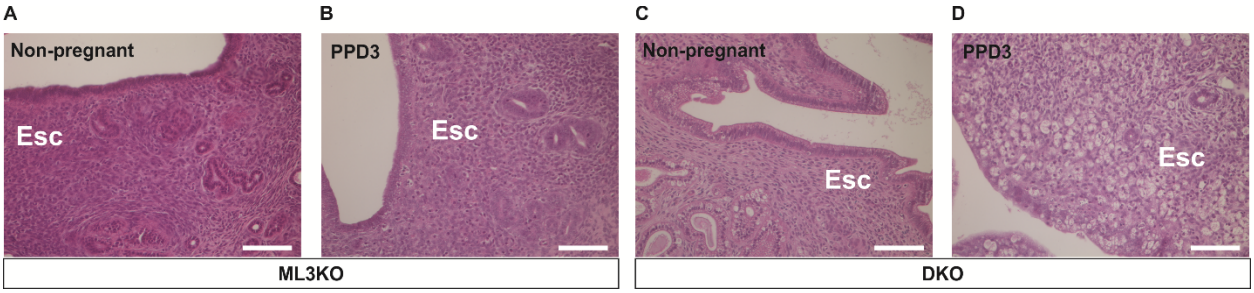


**Figure 2. Pathological vacuoles in postpartum uteri lacking mucolipins 3 and 1.** There is no accumulation of enlarged vacuoles in the control littermates (*Trpml3*$^{-/-}$**,** ML3KO) in either non-pregnant (A) or PPD3 (B) uteri, nor in the virgin uterus of *Trpml3*$^{-/-}$*;Trpml1*$^{-/-}$ (DKO) mice (C) . However, by PPD3 the uterus from DKO mice (D) contains heavily vacuolated endometrial stromal cells (Esc). Scale bars are 50μm.

In control mice lacking mucolipin 3 only (*Trpml3*$^{-/-}$, ML3KO), the uterine endometrium did not exhibit any vacuolization at any stage of the uterus examined (Figure 2A, B). Interestingly, in the mouse model lacking lysosomal channels mucolipins 3 and 1 (*Trpml3*$^{-/-}$*;Trpml1*$^{-/-}$, DKO), there is an accumulation of enlarged vacuoles in PPD3 endometrium ; i.e. luminal epithelial cell, glandular epithelial cell and stromal cells, but not the endometrium from non-pregnant uteri (Figure 2C, D). The presence of the enlarged vacuoles in tissues DKO, but not ML3KO, tissues is consistent with the findings in neonatal intestinal enterocytes (Chapter 2) and auditory hair cells (Chapter 3).

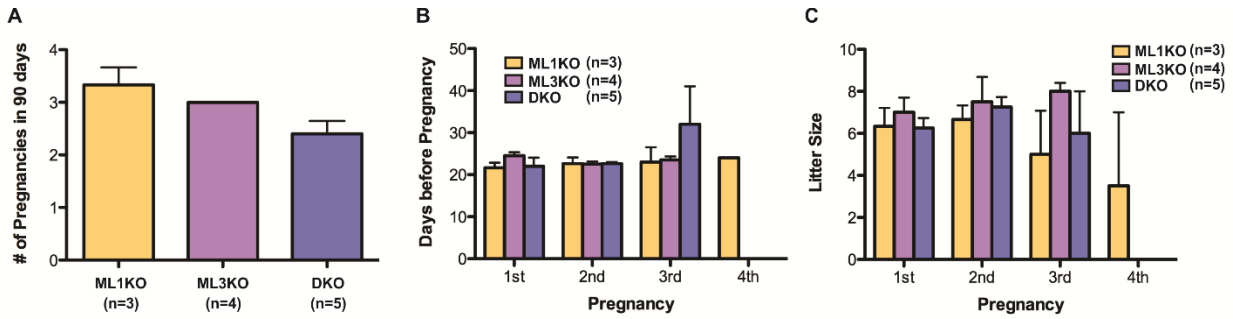


**Figure 3. Mucolipins co-absence may affect long-term fertility.** Two months old female C56BL/6 mice were subjected to a 90-day fertility assessment period. (A) Within a 90-day, DKO mice appeared to be pregnant less frequent than the control ML1KO and ML3KO mice. (B) DKO mice had longer interbirth period after the second pregnancy. (C) The litter size of all genotypes are approximately the same.

Our preliminary observation suggests that female DKO mice may have compromised long-term fertility. DKO mice, but not ML1KO or ML3KO, appear to become pregnant less frequent during our 90-day observation period (Figure 3A). Specifically, after the second pregnancy, DKO mice seem to have longer postpartum recovery period (~30 days) compared to the controls (~21 days) (Figure 3B). The sizes of litter are approximately similar between DKO and control mice, suggesting that mucolipins co-absence does not affect ovulation (Figure 3C). However, due to the current sample size, these analyses are not statistically significant.

**Discussions**

The transient increase in *Trpml3* level correlates with the transient increase in lysosomal accumulation and its enzymatic activity in postpartum uterus (Anton et al., 1969; Bijovsky and Abrahamsohn, 1992). This indicates that changes due to pregnancy or parturition might trigger the formation these vacuoles among mice lacking both mucolipins 3 and 1 and that the presence of at least one type of mucolipin among the littermate controls is sufficient to prevent this phenotype, consistent with the functional redundancy between mucolipins 3 and 1 observed in neonatal intestinal enterocytes and auditory outer hair cells.

Because postpartum endometrial stromal cells readily phagocytose massive amount of extracellular materials for intracellular digestion during regular estrous cycle and postpartum involution (Brandes and Anton, 1969; Miyoshi et al., 1990; Spadacci-Morena and Katz, 2001), we postulated that these cells may utilize the specialized mucolipin-endowed lysosomal system to facilitate postpartum uterine tissue modification. Thus, in the absence of mucolipins 3 and 1, we hypothesized that the endometrial stromal cells may still be able uptake the excess extra cellular matrix through phagocytosis, but fail to degrade such materials through the lysosomal pathway, causing the abnormal enlargement of vacuoles (Figure 2).

Although many studies have suggested that the tissue turnover in the uterus relies mainly on apoptosis, necrosis and, possibly, autophagy (Hopwood and Levison, 1976; Kayisli et al., 2002; Choi et al., 2012), they investigated mainly the tissue dynamic in cycling uterus (i.e. estrus or menstrual cycles). They do not acknowledge the tissue remodeling process after pregnancy at which the uterus returns from its pregnant stage to cycling stage—a process called postpartum uterine involution. Furthermore, a few studies addressing the roles of lysosome in degrading

excess tissue and extracellular matrix during uterine involution have only been done by enzyme reactivity assays and histology, which fail to address the molecular basis of postpartum uterine involution (Anton et al., 1969; Brandes and Anton, 1969; Wang et al., 1999). Here, using our DKO mouse model in which the animal lacks lysosomal mucolipins, we unexpectedly discovered a cellular pathology in the postpartum uterus similar to what we observed in the neonatal intestinal enterocytes and the auditory hair cells (enlargement of endolysosomal vacuoles), thus providing us with a novel model to investigate the molecular basis of mucolipins in lysosomal pathway.

**References**

Anton E, Brandes D, Barnard S (1969) Lysosomes in uterine involution: distribution of acid hydrolases in luminal epithelium. Anat Rec 164:231–251.

Bijovsky AT, Abrahamsohn PA (1992) Changes of the Golgi apparatus and lysosomes during decidualization in mice. Tissue Cell 24:635–642.

Choi J, Jo M, Lee E, Oh YK, Choi D (2012) The role of autophagy in human endometrium. Biol Reprod 86:70.

Henell F, Ericsson JL, Glaumann H (1983) An electron microscopic study of the post-partum involution of the rat uterus. With a note on apparent crinophagy of collagen. Virchows Arch, B, Cell Pathol 42:271–287.

Hopwood D, Levison DA (1976) Atrophy and apoptosis in the cyclical human endometrium. J Pathol 119:159–166.

Kayisli UA, Mahutte NG, Arici A (2002) Uterine chemokines in reproductive physiology and pathology. Am J Reprod Immunol 47:213–221.

Kiracofe GH (1980) Uterine involution: its role in regulating postpartum intervals. J Anim Sci 51 Suppl 2:16–28.

Salamonsen LA (2003) Tissue injury and repair in the female human reproductive tract. Reproduction 125:301–311.

# AUTHOR CONTRIBUTIONS

Intestinal Project (Chapter 2): The work from this project resulted in a co-first author publication: *Remis, N.N., ***Wiwatpanit, T.**, Castiglioni, A.J., Flores, E.N., Cantú, J.A., García-Añoveros, J. (2014). Mucolipin co-deficiency causes accelerated endolysosomal vacuolation of enterocytes and failure-to-thrive from birth to weaning. PLoS Genet 10:e1004833. NNR, AJC, ENF and JAC engineered the mouse line lacking mucolipins 3 and 1, discovered the failure-to-thrive phenotype and determined the spatiotemporal expression of mucolipins in the intestine. I performed ultrastructure examination of the intestine, elucidated that the pathological vacuoles were enlarged endolysosomal hybrid organelle, and lastly, demonstrated that these pathological vacuoles led to reduced endocytosis, resulting in failure-to-thrive phenotype in mice lacking mucolipins 3 and 1. Additionally, for the first time, I demonstrated that human neonatal enterocytes were rich in lysosomes and mucolipin 3. Live enteroid cultures were provided by Dr. Jerrold R. Turner, M.D., Ph.D, Harvard University, MA (formerly at University of Chicago, IL). Human samples were collected and prepared for paraffin or OCT frozen sections by Dr. Catherine Hunter, M.D., and Dr. Isabelle De Plaen, M.D., Feinberg School of Medicine, Northwestern University. Some figures in chapter 2 are modified from Remis et al., 2014. Unless otherwise noted, I collected all the data reported in this chapter. ***equal contributions**

Auditory Project (Chapter 3): The work from this project resulted in a first-author manuscript, conditionally accepted for publication and under revision: **Wiwatpanit, T.**, Remis, N.N., Zhou, Y., Clancy, J.C., Cheatham, M.A. and Garcia-Añoveros, J. Co-deficiency of Lysosomal Mucolipins 3 and 1 in Cochlear Hair Cells Diminishes Outer Hair Cell Longevity and Accelerates Age-Related Hearing Loss. *Journal of Neuroscience*. In Press. Hearing tests and

preliminary data for cochleogram were collected by Dr. Mary Ann Cheatham, Northwestern University, and her lab members. Otherwise, I performed all the experiments reported in this chapter.

In addition to studying hair cell degeneration, I was also interested in the development of the auditory system. Though not reported in this dissertation, the work from this project resulted in a co-first author manuscript in the process of re-submission for publication: ***Wiwatpanit, T.**, *Lorenzen, S.M., *Cantú, J.A., Foo, C.Z., Hogan, A.K., Márquez, F., Clancy, J.C., Schipma., M.J., Cheatham, M.A., Duggan, A. and Garcia-Añoveros. J. Differentiation of nascent outer hair cells into inner hair cells in the absence of INSM1. *Nature*. Awaiting re-submission. Here, I discovered that outer hair cells from mice lacking the transcription factor INSM1 mis-differentiated into inner hair cells. Transcriptomic and *in situ* hybridization reveal that INSM1 acts as a repressor of inner hair cell-specific genes, and, hence, in the absence of INSM1, hair cells in the cochlear outer compartment mis-differentiate into inner hair cells (i.e. they expressed all the inner hair cell markers examined and had anatomical features of inner hair cells). I performed all tissue collections, immunohistochemistry, anatomical examinations and quantifications. In addition, I obtained embryonic organ of Corti for cell sorting for transcriptomic experiments. ***equal contributions**. See APPENDIX A.

I also participated in the writing of a review: Garcia-Añoveros, J. and **Wiwatpanit, T.** (2014). TRPML2 and mucolipin evolution. *Handbook of Experimental Pharmacology.* 222:647-58. Here, we compared sequences of TRPML2 from different species to construct a phylogenetic tree to illustrate the evolution mucolipins. See APPENDIX B.

Finally, during the process of screening for phenotypes from mice lacking mucolipins 3 and 1, I noticed that the endometrial stromal and epithelial cells from postpartum uteri lacking

mucolipins were heavily vacuolated. This phenotype is consistent with that observed in the neonatal intestinal enterocytes and hair cells lacking mucolipins. I later found that in fact postpartum uteri expressed at high level mucolipin 3 compared to non-pregnant uteri. The preliminary work on this project was used as a base for a Friends of Prentice Grant proposal, Northwestern Memorial Foundation, titled “Mucolipins in Postpartum Uterine Involution” (not funded). The preliminary results from this project are reported in APPENDIX C.